MINISTRY OF EDUCATION AND SCIENCE OF UKRAINE
KYIV NATIONAL UNIVERSITY OF TECHNOLOGIES AND DESIGN

Faculty of Chemical and Biopharmaceutical Technologies
Department of Industrial Pharmacy

Master's thesis

on the topic LIPOSOME AND DRUG-TARGETED MOLECULAR PROBES FOR DETECTING LIPID DROPLETS AND TRACKING CANCER CELLS

Completed: student of the group MPhch-20

of the specialty 226 Pharmacy, industrial pharmacy
(code and title of the specialty)

Xiaoqian CHEN
(first name, last name)

Supervisor Andrii HALSTIAN
(first name, last name)

Reviewer Anna KHARYTONENKO
(first name, last name)

Kyiv2021

KYIV NATIONAL UNIVERSITY OF TECHNOLOGIES AND DESIGN

Institute, faculty Chemical and Biopharmaceutical Technologies
Department Industrial Pharmacy
Speciality 226 Pharmacy, industrial pharmacy
(code and title)

Approve
Head of Department Industrial Pharmacy,
Professor, Doctor of Pharmaceutical Science
Vladyslav STRASHNYI

"14" December 2021

ASSIGNMENTS FOR THE MASTER'S THESIS

Chen Xiaoqian
(Full Name)

1. Thesis topic Liposome and drug-targeted molecular probes for detecting Lipid droplets and tracking cancer cells

2. Scientific supervisor Andrii Halstian, Professor, Doctor of Science
(first name, last name, patronymic, academic degree, academic title)
Approved by the order of the higher education al institution on 4thOctober 2021, N286

3. Dead line for student submission of work 14th December 2021

4. Initial data for work: scientific and information sources, methodological and technological literature, scientific periodicals, international and domestic regulations and standards for the development and production of medicines

5. Content of the thesis (list of questions to be developed).*In accordance to the content and task to work(For example: a review of the literature on antibacterial hydrogels, the development of methods for the manufacture of antibacterial hydrogels, the study of the properties of antibacterial hydrogels*

6. Consultants of the master's thesis sections

Section	Surname, initials and position of the consultant	Signature	
		The task was issued	the task accepted
Section 1	Andrii Halstian, Professor, PhD		
Section 2	Jian-Yong Wang, Professor, PhD		
Section 3	Andrii Halstian, Professor, PhD		
Section 4	Jian-Yong Wang, Professor, PhD		

7. Date of issue of the assignment September 20, 2021

Execution schedule

No	The name of the stages of the master's thesis	Terms of performance of stages	Note on performance
1	Introduction	20.09 –27.09.2021	陈晓燕
2	Section1. Summary of Lipid Droplet Fluorescent Probes	28.09. – 11.10.2021	陈晓燕
3	Section2. A novel lipid droplets-specific fluorescence bio-probe with excellent photostability and large Stokes shift for imaging in living cells and zebrafish	12.10 – 25.10.2021	陈晓燕
4	Section3. Two reasonably designed polarity-viscosity sensitive fluorescent probes with large Stokes shift for lighting up lipid droplets in cells	26.10 – 01.11.2021	陈晓燕
5	Section 4. A novel polarity sensitive lipid droplets fluorescent probe synthesized by a rational design strategy and its application in cell imaging	02.11 – 08.11.2021	陈晓燕
6	Conclusions	09.11.-15.11.2021	陈晓燕
7	Draw up a master's thesis (*final version*)	16.11.-04.12.2021	陈晓燕
8	Submission of master's thesis to the department for review (*14 days before the defence*)	06.12.-14.12.2021	陈晓燕
9	Checking the master's thesis for signs of plagiarism(*10 days before the defence*)	14.12-18.12.2021	陈晓燕
10	Submission of master's thesis to the master's department to check the implementation of supplement to the individual curriculum (*10 days before the defence*)	16.12-18.12.2021	陈晓燕
11	Submission of master's thesis for approval by the head of the department(*from 7 days before the defence*)	18.12-21.12.2021	陈晓燕

Student 陈晓燕 Xiaoyan CHEN
(signature) (first name, last name)

Scientific supervisor _____ Andrii HALSTIAN
(signature) (first name, last name)

Head of the scientific and methodological center
for the management of specialist training _____ Olena HRYHOREVSKA

SUMMARY

Xiaoqian Chen. Liposome and drug-targeted molecular probes for detecting lipid droplets and tracking cancer cells. – Manuscript.

LDs are considered to be organelles with extremely low water content and high viscosity. Related to diseases such as diabetes, diabetes, cancer, etc., when the disease is abnormal, lipid droplets in cells will appear, so we have developed four types of lipid droplets.

We designed and constructed a simple coumarin-absorbed p-nitrophenbutylethyl compound as a potential new organic biocatalyst for imaging groups. The internal projection belt shifts to the solar wavelength region. In addition, it is produced by the framework of the donor structure of the Fox also bridge. Stokes camera (100 nm, more than good LD, low biological toxicity and low biological toxicity and introduction. In addition, the biological probe Cou-LDs can also mark the emission of LDs in live zebras

We synthesized two new probes, LDP-1 and LDP-2, which showed a resolution of 4758 cm^{-1} and 3986 cm^{-1}, respectively. In addition, the biological probes LDP1 and LDP show low biological toxicity and good specificity. These two probes are also suitable for life cycle monitoring of cell LD release in HeLa.

At the same time, we have developed a new type of luminescent chemical sensor that can effectively mark the inside of the cell. In addition, the anti-interference, pH stability, and low biological toxicity of decoys have been deeply rooted in cell imaging and zebra fish imaging.

Key words: Lipid droplets, polarity-sensitive, Coumarin, cancer cell, Fluorescent probe, cell imaging

АНОТАЦІЯ

Сяоцянь Чен. Ліпосомні та націлені на ліки молекулярні зонди для виявлення ліпідних крапель і відстеження ракових клітин. – Рукопис.

Ліпідні краплі (LD) вважаються органелами з надзвичайно низьким вмістом води та високою в'язкістю. Пов'язані з такими захворюваннями, як цукровий діабет, рак тобто, коли хвороба є аномальною, у клітинах з'являться ліпідні краплі, тому ми розробили чотири типи ліпідних крапель.

Розроблено просту п-нітрофенбутилетилову сполуку, що поглинає кумарин, як потенційний новий органічний біокаталізатор для груп візуалізації. Внутрішній проекційний спектр зміщується в видимій області світла. Крім того, сполуку виготовляють на основі донорського матеріалу. Камера Стокса (100 нм, більш ніж хороший LD, низька біологічна токсичність і низька біологічна токсичність і введення).

Синтезовано два нових зонди, LDP-1 і LDP-2, які показали роздільну здатність 4758 $см^{-1}$ і 3986 $см^{-1}$ відповідно. Крім того, біологічні зонди LDP-1 і LDP-2 демонструють низьку біологічну токсичність і хорошу специфічність. Ці два зонди також підходять для моніторингу життєвого циклу вивільнення клітинної LD в HeLa. Розроблено новий тип люмінесцентного хімічного датчика, який може ефективно позначати внутрішню частину клітини.

Ключові слова: ліпідні краплі, чутливі до полярності, кумарин, ракова клітина, флуоресцентний зонд, зображення клітин.

CONTENT

Introduction

The relevance. The lipid droplets, which have long been considered an inert fat particle, have not attracted the attention of cell biologists. However, in recent years, more and more researches believe that lipid droplets are a dynamic organelle and represent the frontier of cell biology. As a ubiquitous organelle, lipid droplets have a unique structure in cells. Lipid droplets are similar in structure to plasma lipoproteins. They are divided by cells and transport lipids to different parts of the body through blood circulation. When cells are exposed to a lipid-deficient environment that leads to nutritional imbalance, the breakdown of lipid droplets is activated to provide the necessary energy source for cell survival. When the sudden consumption of glucose in the cell leads to a lack of energy, lipid droplets provide a fast and mobile energy matrix for cell survival.

The earliest description of lipid droplets dates back to the early 19th century. It was described fat droplets in cells and speculated on their origin. In the early days, the high diffraction characteristics of lipid droplets allowed them to be observed under an optical microscope. At the beginning of the 20th century, lipid droplets were considered an important part of most cells, which gave this organelle a new name: liposomes. However, in the late 1960s, artificial liposomes were invented and soon replaced its name. Since then, this organelle has been given

many names, including lipid droplets, liposomes, fat bodies, fat droplets, and liposomes. In plants, they are often called oil droplets. Later, with the rapid development in the field of cell biology, the name lipid droplet gradually replaced other names.

Studies have found that cancer cells have more lipid droplets due to their faster metabolism. Therefore, cancer cells have more lipid droplets than normal cells. This specificity provides the research basis for this article. In this paper, in order to label cell lipid droplets, a variety of novel fluorescent probes . And to achieve precise targeting of lipid droplets in cancer cells, providing a new method for solving cancer diagnosis. This article mainly describes three new types of lipid droplet fluorescent probes. The main conclusions are as follows. Through the fine chemical synthesis of fluorescent probes, UV fluorescence spectroscopy tests are performed on them to analyze the stability of the probes, selectivity, pH resistance, and cytotoxicity. And imaging HeLa cells to study the targeting of the lipid droplets of cancer cells by fluorescent probes based on the coumarin dye as the parent. The study found that these three fluorescent probes can accurately target the lipid droplets of cancer cells. Thus, the research presented in this work is relevant.

Objective of the study: create molecular probes with liposomes and drugs to detect lipid droplets and track cancer cells.

The object of research is properties of molecular probes with liposomes.

The subject of research is molecular probes for detecting lipid droplets and tracking cancer cells.

Research methods. The ^{1}H NMR and ^{13}C NMR spectrums were obtained from INOVA-400 MHz nuclear magnetic resonance instruments, respectively. High-resolution electrospray mass spectra (HRMS) were obtained from Bruker APEX IV-FTMS 7.0T mass spectrometer. All the UV–vis absorption spectra and emission spectra were obtained from Shimadzu UV-1800 spectrometer and Shimadzu RF-5301PC spectroscope respectively. The fluorescence images of cells were obtained with Nikon A1MP confocal microscopy with a CCD camera, Both TLC and silica gel were purchased from the Qingdao Ocean Chemicals.

Practical value: A novel organic bio-probe Cou-LDs exhibited favorable merits including large Stokes shift (over 100 nm), good selectivity, low biological toxicity, and LDs-specificity. Furthermore, the bio-probe Cou-LDs could also marking LDs distribution in living zebrafish, which may be suitable for studying some physiological processes.

Scientific novelty: A novel organic bio-probe Cou-LDs was designed and constructed for LDs cell imaging with much more hydrophobic and viscous environment compared to cytosol.

SECTION 1. Summary of Lipid Droplet Fluorescent Probes

1.1 Fluorescence mechanism

At present, scientists have researched and discovered and demonstrated the detection mechanisms of fluorescent probes: photo-induced electron transfer (PET), intramolecular charge transfer (ICT), fluorescence resonance energy transfer (FRET), cross-bond energy transfer (TBET), aggregation induced luminescence (AIE), excited state intramolecular charge transfer (ESIPT), etc.

1.1.1 Photo-induced electron transfer (PET)

The fluorescent probe of the PET mechanism consists of an acceptor containing an electron donor, a spacer, and a fluorophore that absorbs and emits light.The acceptor is responsible for binding the guest, and the spacer has the function of separating the fluorophore and the acceptor, but can also connect the constituent molecules.When light irradiates the probe molecule in an excited state, electrons are transferred from the receptor to the fluorophore or from the fluorophore to the receptor in the molecule, and the probe molecule does not emit fluorescence.When the receptor binds to the detection substance, the effect of PET is inhibited, and the fluorophore emits fluorescence, as shown in Fig. 1.1.The fluorescence probe of the PET mechanism generally has a huge change in

fluorescence before and after it is combined with the detection substance. Therefore, this type of probe is often used as a switch for molecular fluorescence[1].

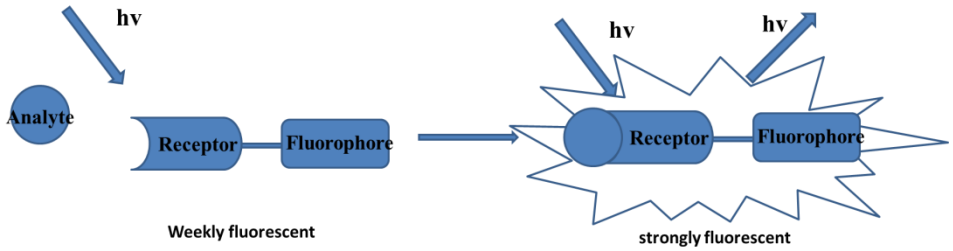

Figure. 1.1 Schematic diagram of luminescence of fluorophore with PET mechanism

Recently, Huang and his team members introduced a new dual-mode signal analysis method based on the hyperchromic effect and light-induced electron transfer of copper nanoclusters protected by polyethyleneimine, which is simple, sensitive, fast and Selectively monitor alkaline phosphatase .

1.1.2 Intramolecular charge transfer (ICT)

The fluorescent probe of the ICT mechanism is usually formed by connecting the electron withdrawing group and the electron pushing group through π electrons. The molecular substrate has two states: electron-deficient and electron-rich. When the electron-deficient state is connected to the electron-withdrawing group, ICT is enhanced, and the spectrum is red-shifted. When the electron-deficient state is connected to the electron-pushing group, ICT is weakened and the spectrum is blue-

shifted; when the electron-rich state is connected to the electron withdrawing group, ICT is weakened, and when it is connected to the electron pushing group, ICT is strengthened. As shown in Fig. 1.2, Molecular fluorescent probes with ICT properties have a strong solvation effect, and their fluorescence spectrum redshifts with the increase of solvent polarity[2-4].

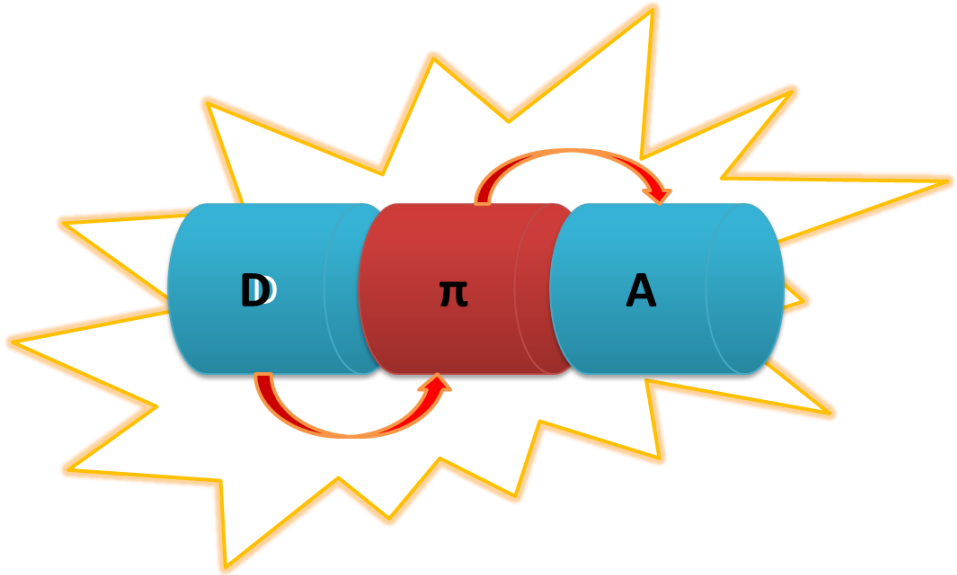

Figure. 1.2 Schematic diagram of fluorophore luminescence with ICT mechanism

Lin's team designed a dicyanoisophorone NIR fluorescent probe MSO-SO2 for ER. Among them, levulinic acid can be used as a specific recognition site and electron withdrawing group.In the absence of SO2, the probe MSO-SO2 emits extremely weak fluorescence due to the inhibition of the intramolecular charge transfer (ICT) process;After responding to SO2, the C=O bond of MSO-SO2 is broken, and the molecule immediately releases the group MSO with near-infrared fluorescence, and emits strong red fluorescence[3].

1.1.3 Fluorescence resonance energy transfer (FRET)

If two fluorescent probe molecules, one is the donor and the other is the acceptor, if the absorption spectrum of the acceptor molecule overlaps with the emission spectrum of the donor molecule and the distance between them is less than 10 nm, Then energy resonance transfer can occur between the two probe molecules. Specifically, when the donor molecule is excited, it will not show fluorescence, but transfer energy to the acceptor through electric dipole interaction, excite the acceptor, and show fluorescence (the acceptor is a fluorescent emitting group). As shown in Fig. 1.3, during the energy transfer process, no photon emission or reabsorption occurs, so it is non-radiative.

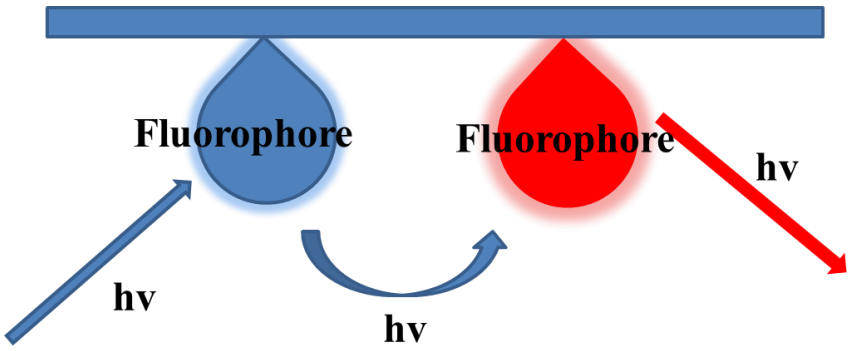

Figure. 1.3 Schematic diagram of fluorophore luminescence with FRET mechanism

In 2016, Jia's group prepared a small molecule fluorescent probe PNcy3cy5 with a FRET mechanism in 2016, and used the different reactivity of Cy3 and Cy5 to OONO- through fine-tuning. It shows high detection sensitivity and generates a ratio fluorescent signal. This probe can also be specifically located in the mitochondria mainly produced by

endogenous OONO-, and it is a promising biological molecular tool[5].

1.1.4 Cross-bond energy transfer (TBET)

The fluorescent probe with cross-bond energy transfer is that the donor and acceptor are connected in the same molecule through the rigid structure of a part of the π-electron system, such as phenylacetylene, diphenylacetylene and other structural units. Compared with FRET, the donor and acceptor have a smaller spatial distance, and the existence of bonds makes the spatial orientation fixed and difficult to change, but electron exchange can occur through the overlap of the electron cloud, so that energy is transferred from the donor to the acceptor[6, 7].

In 2014, Zhou's research team adopted a bond energy transfer (TBET) strategy to design and synthesize a small molecule ratio two-photon fluorescent probe for real-time imaging of living cells and tissues. The two fluorophores share electrons. The yoke bond is directly connected to form the TBET probe Np-Rh, which shows a two-photon fluorescence response with high efficiency energy transfer (93.7%) and two well-resolved emission peaks separated by a target modulation ratio of 100nm[8].

1.1.5 Aggregation induced luminescence (AIE)

In 2001, the team of Professor Tang Benzhong of the Hong Kong

University of Science and Technology discovered a relatively special phenomenon, that is, some molecules do not emit light in dilute solution, but the fluorescence intensity is greatly enhanced in the aggregate state, and the concept of aggregation-induced luminescence was first proposed. The mechanism of aggregation-induced luminescence can be explained by the limited intramolecular motion. Some groups inside the molecule are more active. When in the excited state, the light energy is dissipated in the form of heat in the form of vibration, so it does not emit light or emits weak light. , And when the molecules regroup together, they restrict each other's internal movement and reduce energy loss, so the light output efficiency is very high, which shows the phenomenon of fluorescence enhancement. The opposite is aggregation-induced quenching (ACQ), that is, molecules that fluoresce strongly at low concentrations, but do not emit light or faintly at high concentrations[9].

Dong’s team discovered in 2007 that 1,2-diphenyl-3,4-bis(diphenylmethylene)-1-cyclobutene can be effectively induced to emit light through the formation of aggregates. The crystalline aggregates emit brighter and bluer light than their amorphous counterparts[10].

1.1.6 Excited state intramolecular charge transfer (ESIPT)

ESIPT fluorescent probe refers to the proton transfer reaction between adjacent proton donor and acceptor after being excited inside the

probe molecule after being excited by light, in which the proton group will appear tautomerism. The enol structure will become a keto structure and the emission wavelength of the molecule will be red-shifted[11, 12]. Molecules with ESIPT constitute a very rich field of research because they have large Stokes shifts[13]. Due to its unique photophysical properties, ESIPT molecules have a wide range of applications in luminescent materials for sensors, dye lasers, light stabilizers, bioluminescent probes and electroluminescent devices[14, 15].

In 2019, the Mishra team[16] chose a fluorescent, single embedded ESIPT core 6(a-c) azo dye,

They focused on evaluating the effects of solvents of different polarities and viscous organic solvents, as well as the effects of pH on the UV-visible absorption and emission spectra of electrospray polymer cores containing azo dyes. The results showed that the synthesized dye could be used as a viscosity sensor in the deep red area.

1.2 Lipid droplets

Lipid droplets, which have long been considered an inert fat particle, have not attracted the attention of cell biologists. However, in recent years, more and more studies believe that lipid droplets are a dynamic organelle and represent the frontier of cell biology. Lipid droplets, as a ubiquitous organelle, have a unique structure in cells. They exist in most

eukaryotic cells and are composed of neutral lipids (such as cholesterol or triglycerides) wrapped in a monolayer of phospholipids[17]. There are many proteins on the surface of lipid droplets, which play a very important role in biological functions[18, 19]. Lipid droplets are formed in the endoplasmic reticulum membrane, grow and contract rapidly, pass through the cytoplasm, and contact other organelles to exchange proteins and lipids. The composition of their lipids and proteins is dynamic with changes in cell state and nutrient utilization Variety. Lipid droplets are similar in structure to plasma lipoproteins, which are secreted by cells and transport lipids to different parts of the body through blood circulation. When cells are exposed to a lipid-deficient environment to cause nutritional imbalance, the breakdown of lipid droplets is activated to provide the necessary energy source for cell survival. When the sudden consumption of glucose in the cell leads to a lack of energy, lipid droplets provide a fast and mobile form of energy substrate for cell survival.

The earliest description of lipid droplets can be traced back to the early 19th century. Both Richard Altman and E.B. Wilson described the fat droplets in cells and speculated their origin [20].In the early days, the high diffraction properties of lipid droplets allowed them to be observed under an optical microscope. In the early 20th century, lipid droplets were considered an important part of most cells, which gave this organelle a new name: liposomes. However, in the late 1960s, artificial liposomes

were invented and soon replaced its name. Since then, this organelle has been given many names, including lipid droplets, liposomes, fat bodies, fat droplets and liposomes. In plants, they are often referred to as oil droplets. Later, with the rapid development of the field of cell biology, the name lipid droplet gradually replaced other names.

1.2.1 The structure of lipid droplets

Lipid droplets are organic cores composed of neutral lipids (triacylglycerols and sterol esters) and are wrapped by a monolayer of phospholipids (Fig. 1.4) [17]. This structure provides a unique interface for cells to separate the water and organic phases. A large number of proteins are secreted on the surface of lipid droplets, including structural proteins (perilipin family proteins), lipid synthase (acetyl coenzyme, carboxylase, acyl-CoA synthase, etc.), lipase (fatty tissue triacylglycerol lipase ATGL) and membrane transporters (Rab5, Rab18 and ARF1). More complicated is that different lipid droplets in cells can contain different proteins (Ducharme and Bickel), and the rate of obtaining triglycerides is also different, which indicates that cells contain different types of lipid droplets with special functions[19].

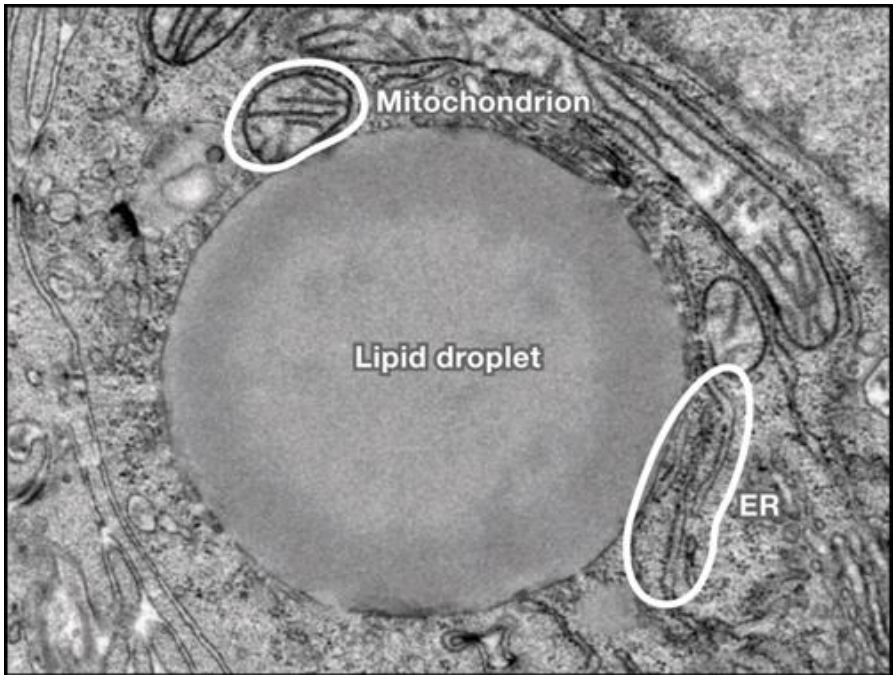

Figure. 1.4 The composition of lipid droplets

1.2.2 Lipid droplet formation

When fatty acids (FAs) are carried by albumin and lipoproteins from outside the cell into the cell, the life cycle of lipid droplets begins to form. Fatty acids release triglycerides in lipoproteins through the hydrolysis of lipoproteins, and passively diffuse into cells through the action of fatty acid transporters or fatty acid translocators[21]. Fatty acids can also be synthesized from carbohydrates in many types of cells. Next, the fatty acid enters the biological activity pool by combining with coenzyme a to form fatty acid acyl-coenzyme a in a reaction that requires energy. Fatty acid acyl-coenzyme a is used by glycerol synthase (glycerol-3-phosphate acyltransferase and sn-1-acylglycerol-3-phosphate acyltransferase) in the

endoplasmic reticulum to finally generate diacylglycerol. Diacylglycerols are converted into neutral lipids (triglycerides) by the DGAT enzyme or enter the phospholipid synthesis pathway.

1.2.3 Enlargement of lipid droplets

The size of lipid droplets varies greatly, and their diameter ranges from 20 nm to 100 μm. Therefore, lipid droplets can grow. One possible mechanism is that, like balloons, lipid droplets swell like unicellular organelles. If lipid droplets continue to adhere to the endoplasmic reticulum, protein and newly synthesized lipids may diffuse to the sides of the lipid droplets and increase their volume[21]. If the lipid droplets are separated from the endoplasmic reticulum, these proteins and lipids may be transported to the lipid droplets through the vesicle, because the vesicle bilayer membrane must fuse with the monolayer membrane at the lipid droplet. In addition, the neutral lipids in the nucleus can target enzymes on the surface of lipid droplets (such as DGATs). In either case, the increase in the volume of neutral lipids needs to match the increase in the corresponding surface phospholipids. Consistent with this view, the key enzyme of phospholipid synthesis, CTP: phosphocholine cytidine transferase, is located on the surface of the lipid droplet during the growth process of the lipid droplet [22]. Similarly, smaller lipid droplets can form larger lipid droplets through fusion, which may also promote the growth

of lipid droplets. It should be noted that the fusion mechanism will reduce the need for phospholipid synthesis during the growth of lipid droplets, because fusion will reduce the specific surface area of the lipid droplets.

1.2.4 The role of lipid droplets

For many cells and organisms, the energy supply in the environment fluctuates between surplus and starvation, and the ability to store energy may provide a competitive evolutionary advantage.

Energy in cells is mainly stored in the form of triglycerides, which are hydrophobic and highly concentrated molecules used to store energy. In cells, energy is stored in lipid droplets [21]. In fact, the main cells involved in this process are highly specialized adipocytes, in which lipid droplets usually occupy most of the space. In mammals, energy storage and catabolism in lipid droplets are highly regulated by hormones and signaling pathways. Lipid droplets are also the reservoir of the components of biological membranes (phospholipids and sterols). When energy is needed, the lipids in lipid droplets can be catabolized to produce corresponding biological membranes. In yeast, the hydrolysis of triglycerides is related to the cell cycle and increases rapidly with the expansion of the membrane[23].

Lipid droplets are also involved in intracellular protein metabolism. For example, during the development of Drosophila, histones accumulate

on the surface of lipid droplets until they are incorporated into the rapidly dividing nucleus[24].In the process of hepatocyte virus replication, the core protein of hepatitis C virus is also located in lipid droplets[25]. Lipid droplets play a great role in the function of spliceosome and proteasome. In the proteasome, lipid droplets can serve as a platform for the deposition and degradation of certain proteins[26].Lipid droplets have been proven to play a very important role in various biological functions, such as regulating the storage and metabolism of neutral lipids, protein degradation, membrane construction and maintenance, and signal transduction. Abnormal intracellular lipid droplets can lead to the occurrence of many diseases, including cancer, obesity, fatty liver, hyperlipidemia, atherosclerosis, inflammation, viral infection, type II diabetes and neurodegeneration in Alzheimer's disease .

1.2.5 The significance of lipid droplets

In the past few decades, lipid droplets have been studied mostly in morphology, and other aspects have received little attention. In 1991, in fat cells, the phosphoprotein perilipin associated with lipid droplets was first discovered[27]. This discovery aroused the attention of scientists to lipid droplets. Since then, research on lipid droplets has increased dramatically. It mainly includes basic research related to obesity-related diseases and oil production. Lipid droplets have developed new areas for

biological research and greatly promoted the development of cell biology. Lipid droplets, whose role has been underestimated for a long time, are now finally recognized as an important organelle with complex dynamic structure and biological significance

The overexpression of triglycerides usually induces obesity and metabolic syndrome, often leading to cardiovascular disease and type II diabetes. Lipid droplets play an important role in the storage of triglycerides. In fact, many diseases, such as obesity, diabetes and fatty liver, are diseases caused by excessive lipid droplets. Lipid droplets in fat cells, muscle cells, liver cells, and cardiomyocytes may protect cells from excessive fat. However, in many cases, excessive lipid deposition may exceed the cell's ability to withstand it, leading to dysfunction, called lipotoxicity[28]. Interestingly, the Fsp27/CIDEC protein can regulate the storage of fat by adipocytes[29], and may also regulate the storage capacity of lipid droplets[30]. Lipid droplets also play an important role in atherosclerosis. In atherosclerosis, cholesteryl esters cause the accumulation of lipid droplets in macrophages to form foam cells, which are a sign of atherosclerotic lesions. In foam cells, lipid droplets have the effect of buffering excess unesterified sterols in the cells. If macrophages are overwhelmed by excessive lipids, cell apoptosis and cell necrosis may occur, causing pathological changes, and ultimately leading to stroke and heart attack[31]. In addition to metabolic diseases, lipid droplets are also

involved in the cell replication of a variety of infectious pathogens, including chlamydia and hepatitis C virus[32], providing a new therapeutic perspective for these diseases. In addition to diseases, in-depth research has been conducted on the application of lipid droplets in nutrient sources or biofuels in petroleum production. For a long time, researchers have changed the fat production of animals or crops through breeding, and may further increase their fat production through genetic engineering. In addition, in industrial production, efforts to use lipid droplets in algae or bacteria as a source of biofuel to provide an energy source are rapidly increasing. Traditionally, vegetable oil stored in liposomes can be obtained from crops such as Brassica napus and further processed into biodiesel. The current research on the engineering technology of photosynthetic microorganisms such as algae is expected to bring the industrial-scale production of petroleum into a new field.

1.3 Research Progress of Fluorescent Probes for Lipid Droplets

In recent years, different lipophilic fluorescent probes have been developed, expanding the toolbox that can be used to detect lipid droplets. The ingenious design of the probe improves the specificity of the compound to organelles, so that the compound has better photophysical properties, enhanced cell permeability, and lower cytotoxicity. In this section, we have listed a series of fluorescent probes for targeting lipid

droplets, with fluorescence emission wavelengths ranging from blue to the near infrared (NIR) region. For clarity, we group the emission colors of fluorescent probes in low-polar solvents as follows (Fig. 1.5): blue (λem <500 nm), green (λem = 500 – 550 nm), yellow (λem =550 – 600 nm), red to near infrared (λem> 600 nm).

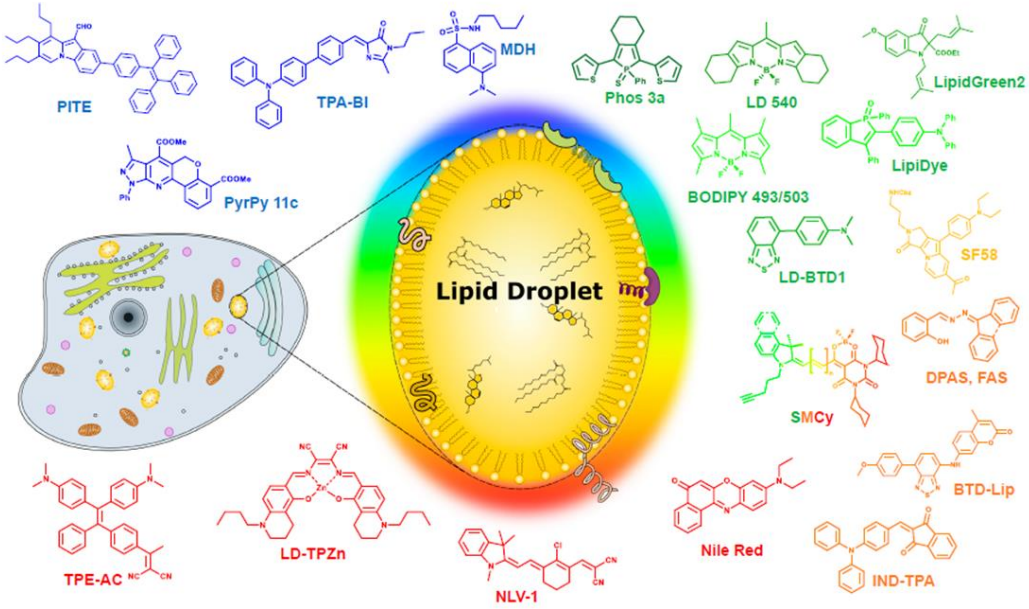

Figure. 1.5 Various lipid droplet fluorescent probes

1.3.1 Lipid droplet probe with blue light

Yang et al. [33] reported a blue commercial dye targeting lipid droplets with monosalvianolic pentane (MDH) (Figure 1.5) as the fluorophore. MDH has good fluorescence in multicolor single photon excitation (1PE) imaging. At the same time, it has two-photon (2PE) imaging performance under 760 nm excitation.

Inspired by MDH as a commercial dye for lipid droplet targeting, PyrPy10d and PyrPy11c blue dyes were developed with dihydropyridine

and pyrazopyridine as the core[34]. These dyes exhibit solvochromic behavior. As the polarity of the solvent increases, the color shifts to red. This feature proves that the molecule undergoes an intramolecular charge transfer (ICT) process. The introduction of ester groups in the pyridine core can improve the ICT process and cell permeability. In addition, the introduction of the second ester group greatly improves the selectivity of the compound to lipid droplets.

PITE[35] is a combination of pyroindole (PI) and tetraphenylethylene (TE) (Figure 1.5). PI emits strong green fluorescence in organic solvents, but due to its poor solubility, the fluorescence is quenched in aqueous solutions, while TE is an aggregation-induced emission (AIE) molecule. PI and TE are coupled to form molecules with new properties, and PITE can specifically target lipid droplets in cells. PITE has absorption peaks at 320 nm and 420 nm, caused by TE and PI, and emission peaks at 490 nm. It shows high targeting of lipid droplets in yeast cells and HeLa cells.

Tang Benzhong's group developed a series of AIE probes targeting lipid droplets, named TPE-AmAl[36] and TPA-BI[37] (Fig. 1.6). TPE-AmAl is composed of TE units with AIE properties. Alkylamino groups are used as electron donors and carbonyl groups are used as electron acceptors to promote the ICT process. TPE-AmAl aggregates in an aqueous solution, the emission spectrum is at 610 nm, but it emits blue

fluorescence in the lipid droplets in the cell. This difference is caused by the non-polar environment of the lipid droplets and the solvation properties of the dye (blue shift in low-polar solvents). Nile red was used as a commercial dye to verify its targeting of lipid droplets.

TPA-BI uses triphenylamine (TPA) as an electron donor and has the ability to enhance two-photon absorption (2PA). When the solvent changes from n-hexane to acetonitrile, TPA-BI exhibits a solvation effect from blue (447 nm) to red (619 nm), covering almost the entire visible spectrum. TPA-BI can perform cell imaging at 1PE and 2PE. In 1PE imaging, TPA-BI not only exhibits excellent lipid droplet targeting, but also exhibits high photostability. The cross-sectional value (δ2PA) of TPA-BI at 840 nm is as high as 213 GM, and its imaging in 2PE cells was evaluated. The results show that TPA-BI outperforms 1PE in 2PE.

Although the reported blue probes successfully target intracellular lipid droplets, they all have some common limitations, such as low brightness, high background fluorescence, and UV-induced phototoxicity.

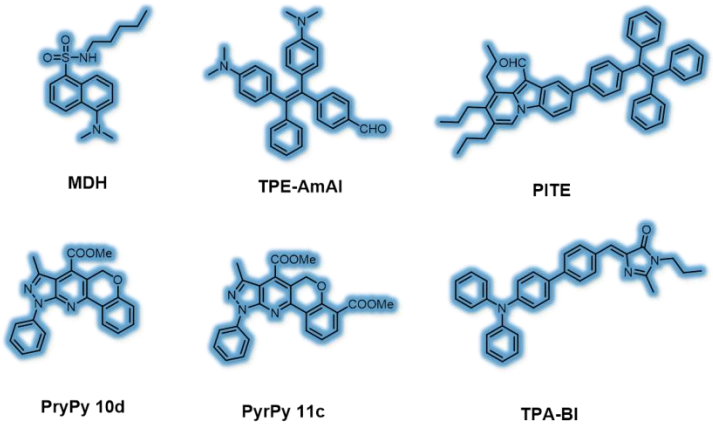

Figure. 1.6 Structures of blue emitting probes for LDs

1.3.2 Green glowing lipid droplet probe

N et al. developed lipid droplet probes LipidGreen (λex/em=485/515nm) and LipidGreen2 (λex/em=456/534nm) that emit green light (Fig. 1.7)[38]. In co-localization experiments with lipid droplet-associated protein (Periplin) and LipidTOX™, both dyes have been shown to stain lipid droplets.

The lipophilic BODIPY derivative LD540 was synthesized for lipid droplet imaging. The dye emits bright fluorescence at 545 nm in sunflower oil[39]. Another type of fluorescent dyes reported to be used for dyeing lipid droplets are AF8, AF10 and AFN based on azolinone[40]. In DMSO, the absorption maximums of AF8 and AF10 are at 375 nm and 352 nm, respectively, and their emission peaks are at 479 nm and 477 nm. Interestingly, in DMSO, the absorption maximum of AFN is at 432 nm, the emission peak is at 592 nm, and the Stokes shift is 160 nm. AF8 and AF10 did not show solvent discoloration effect, while AFN showed solvent discoloration effect. The solvation and discoloration of AFN is caused by the ICT process. Although AF8 and AF10 exhibit interesting photophysical properties, only AFN can enter cells and have a good co-localization effect with Nile Red, showing its specific recognition of lipid droplets.

The subject of Tang Benzhong was combined into a series of two-photon lipid droplet probes containing naphthalene[41], referred to as

NAP (NAP-Ph, NAP-Br, NAP-CF3 and NAP-Py, as shown in Fig. 1.7). These probes have AIE properties, exist in an aggregated state in aqueous solutions, and their emission wavelength is at 523 -540 nm. NAP AIEgens exhibits a large Stokes shift (110 nm) and a good δ2PA (45-100 GM at 860 nm), so it can perform two-photon imaging in living cells and tissues. This type of probe can specifically stain lipid droplets at a very low concentration (50 nM) and a short time (15 min incubation). Appelqvist et al. introduced a green lipid droplet dye based on the benzothiazole (BTD) fluorophore, named LD-BTD1 (Figure 1.6)[42]. BTD is cross-coupled with the electron-donating group dimethylaminophenyl to form a push-pull fluorophore. In hexane, the absorption peak is at 420 nm and the emission peak is at 511 nm. As the polarity of the solvent increases, LD-BTD1 exhibits a significant solvation discoloration effect. Shigehiro Yamaguchi synthesized a benzophosphoroxy fluorophore that is extremely sensitive to polarity for lipid droplet recognition, and its name is LipiDye (Figure 1.6)[43]. In toluene, the absorption peak is at 415 nm, and the emission peak is at 528 nm. Its ICT process makes it show obvious solvation discoloration performance. Once LipiDye stains lipid droplets, its emission maximum is between 521□530 nm. Niko et al. used a similar method to synthesize a probe PA with push-pull effect (Figure 1.6)[44]. The absorption peak is located at 430 nm, and the emission range is between 480 □ 600 nm. This

type of probe also has an obvious solvation effect. Nilsson synthesized a series of phosphorus-containing compounds substituted by pyridyl and thienyl groups (Phos, as shown in Figure 1.6)[45]. The results show that the introduction of thienyl group can cause the red shift of absorption wavelength and emission wavelength more than the introduction of pyridyl group. The study also found that the thiophene derivatives (Phos 2a and Phos 3a) of the phosphorus-containing compounds have better lipid droplet targeting performance in cells than pyridine derivatives. Moliner et al. used natural products as intermediates to design the phenazine lipid droplet probe P1 (Figure 1.6)[46]. In dioxane, the absorption peak of P1 is located at 428 nm, and it emits fluorescence at 500 nm, forming weakly emitting aggregates in water. P1 can achieve better co-localization effect with Nile Red dye in HeLa cells.

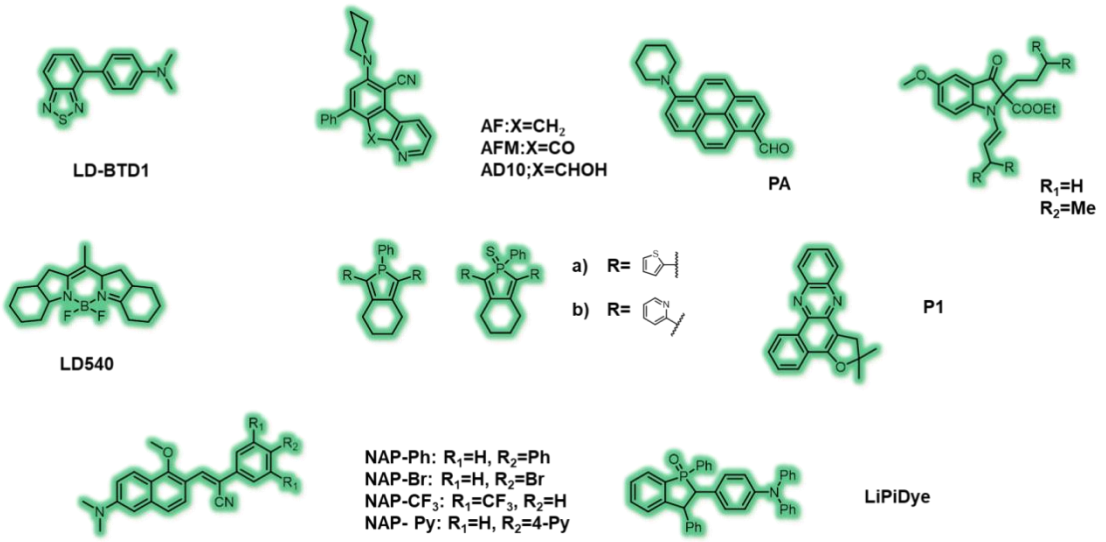

Figure. 1.7 Structures of green emitting probes for LDs

1.3.3 Yellow glowing lipid droplet probe

Seung Bum Park reported a series of Seoul-Fluor-based fluorescent dyes for targeting cell lipid droplets (Figure 1.8)[47]. By introducing the electron-donating group diethylamino group into the Seoul-Fluor core, the fluorescent molecule SF44 was synthesized. This molecule has an obvious solvent discoloration effect. Its emission range is from 561 nm to 624 nm (from ether to acetonitrile). Caused by the ICT process. By improving the compound, the lipophilic molecule SF58 was further rationally designed, and the improved molecule was tested with SF44 for lipid droplets in microalgae. Benzhong Tang's group recently synthesized AIEgens with FAS and DPAS for targeting lipid droplets in cells (Figure 1.8)[48]. They have undergone an excited state intramolecular proton transfer (ESIPT) process, and their keto structure exists in an aggregate state, resulting in a larger Stokes shift and enhanced fluorescence emission. FAS and DPAS showed two emission peaks in the solution. The emission in the short-wavelength region corresponds to the enol configuration, while the emission in the long-wavelength region corresponds to the ketone configuration. FAS and DPAS have good colocalization coefficients with BODIPY 493/503, proving their lipid droplet targeting in cells.

Brenno A. D. Neto synthesized the coumarin lipid droplet dye BTD-Lip[49] based on benzothiadiazole (BTD), which serves as the electron

acceptor. Connecting p-methoxyphenyl as an electron donor to BTD promotes the ICT process in the excited state. The ICT molecule BTD-Lip has a significant solvation effect, ranging from 585 nm to 643 nm (from n-hexane to DMSO). BTD-Lip can identify lipid droplets in CaCo-2 cells, and has a good colocalization coefficient with BODIPY 493/503. BTD-Lip can also identify lipid droplets in Caenorhabditis elegans. Tang Benzhong's subject was combined into a yellow-emitting lipid droplet targeting dye IND-TPA[50]. In THF, the absorption peak is at 478 nm and the emission peak is at 594 nm. IND-TPA exhibits atypical AIE behavior: in the THF/water solution, when the ratio of water increases to 70%, the fluorescence intensity decreases by 13.8 times, and when the ratio of water increases to 90%, the fluorescence intensity increases by 20.4 times. This is due to the twisted intramolecular charge transfer (TICT) effect. It has a good co-localization effect with commercial lipid droplet dye BODIPY 493/503, further confirming the specific recognition of lipid droplets by this probe. IND-TPA has a high signal-to-background ratio. Subsequently, the research group reported the first light-activated AIE probe BZT3a for lipid droplet imaging (Figure 1.8)[51]. BZT3a undergoes photo-oxidation under 365nm light to generate BZT4a in oxidized form. Solid BZT4a has absorption at 365 nm and emission peak at 570 nm. Further studies have shown that in cells, BZT3a and the commercial lipid droplet dye BODIPY 493/503 have a good co-

localization coefficient. Interestingly, BZT3a can be photoactivated under two-photon irradiation at 780 nm. Although its brightness is poorer than commercial BODIPY 493/503, it has simple chemical synthesis, strong cell permeability, larger Stokes shift and excellent lipid droplet targeting performance.

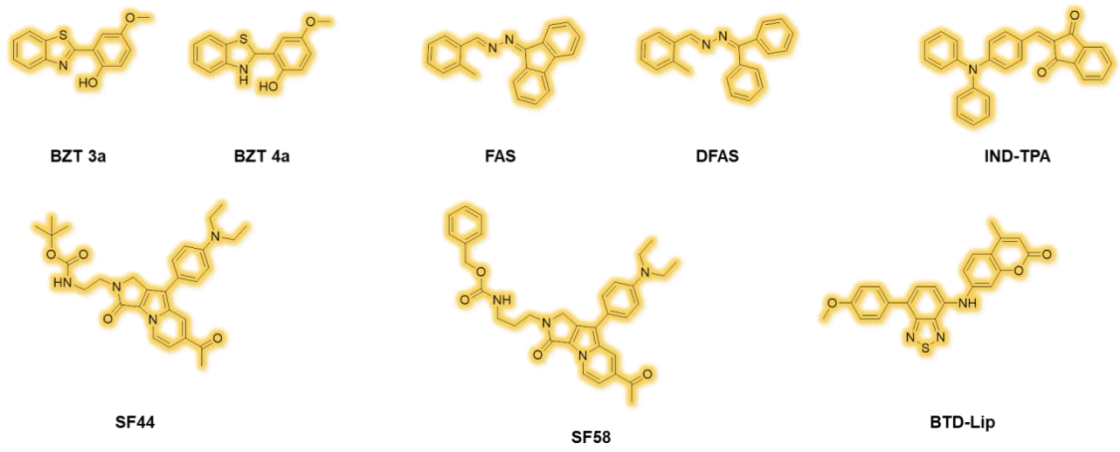

Figure. 1.8 Structures of yellow emitting probes for LDs

1.3.4 Red and near infrared lipid droplet probe

The main advantages of red fluorophores are: (1) low background signal from autofluorescence from biological samples, (2) effective excitation of dyes in thicker tissue samples, and (3) less light scattering.

Jun-Long Zhang designed a red-emitting lipid droplet probe LD-TPZn based on Zn (II) complex[52]. In DMSO, the absorption peaks of LD-TPZn are located at 390, 440 and 599 nm, the emission peaks are located at 637 nm, and the quantum yield is 0.44. Co-localization experiments with BODIPY 493/503 and intracellular lipid droplet-associated protein periliplin-1 confirmed that LD-TPZn has a good

targeting effect on intracellular lipid droplets. At 880 nm, LD-TPZn has a two-photon absorption cross section of 110 GM, which can be used for lipid droplet imaging of adipose tissue.

Recently, Nikhil R. Jana reported a fluorescent probe LQD based on quantum dots (Fig. 1.8), which can be selectively used for lipid droplet recognition[53]. The LQD is composed of a red-emitting CdSe quantum dot core and polyacrylate wrapped in a ZnS shell. LQD has a narrow emission peak at 600 nm in colloidal solution. As quantum dots, LQDs have a wide excitation window and can use blue lasers to image lipid droplets. LQD enters cells through endocytosis and has a good colocalization coefficient with Nile Red. Benzhong Tang's group explored the photo-activated lipid droplet probe PhotoAFN 2a-c[54]. In tetrahydrofuran solution, the emission spectrum range is 610 - 624 nm, and in solid state, the emission spectrum range is 571 - 620 nm.

As a TICT molecule, PhotoAFN 2a-c exhibits a significant solvent effect (blue shift with decreasing solvent polarity). In addition, the probe can distinguish lung cancer cells from normal lung cells. Subsequently, the subject was combined into the near-infrared AIE probe TPE-AC[55], which aggregates in water and exhibits near-infrared emission at 780 nm, with an absolute quantum yield of 5% in solid state. When staining lipid droplets in cells, TPE-AC has a good overlap with commercial dyes BODIPY 493/503. Compared with commercial dyes, this probe also has

better photostability. Similarly, the research group used triphenylamine as the core and redesigned the near-infrared luminescent materials TPMN, TTMN, MeTTMN and MeOTTMN (Figure 1.9)[56].

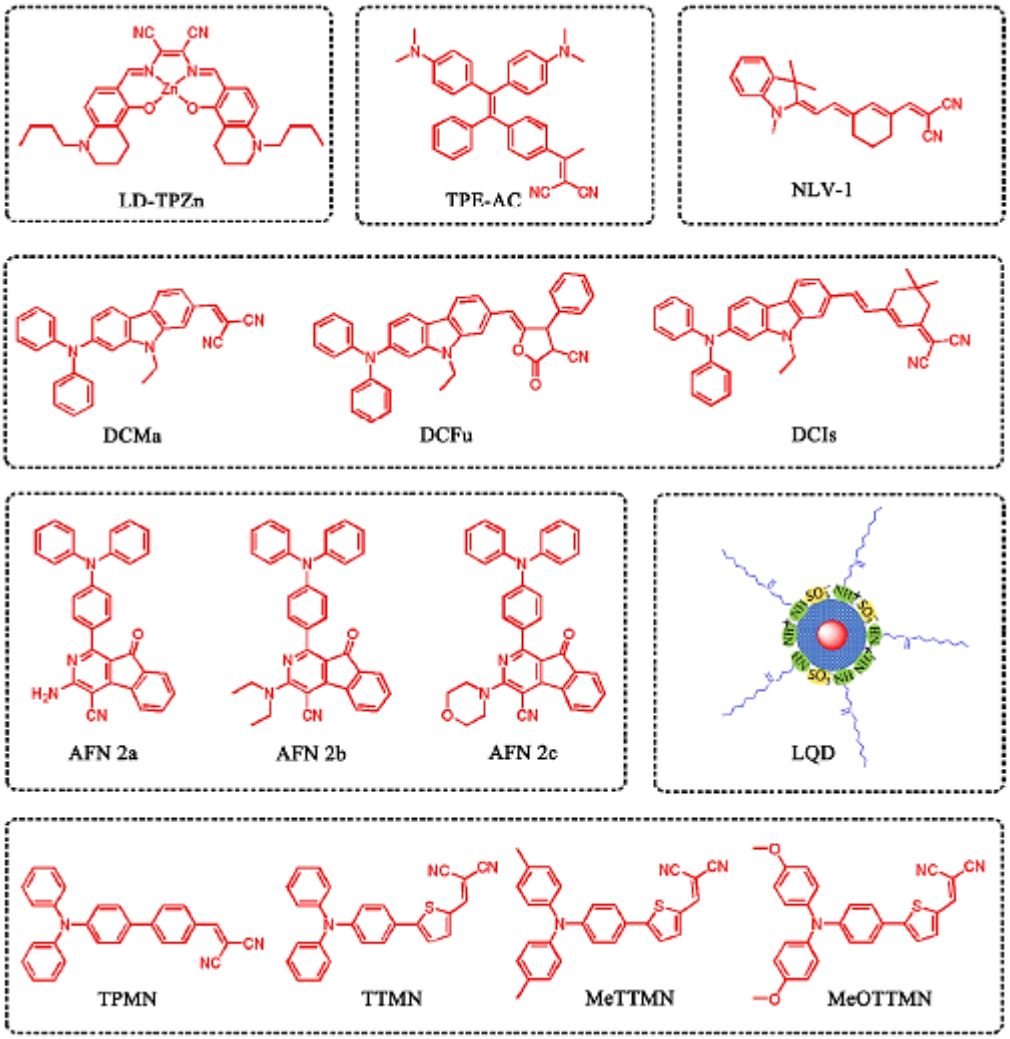

Figure. 1.9 Structures of red emitting probes for LDs

These AIEgens exhibit some interesting characteristics, such as: one-pot synthesis, larger Stokes shift, and higher quantum yield. Through co-localization experiments with commercial lipid droplet dye BODIPY 493/503, it was found that it has good targeting ability to lipid droplets. In

addition, this type of AIEgens has a good ability to generate active oxygen and has potential photodynamic applications. In addition, TPMN, TTMN and MeTTMN have good imaging effects in zebrafish embryos. Then synthesized the near-infrared AIE probes DCMa, DCIs and DCFu with push-pull electronic effects[57]. These luminescent molecules exhibit a strong solvent discoloration effect. In polar solvents, they do not emit light due to the TICT effect. In the aggregate state, their emission range is from 665 nm to 775 nm, and has a good co-localization effect with BODIPY 505/515.

Lin's research group developed the near-infrared probe NLV-1 (Fig. 1.9)[58]. NLV-1 is an anthocyanin composed of indole aniline and malononitrile. The probe emits strong light in high-viscosity media, but does not emit light in low-viscosity media due to the free rotation of molecules. Due to this characteristic, NLV-1 can detect viscosity changes in lipid droplets. The absorption peak of the probe in methanol is at 644 nm, the emission peak is at 704 nm, the absorption peak in glycerol is at 680 nm, and the emission peak is at 719 nm, and the fluorescence intensity is increased by 13.77 times. Although NLV-1 can target lipid droplets in cells, NLV-1 will only fluoresce when the lipid droplet environment viscosity increases after treatment with a viscosity modifier. This property is indeed useful for studying the viscosity changes of lipid droplets, but it is unrealistic to use NLV-1 as a lipid droplet label under

physiological conditions.

1.4 The research significance and work of this course

LDs are generally considered to be organelles with extremely low water content and high viscosity. It is closely related to human diseases such as obesity, diabetes, and cancer. Cancer cells are abnormal and the lipid droplets in the cell will increase. Therefore, we have developed four probes for detecting lipid droplets and used to identify the lipid droplets in cancer cells.

1. simple coumarin-substituted p-nitrostyrylacetonitrile as a potential new organic biological probe for imaging lipid droplets. In addition, the donor-acceptor structural framework separated by styrene bridges also produced a relatively significant Stokes shift. This sensitive probe shows advantageous advantages, including large Stokes shift (over 100 nm), good selectivity, low biological toxicity, and LDs specificity. In addition, the biological probe Cou-LDs can also mark the distribution of LDs in live zebrafish, which can be used for cancer imaging.

2. Two new probes, LDP-1 and LDP-2, were synthesized, which showed large Stokes shifts of 4758 cm-1 and 3986 cm-1, respectively. These two probes emit strongly in hydrophobic and high-viscosity environments. In addition, the biological probes LDP-1 and LDP-2 exhibit low biological toxicity and good selectivity. These two probes are

also suitable for selectively monitoring the distribution of LDs in live HeLa cells, successfully identifying lipid droplets in cancer cells.

3. We have developed a new type of fluorescent chemical sensor that can effectively label intracellular lipid droplets. Interestingly, due to the reasonable design of the molecular structure of the probe ATOP-LD, it also exhibits polarity-sensitive properties, and it has strong electron-donating and electron-withdrawing groups. In addition, the probe itself has excellent anti-interference, pH stability and low biological toxicity, and has been successfully applied to cell imaging and zebrafish imaging.

SECTION 2. A novel lipid droplets-specific fluorescence bio-probe with excellent photostability and large Stokes shift for imaging in living cells and zebrafish

2.1 Introduction

Lipid droplets (LDs) are highly dynamic spherical organelles with diameters ranging from 40 nm to 100μm, which can be found in most eukaryotic cells.[59]They mainly consist of a phospholipid monolayer and neutral lipids. [60] LDs are not only related to the storage of lipids, [61] but also play pivotal roles in energy homeostasis,[62]membrane trafficking, [63] protein storage, [64]and preventing lipo-toxicity and apoptosis. Moreover, the abnormity of LDs is strongly relative to various diseases, includingobesity,[65] neurodegeneration,[66] lipoatrophic diabetes, [67] atherosclerosis, and so on. More importantly,recent studies have shown that the number, size, andcomposition of LDs could be used as cancer markers. [68] Hence, monitoring LDs is highly important to understand the biological properties of lipid droplets, and early diagnosis of some diseases, which is beneficial for protecting people's health.

So far, many techniques have been reported for imaging LDs, including the immunohistochemistry of LD-associated membrane proteins [69],the Raman microscopy [70], the NMR spectrum [71], transmission electron microscopy (TEM) and the spectrally resolved

fluorescence lifetime measure-ments [72,73]. Compared with the above method, Fluorescence imaging has significant advantages like high sensitivity, high spatialresolution, easy operation, and low cost. [74,75] So far, a quite number of fluorescent probes have been reported for LDs-specific imaging. For example, BODIPY 493/503 [76] and Nile Red [77] are commonly used two commercial markers for LDs' detection that show some limitations such as short Stokes shift [78] and poor photostability [79], respectively. Specifically, LD-targeting fluorescent probes have been developed and demonstrated as effective tools for the visualization of the dynamic morphology of LDs and their related activities in real time in vitro. To date, both intramolecular charge transfer (ICT) and aggregation-induced emission (AIE) fluorescence mechanisms have been exploited to create LD probes[80-95]. In general, for ICT fluorescent probes, blue shifts in the fluorescence emission maxima and increases in fluorescence emission intensities are seen in non-polar environments. This promising attribute makes imaging agents based on ICT mechanisms significantly brighter when they are localized within the neutral lipid core of LDs, thus minimalizing interference from background fluorescence. Despite this recent recognition of the importance of LDsand the emerging correlations between LDs and metabolic diseasesand cancer, many fundamental questions still remain unanswered. Despite the progress made in understanding the role of LDs,

a number of fundamental questions remainunanswered. Therefore, it is of great significance to develop a lipid droplet-specific fluorescent biological probe based on the ICT mechanism with large Stokes shifts and good photostability.

In this report, we proposed a simple coumarin-substituted p-nitrostyrylacetonitrile as potential molecules Cou-LDsfor imaging lipid droplets. The fluorophore coumarin was widely used in the field of biological imaging due to the high fluorescence quantum yield and excellent photostability. And the presence of diethylamino electron donating groups helps in shiftingthe intramolecular charge transfer bands to the red-wavelength regions. Further, the donor acceptorstructural framework separated by the styryl bridge also yields a relatively significant Stokes shift. In addition, ICT-based platforms typically display good photostability, permitting both real-time tracking of LDs and their interactions with other organelles to be readily monitored.

2.2 Synthesis of probes

2.2.1 Reagent

Short name	Name	Supplier
DCM	Dichloromethane	Damao Chemical Reagent Factory

THF	Tetrahydrofuran	Damao Chemical Reagent Factory
EtOAC	ethyl acetate	Damao Chemical Reagent Factory
EtOH	Etanol	Damao Chemical Reagent Factory
CH_3CN	Acetonitrile	Damao Chemical Reagent Factory
DMSO	Dimethyl Sulfoxide	Damao Chemical Reagent Factory
DMF	N,N-DiMethylforMaMide	Damao Chemical Reagent Factory
Arg	L-Arginine	J&K Scientific
Cys	L-Cysteine	J&K Scientific
Ser	L-Serine	J&K Scientific
GSH	L-Glutathione	Energy Chemical
Pip	Piperidine	Energy Chemical

2.2.2 Materials

Unless other noted, all the solvents, reagents and materials were obtained from commercial companies and used without other purification. Twice-distilled water was applied to all measurements and experiments. NMR spectra were examined from AVANCE III 400 MHz Digital NMR Spectrometer with TMS as an internal standard; Electronic absorption spectra were recorded on a LabTech UV Power spectrometer; Fluorescence spectra were obtained with a HITACHI F4600 fluorescence spectrophotometer; The fluorescence images of cells were obtained with Nikon A1MP confocal microscopy with a CCD camera; The pH

measurements were implemented on a Mettler-Toledo Delta 320 pH meter; analysis was exhibited on silica gel plates and column chromatography was carried out over silica gel (mesh 200-300). Both TLC and silica gel were purchased from the Qingdao Ocean Chemicals.

2.2.3 Synthesis of probe Cou-LDs

Synthesis of compound 2

The mixture of diethyl malonate (1.60 g, 10 mmol), 4-(diethylamino)-2-hydroxybenzaldehyde (1.93 g, 10 mmol), anhydrous ethanol (15 mL) and piperidine (0.25 g, 3 mmol) was reacted at reflux under nitrogen for 6 h. After the reaction, the remaining solvent was removed by evaporation under reduced pressure. Then 30 mL of the mixed solution HCl/glacial acetic acid (1:1, v/v) was added to the reaction system at 120°C and the reaction was continued for 7 h. After the reaction, the resulting mixture was poured into 40 mL of deionized water and the pH was adjusted to neutral with 40 % sodium hydroxide solution and a dark brown precipitate was produced. The precipitate was filtered and washed several times with water and ethanol to obtain the target product (1.98 g, 91 %). 1H NMR (400 MHz, CDCl3) δ 7.54 (d, J = 9.3 Hz, 1H), 7.24 (d, J = 8.8 Hz, 1H), 6.56 (d, J = 8.8 Hz, 1H), 6.46 (s, 1H), 6.02 (d, J = 9.3 Hz, 1H), 3.40 (q, J = 7.2 Hz, 4H), 1.20 (t, J = 7.2 Hz, 6H).

Synthesis of compound 3

DMF (1 mL) was added to the dry eggplant bottle after three cycles of vacuum and nitrogen filling, POCl3 (1.61 g, 10.5 mmol) dissolved in DMF (1 mL) was slowly added to the eggplant bottle with a syringe and stirred for 45 min at 50 °C. Compound 2 (0.76 g, 3.5 mmol) was dissolved in DMF (5 mL) and added to the above mixed system and stirred for 2 h at 60 °C. After the reaction, the mixture was slowly poured into 100 mL of ice water and the pH was adjusted to neutral with 20% NaOH. The precipitate was filtered and washed several times with deionized water and anhydrous ethanol to obtain a yellow solid powder with the yield of 81 %. 1H NMR (400 MHz, CDCl3) δ 10.13 (s, 1H), 8.26 (s, 1H), 7.43 (d, J = 9.0 Hz, 1H), 6.68 (dd, J = 9.0, 2.6 Hz, 1H), 6.53 (d, J = 2.7 Hz, 1H), 3.48 (q, J = 7.1 Hz, 4H), 1.26 (t, J = 7.2 Hz, 6H).

Systhesis of Probe Cou-LDs

Compound 3 (0.20 mmol, 49.1mg), piperidine (5.0 mg, 0.06 mmol), and p-nitrobenzene acetonitrile (0.20 mmol, 32.4mg) were dissolved in ethanol (2.0 mL) into a 10 mL reaction tube in turn and stirred at 25°C for 24 hours. The crude product was purified by column chromatography (petroleum ether: ethyl acetate = 5:1) to obtain Cou-LDs of the product (83 % yield, orange red solid, 57.4 mg).1H NMR (400 MHz, CDCl3) δ 8.82 (1 H, s), 8.28 (2 H, d, J = 8.1), 8.06 (1 H, s), 7.84 (2 H, d, J = 8.2), 7.44 (1 H, d, J = 8.8), 6.66 (1 H, d, J = 8.3), 6.48 (1 H, d, J = 19.2), 3.49 (4 H, d, J = 6.8), 1.27 (6 H, t, J = 6.5).

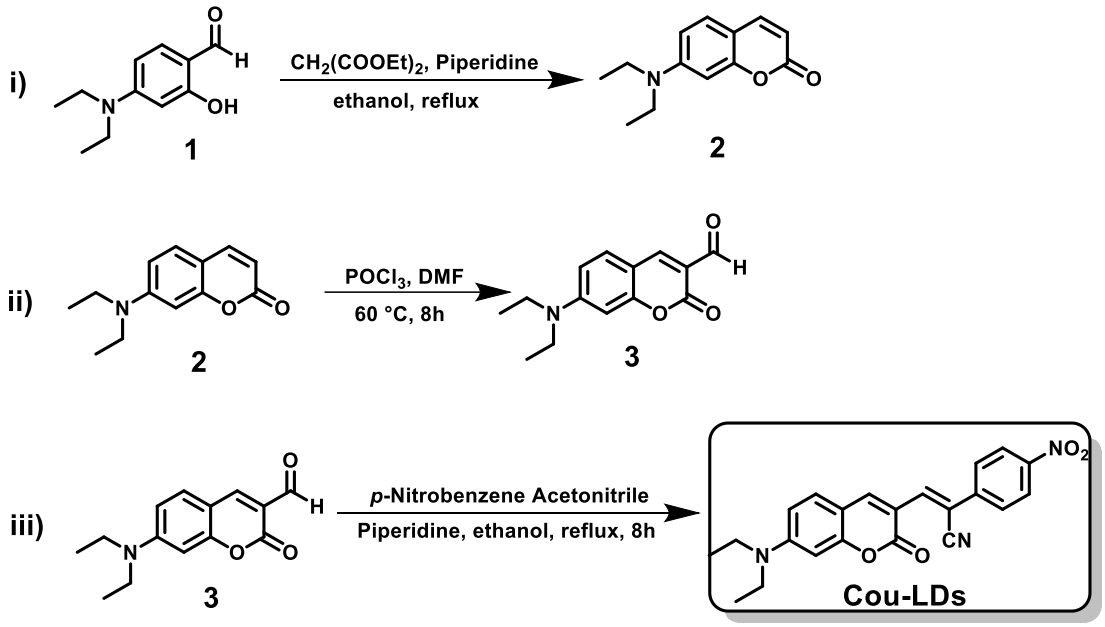

Scheme 2.1. Synthesis of probe **Cou-LDs**.

2.2.4 Probe design

As a donor (D)-π-acceptor (A) organic molecule, probe Cou-LDs with diethyldiamino as a strong electron-donating group was designed for argeting LDs. The presence of diethylamino electron donating groups helps in shiftingthe intramolecular charge transfer bands to the red-wavelength regions. Further, the donor acceptorstructural framework separated by the styryl bridge also yields a relatively significantStokes shift. Aditionally, due to the ICT effect, designed probe Cou-LDs exhibited strong fluorescent intensity with hydrophobic nature for monitoring LDs.

2.3 Result and Discussion

2.3.1 General procedure for analysis

Parent stock solution of the fluorescent probe **Cou-LDs** (1.0 mM) wasprepared in absolute DMSO 20.0 μL of stock solution was transferred into atest tube, and then diluted to 2.0 mL with the mixture of organic solvent. All spectra were obtained in a quartzcuvette (path length = 1 cm). The solutions of Na^{+}, Zn^{2+}, Al^{3+}, and Ca^{2+}were prepared from their chloride salts. Hypochlorous acid (HClO) and Hydrogen peroxide (H_2O_2) was provided from its commercially available 30% aqueous solution to afford the desired concentration.Cysteine (Cys) and glutathione (GSH) were prepared by dissolving thecorresponding solid in ultrapure water. PBS solution was prepared with$Na_2HPO_4$and KH_2PO_4, and adjusted to pH 7.4.

2.3.2 Cell culture and cytotoxicity assays

HeLa cells were provided by Jiangsu Kaiji Biotechnology Co., Ltd. The living HeLa cells were cultured in the Dulbecco's modified Eagle's medium (DMEM) supplemented with fetal bovine serum (10% FBS) under the atmosphere containing 5% CO2 and 95% air at 37 °C. The cytotoxic effects of the probe (Cou-LDs) were tested by the MTT assay. The living cells line were treated in DMEM (Dulbecco's Modified Eagle

Medium) supplied with fetal bovine serum (10%, FBS), penicillin (100 U/mL) and streptomycin (100 μg/mL) under the atmosphere of CO2 (5%) and air (95%) at 37 °C. The HeLa cells were then seeded into 96-well plates, and 0, 5, 10, 20, 30, 40 μM (final concentration) of the probe (Cou-LDs) (99.9% DMEM and 0.1% DMSO) were added respectively. Subsequently, the cells were cultured at 37 °C in an atmosphere of CO2 (5%) and air (95%) for 24 hours. Then the HeLa cells were washed with PBS buffer, and DMEM medium (500 μL) was added. Next, MTT (50 μL, 5 mg/mL) was injected to every well and incubated for 4 h. Violet formazan was treated with sodium dodecyl sulfate solution (500 μL) in the H2O-DMF mixture. Absorbance of the solution was measured at 570 nm by the way of a microplate reader. The cell viability was determined by assuming 100% cell viability for cells without Cou-LDs.

2.3.3 Imaging of Lipid droplets in HeLa cells

HeLa cells were grown in modified Eagle's medium (MEM) replenished with 10% FBS with the atmosphere of 5% CO2 and 95% air at 37 °C for 24 h. For fluorescence imaging experiments, the cells were divided into two samples; one was incubated with the probe Cou-LDs (10 μM) and BODIPY493/503 (10 μM) for 30 min. All HeLa cells were washed three times with PBS buffer after incubation. The experiments of cell imaging were acquired with a Nikon A1MP confocal microscopy

with the equipment of a CCD camera. Cell images were collected from green and red channel.

2.3.4 Photophysical properties of the probe in different solvents

The absorption and emission spectra of probe Cou-LDs in different solvents including ethyl acetate (EtOAc), acetone, tetrahydrofuran (THF), PBS buffers (pH = 7.4), ethanol (EtOH), d imethyl sulfoxide (DMSO), N,N-dimethylformamide (DMF), methanol (CH3OH), acetonitrile (CH3CN), were depicted in Fig. 2.1. The absorption spectra of probe Cou-LDs exhibited a small shift in organic solvents around at 500 nm with almost same absorption intensity (Fig. 1a)). On the contrary, Cou-LDs exhibited the large emission shift of around 45 nm from THF to DMSO (Fig. 1b)). Simultaneously, the emission spectra of probe Cou-LDs showed an increasing fluorescence intensity in liposoluble solvents especially in EtOAc and THF. there is largest decrease amolst 34-fold in the emission intensity by increasing the solvent polarity (Fig. 2.1b)). The resluts indicated that the photophysical properties of Cou-LDs are related to the solvent polarity so the probe Cou-LDs could be applied for monitoring LDs in living cells.

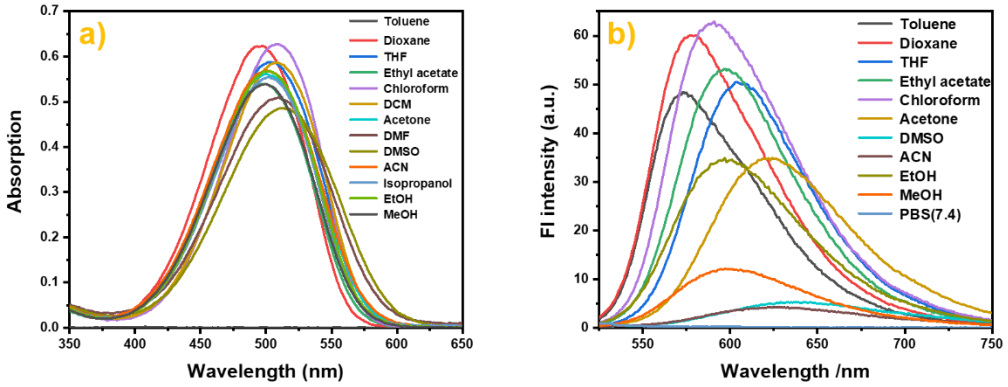

Figure 2.1. The absorbance and fluorescence spectra of probe **Cou-LDs** (10 μM) in different solvents.

2.3.5 Fluorescence spectra of probe Cou-LDs in different ratio of EtOAc and MeOH

In order to verify the solvent effect on optical properties of probe Cou-LDs, different concentration of EtOAc in MeOH were applied for this research, which were depicted in Fig. 2.2. The result showed that when the concentration of EtOAc increased from 0 to 100%, the fluorescence intensity was increased almost 11-fold exhibiting a slight blue shift from 620 nm to 600 nm with large Stokes shift (100 nm) using the excitation wavelength at 500 nm. The phenomenon of obvious emission enhancement indicated that probe Cou-LDs was suitable for detecting LDs.

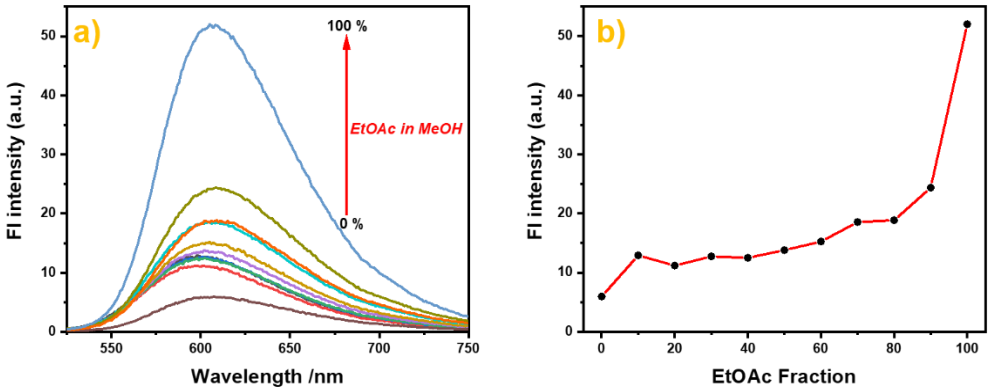

Figure 2.2. The fluorescence spectra of probe **Cou-LDs** (10 μM) in different ratios of EtOAc/MeOH.

2.3.6 Fluorescence spectra of probe Cou-LDs response to viscosity

Viscosity is an important physicochemical parameterand many physiological diseases are related to the alterationof the viscosity in the local environment, such as hypercholesterolemia, atherosclerosis, cell malignancy and diabetes.To confirm the fluorescence response of probe Cou-LDs could response to the viscosity, the fluorescence spectra of probe Cou-LDs were examined in a methanol−glycerol system. As the viscosity increased from 1.53 cp (100% methanol) to 614 cp (100% glycerol), the fluorescence intensity at 600 nm of probe Cou-LDs increased dramaticly (Fig. 2.3). The results indicate that the probe Cou-LDs also could to monitor viscosity.

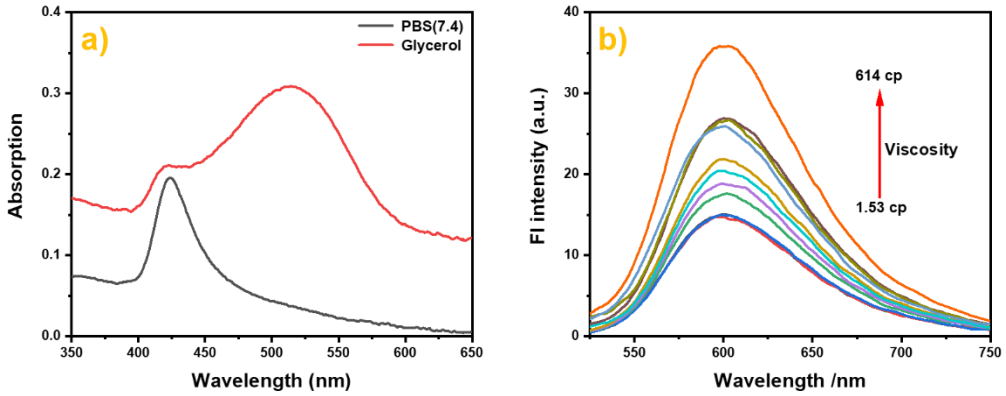

Figure 2.3. The fluorescence spectra of probe Cou-LDs (10 μM) in different ratios of Methanol /Glycerol.

2.3.7 The selectivity of probe Cou-LDs

Other than complex pH environment, intracellular microenvironments also contain numerous biologically relevant cations, anions, reactive sulfur species (RSS) and reactive oxygen species (ROS), which could affect the performance of fluorescent probe. As showed in Figure 4, the fluorescence intensity at 600 nm of the probe Cou-LDs (10 μM) has no obvious change when the system was added different interfering species, which indicate the anti-interference performance of the probe Cou-LDs is excellent. These above results demonstrate that the probe Cou-LDs is stable in complex physiological environments and which is benifical for cell imgaging.

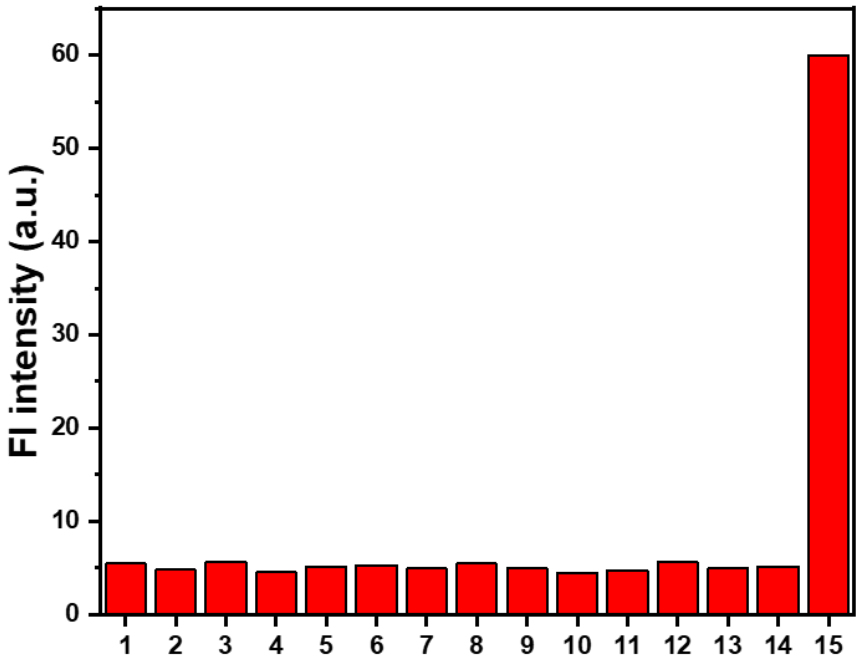

Figure 2.4. The fluorescence spectra of probe Cou-LDs (10 μM) in PBS solution in the presence ofdifferent interfering species (500 μM) (1: blank; 2: TBHP; 3: Na^{+}; 4: Cl^{-}; 5: HCO_3^{-}; 6: Cys; 7: GSH; 8: HSO_3^{-}; 9: ClO^{-}; 10: NO^{2-}; 11: CO_3^{2-};12: SO_4^{2-}; 13: H_2O_2; 14: Ca^{2+};15: Toluene)

2.3.8 The MTT and co-localization fluorescence imaging in HeLa cells of probe Cou-LDs

The first step for cell imaging with probe Cou-LDs was verify the biological toxicity. The MTT assay was establised for the cytotoxicity test in living HeLa cells. The test indicated that the survial rate of HeLa cells incubated with probe Cou-LDs for 24 h was more than 90% exhibiting low biological toxicity, which showed that probe Cou-LDs could be an practical tool for LDs marking under complex biological environment.

Subsequently, the co-localization fluorescence imaging of probe Cou-LDs was completed in living HeLa cells compared with the commercial organic dye BODIPY493/503 due to their different emission wavelength. We found that green fluorescence imaging was conducted by probe Cou-LDs (Fig. 2.5)). The merged imaging was also shown in Fig. 2.5). Moreover, the parameters of co-localization imag was obviouly depcited indicating that the red and green channel was overlapped largely with pearson correlation coefficient up to 0.91. All the excellent results indicate that this novel probe Cou-LDs can be used for LDs marker in living biosamples specificaly.

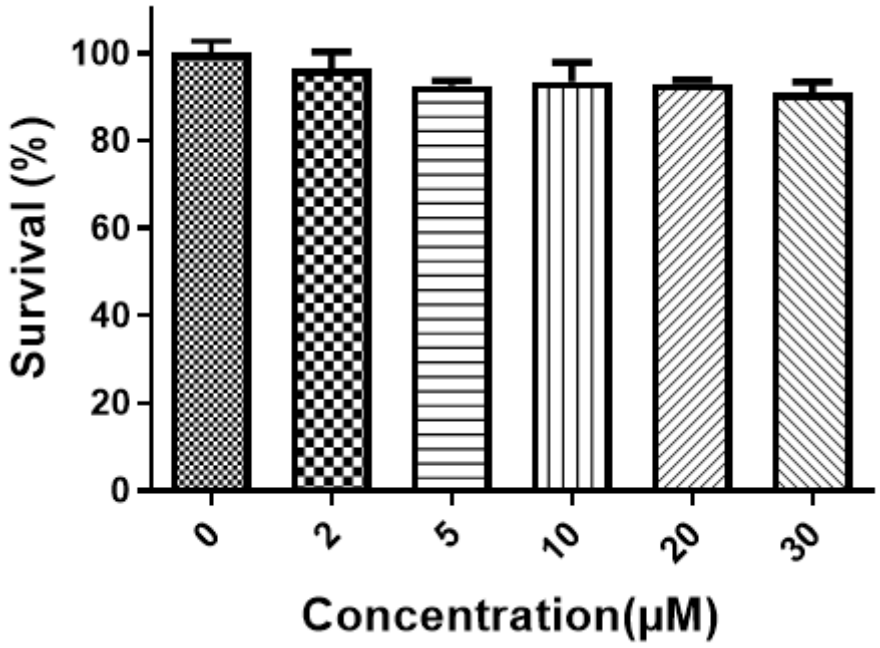

Figure 2.5. Cytotoxicity assays of probe Cou-LDs at different concentrations (0 μM; 2μM; 5 μM; 10 μM; 20 μM; 30 μM) for HeLa cells

2.4 Conclusion

In summary, a novel organic bio-probe Cou-LDs was designed and constructed for LDs cell imaging with much more hydrophobic and viscous environment compared to cytosol. The presence of diethylamino electron donating groups helps in shiftingthe intramolecular charge transfer bands to the red-wavelength regions. Further, the donor acceptorstructural framework separated by the styryl bridge also yields a relatively significantStokes shift. This ideal probe exhibited favorable merits including large Stokes shift (over 100 nm), good selectivity, low biological toxicity, and LDs-specificity. Furthermore, the bio-probe Cou-LDs could also marking LDs distribution in living zebrafish, which may be suitable for studying some physiological processes. Further applications of this bio-probe for the investigation of the physiological processes are under progress.

SECTION 3. Two reasonably designed polarity-viscosity sensitive fluorescent probes with large Stokes shift for lighting up lipid droplets in cells

3.1 Introduction

Lipid droplets (LDs) are dynamic organelles in cells existing in almost all organisms [96-97]. The interior of LDsare mainly composed ofhydrophobic lipids [98]. LDs play a very important role in biological activity, which can maintain some basic cell activity balance including cell energy balance and metabolic balance. LDs can be used for assisting intracellular protein transport and maturation [99]. Therefore, abnormal concentration of LDs are often associated with a series of diseases [100]. When the concentration of LDs in neurons or glial cells increased, it was usually accompanied by the problem of neurodegeneration.[101-102]In addition, researchers found that abnormal metabolism of LDs were often closely related to cancer, diabetes, obesity, virus proliferation and other diseases[103-105]. Therefore, it is very necessary to study LDs in cells.

LDs are usually in the range of half a micron to tens of microns in size, so they can be easily detected by TEM. But the dynamic changes of LDs in living cells can not be observed.[106] Fluorescence imaging technology provides an ideal solution for studying the activity of LDs. Since Fowler and co-workers first reported Nile Red,12 many probes

have appeared to detect LDs in living cells.[107-113] However, the present fluorescent probes still have some shortcomings, such as too complicated synthesis route, short emission wavelengths, background interference etc.[114-115] The background interference of probe in biological imaging is mainly caused by small Stokes shift.[116] Most of the known probes are visible light emitting fluorescent probes, but some natural biomolecules can produce autofluorescence below 630 nm. In order to avoid background interference, it is necessary to develop LDs probes with emission wavelength exceeding 630 nm.[117] In addition, LDs exist in hydrophobic and high viscosity environments, so as long as the probe exhibits the characteristics for distinguishing the two characteristics, which could be used as an LDs probe.[118-119] Therefore, it is very meaningful for developing a probe exhibiting large stokes shift to sense LDs.

In this chapter, two novel bio-probes (LDP-1 and LDP-2) ere synthesized by simple methods. The two probes couldsense the hydrophobic and high viscosity environment at the same time. The experimental results showed that LDP-1 and LDP-2 exhibited significant polarity sensitivity and strong emission at high viscosity.[120-125] The two probes also exhibited large Stokes shifts of 4758 cm–1 and 3986 cm–1 respectively, excellent selectivity, and low biological toxicity. Furthermore, the Pearson's correlation were as high as 0.97 and 0.89 by

co-localization experiments, which indicated that the two probes could also selectively sense LDs in HeLa cells.

3.2 Synthesis of probes

3.2.1 Reagent

Short name	Name	Supplier
DCM	Dichloromethane	Damao Chemical Reagent Factory
THF	Tetrahydrofuran	Damao Chemical Reagent Factory
EtOAC	ethyl acetate	Damao Chemical Reagent Factory
EtOH	Etanol	Damao Chemical Reagent Factory
CH_3CN	Acetonitrile	Damao Chemical Reagent Factory
DMSO	Dimethyl Sulfoxide	Damao Chemical Reagent Factory
DMF	N,N-DiMethylforMaMide	Damao Chemical Reagent Factory
Arg	L-Arginine	J&K Scientific
Cys	L-Cysteine	J&K Scientific
Ser	L-Serine	J&K Scientific
GSH	L-Glutathione	Energy Chemical
Pip	Piperidine	Energy Chemical

3.2.2 Materials

The ^{1}H NMR and ^{13}C NMR spectrums were obtained from INOVA-400 MHz nuclear magnetic resonance instruments, respectively.High-resolution electrospray mass spectra (HRMS) were obtained from Bruker APEX IV-FTMS 7.0T mass spectrometer. All the UV–vis absorption spectra and emission spectra were obtained from Shimadzu UV-1800 spectrometer and Shimadzu RF-5301PC spectroscope respectively. The fluorescence images of cells were obtained with Nikon A1MP confocal microscopy with a CCD camera, Both TLC and silica gel were purchased from the Qingdao Ocean Chemicals.

3.2.3 Synthesis of probes

Synthesis of probe (E)-2-(3-(2-(7-(diethylamino)-2-oxo-2H-chromen-3-yl)vinyl)-5,5-dimethylcyclohex-2-en-1-ylidene)malononitrile (LDP-1)

As described in Scheme 2, LDP-1 was synthesized in a simple way. According to the existing literature, compound 1 was synthesized.[126] The compound 1 (490.3 mg, 2.00 mmol) was dissolved in acetonitrile (10 ml). The compound 2 (391.2 mg, 2.10 mmol) and piperidine (20 □L, 0.20 mmol) was added to acetonitrile. After were refluxed at 115 ℃ for 8 h, the solution were filtered. Probe LDP-1 (708.0 mg) was obtained in yield of 86 %. 1H NMR (400 MHz, CDCl3) δ 7.79 (s, 1H), 7.32 (d, J = 8.9 Hz,

1H), 7.26 (s, 1H), 7.22 (s, 1H), 7.12 (d, J = 16.1 Hz, 1H), 6.83 (s, 1H), 6.70 – 6.58 (m, 1H), 6.51 (s, 1H), 3.45 (q, J = 7.0 Hz, 4H), 2.58 (s, 2H), 2.46 (s, 2H), 1.24 (t, J = 7.1 Hz, 7H), 1.06 (s, 6H). 13C NMR (100 MHz, CDCl3): δ 168.9, 160.9, 156.7, 154.2, 151.7, 140.5, 131.6, 129.8, 129.4, 123.3, 115.8, 113.8, 112.9, 109.7, 109.1, 97.2, 45.1, 42.9, 39.1, 31.9, 27.9, 12.3; HRMS (ESI): calcd for C26H27N3O2 [M+H]+ 414.2170, found 414.2176 (Fig.S1, S2, S3).

Synthesis of probe (E)-2-(3-(4-(diethylamino)styryl)-5,5-dimethylcyclohex-2-en-1-ylidene)malononitrile (LDP-2)

As described in Scheme 2, LDP-2was synthesized in a simple way. Thecompound 3 (177.3 mg, 1.00 mmol) was dissolved in acetonitrile(5 mL). The compound 2 (195.6 mg, 1.05 mmol) and piperidine (10 mL, 0.10 mmol) were added. Reflux at 40 ℃ for 8 h under N2 protection. After the reaction completed, decompression concentration. The crude product were purified by column chromatography on silica gel (EtOAC/PE, 1/2) to afford probe LDP-2 (250.0 mg) in yield of 73 %. 1H NMR (400 MHz, CDCl3) δ 7.79 (s, 1H), 7.32 (d, J = 8.9 Hz, 1H), 7.22 (s, 1H), 7.12 (d, J = 16.1 Hz, 1H), 6.83 (s, 1H), 6.70–6.58 (m, 1H), 6.51 (s, 1H), 3.45 (q, J = 7.0 Hz, 4H), 2.58 (s, 2H), 2.46 (s, 2H), 1.24 (t, J = 7.1 Hz, 7H), 1.06 (s, 6H). 13C NMR (100 MHz, CDCl3): δ 169.2, 155.5, 149.2, 138.4, 129.8, 123.7, 122.8, 121.1, 114.4, 113.6, 111.5, 44.5, 43.0, 39.2, 31.9, 28.0, 12.7; HRMS (ESI): calcd for C23H27N3 [M+H]+

346.2271, found 346.2278 (Fig.S4, S5, S6).

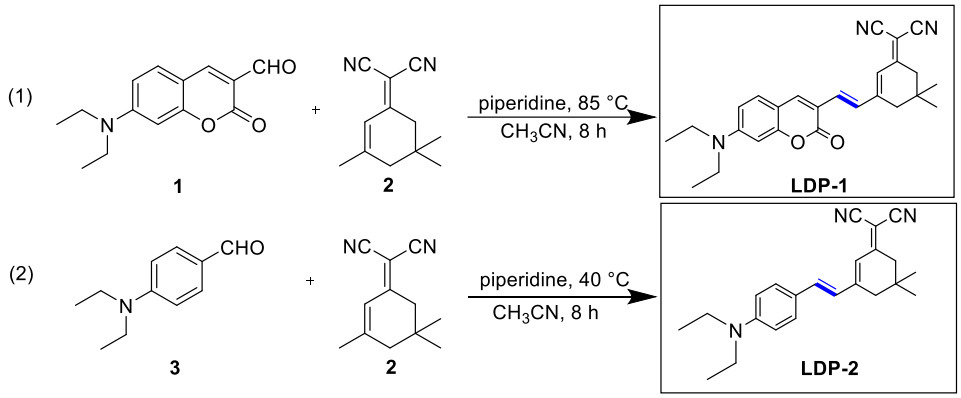

Scheme 3.1. Synthesis of **LDP-1** and**LDP-2**

3.2.4 Probe design

As described above, LDs are accompanied by a unique environment, namely high viscosity and nonpolarity. On this basis, two fluorescent probes with D-π-A structure were designed and constructed.In order for the probe to better respond to polarity and viscosity. The group of N,N-diethyl as strong electron donor and dicyanomethyl isophorone as strong electron acceptor were used for construction of probes **LDP-1** and **LDP-2** [127-128]. Fluorescent probes based on intramolecular charge transfer (ICT) mechanism were widely used as detection mechanism. ICT effect refers to the process in which molecules with push-pull electronic structure undergo intramolecular charge transfer in excited state, which leads to the separation of positive and negative charges in molecules. Due to that characteristic of ICT, the probe would show strong emission behavior sensitive to polarity (red shift or blue shift) [129]. In addition, the rotation behavior around the

double C=C bond will hinder the fluorescence emission of the probe[130-131]. The emission of the probe in a high viscosity environment was stronger than that in a low viscosity.

3.3 Result and Discussion

3.3.1 General procedure for analysis

Parent stock solution of the fluorescent probe LDP-1 and LDP-2 (1.0 mM) wasprepared in absolute DMSO 20.0 μL of stock solution was transferred into atest tube, and then diluted to 2.0 mL with the mixture of organic solvent. All spectra were obtained in a quartzcuvette (path length = 1 cm).

The solutions of K+, Zn2+, Al3+, Cu2+, Fe3+andwere prepared from their chloride salts. Hydrogen peroxide (H2O2) was provided from its commercially available 30% aqueous solution to afford the desired concentration.Cysteine (Cys) and glutathione (GSH) and L-Serine (Ser) and L-Arginine (Arg) were prepared by dissolving thecorresponding solid in ultrapure water. PBS solution was prepared withNa2HPO4and KH2PO4, and adjusted to pH 7.4.

3.3.2 Cell culture and cytotoxicity assays

Hela cells were provided by Jiangsu Kaiji Biotechnology Co., Ltd. The living HeLa cells were cultured in the Dulbecco's modified Eagle's medium (DMEM) supplemented with fetal bovine serum (10%

FBS) under the atmosphere containing 5% CO2 and 95% air at 37 °C. The cytotoxic effects of the probe (LDP-1 and LDP-2) were tested by the MTT assay. The living cells line were treated in DMEM (Dulbecco's Modified Eagle Medium) supplied with fetal bovine serum (10%, FBS), penicillin (100 U/mL) and streptomycin (100 μg/mL) under the atmosphere of CO2 (5%) and air (95%) at 37 °C. The HeLa cells were then seeded into 96-well plates, and 0, 5, 10, 20, 30, 40 μM (final concentration) of the probe (LDP-1 and LDP-2) (99.9% DMEM and 0.1% DMSO) were added respectively. Subsequently, the cells were cultured at 37 °C in an atmosphere of CO2 (5%) and air (95%) for 24 hours. Then the HeLa cells were washed with PBS buffer, and DMEM medium (500 μL) was added. Next, MTT (50 μL, 5 mg/mL) was injected to every well and incubated for 4 h. Violet formazan was treated with sodium dodecyl sulfate solution (500 μL) in the H2O-DMF mixture. Absorbance of the solution was measured at 570 nm by the way of a microplate reader. The cell viability was determined by assuming 100% cell viability for cells without LDP-1 or LDP-2.

3.3.3 Imaging of lipid droplets in HeLa cells

HeLa cells were grown in modified Eagle's medium (MEM) replenished with 10% FBS with the atmosphere of 5% CO2 and 95% air at 37 °C for 24 h. For fluorescence imaging experiments, the cells

were divided into two samples; one was incubated with the LDP probe (10 μM) and BODIPY493/503 (10 μM) for 30 min. All HeLa cells were washed three times with PBS buffer after incubation. The experiments of cell imaging were acquired with a Nikon A1MP confocal microscopy with the equipment of a CCD camera. Cell images were collected from green and red channel.

3.3.4 Photophysical properties of the probe in different solvents

Transfer 20.0 μL of the stock solution to a test tube, and then dilute it to 2.0 mL with organic solvent mixture. As shown in the Figure3.1, we tested the absorption and emission of the probe in a series of different solvents. The absorption of the two probes in different solvents did not change much, but the maximum emission wavelength were obviously red shifted. The maximum emission wavelength of probe LDP-1 in Dioxanewas 625 nm, while the maximum emission wavelength in DMSO was redshifted to 710 nm. The same is true. The maximum emission wavelength of probe LDP-2 in Dioxanewas 615 nm, while the maximum emission wavelength in DMSO was redshifted to 695 nm. The maximum emission wavelengths of LDP-1 and LDP-2 showed red shifts of 85 nm and 80 nm with the increase of polarity. In addition, from the photos taken, we could clearly observe the discoloration behavior of solvents

(Fig.3.1). With the increase of the polarity of the solvent, the color of the two probes gradually turns red.

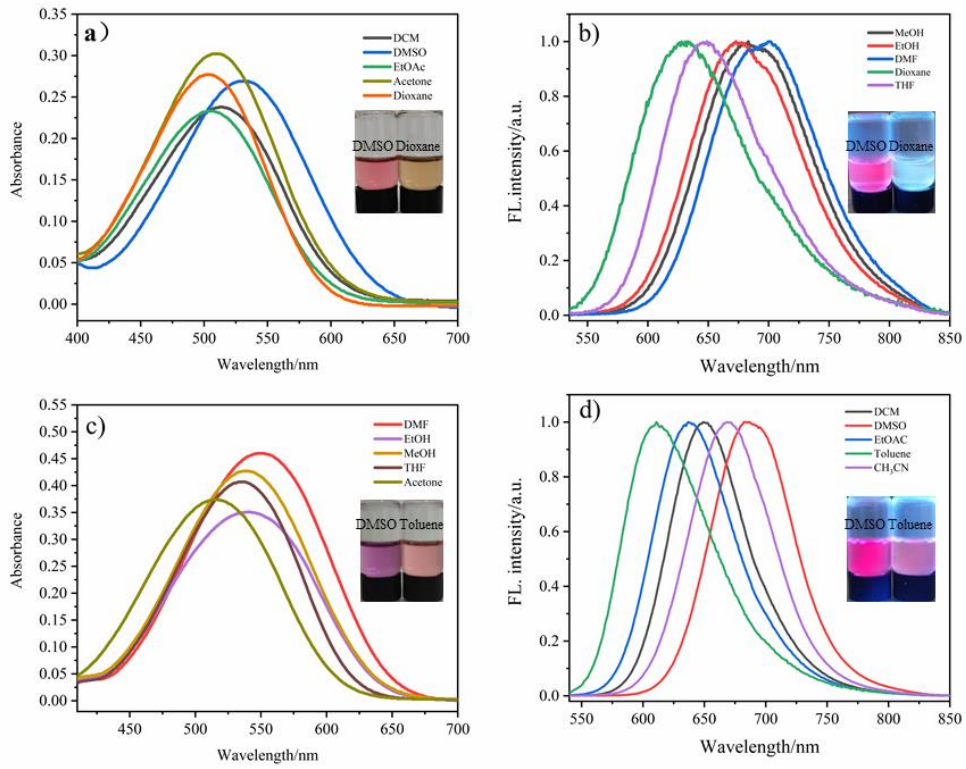

Figure 3.1. (a) Absorption and (b) fluorescence spectra of LDP-1 (10 μM, λex =520nm). (c) Absorption and (d) fluorescence spectra of LDP-2 (10 μM, λex= 530nm) in various solvents

The maximum absorption wavelength of LDP-1 in acetonitrile is 520 nm and the maximum emission wavelength is 691 nm. The maximum absorption wavelength of LDP-2 in acetonitrile is 533 nm and the maximum emission wavelength is 672 nm. According to the experiment results, we found that LDP-1 and LDP-2 all exhitbited large Stoke shifts (170 nm and 140 nm) (Table 3.1, Table 3.2, Fig.3.1). Then, we associated the maximum emission wavelength with the ET(30) value of the solvent to obtain the relationship between them.

ET(30) is a solvent polarity parameter representing solute-solvent interactions at the microscopic level.[132-135]Generally, the greater the polarity of solvent, the greater the ET (30) value.On the whole, with the increase of ET(30), the maximum emission wavelengths of both probes tended to increase.(Fig.3.2). This indicated that the effectof red shift with the increase of solvent polarity was showed. To further verify that the probes were sensitive to the polarity, we related the emission behavior of the probes to the dielectric constant of the solvents. (Fig. 3.3). Generally speaking, the dielectric constant increases as the polarity increases. The maximum emission wavelength was directly proportional to the dielectric constant of the solvents ($R2 > 0.95$). The above results showed that LDP-1 and LDP-2 were sensitive to polarity.

Finally, we calculated the HOMO and LUMO distributions of probes (calculated by Gaussian '09) (Figure3.4). According to the calculation results, the HOMO was localized in the N,N-diethyl group and coumarin or benzene ring spacer, the LUMO was localized to the dicyanomethylideneisophorone group. The HOMO and LUMO energy gaps of the two probes were 2.7 eV (LDP-2) and 2.5 eV (LDP-1). This proves the characteristics of intramolecular charge transfer (ICT) of probes LDP-1 and LDP-2.

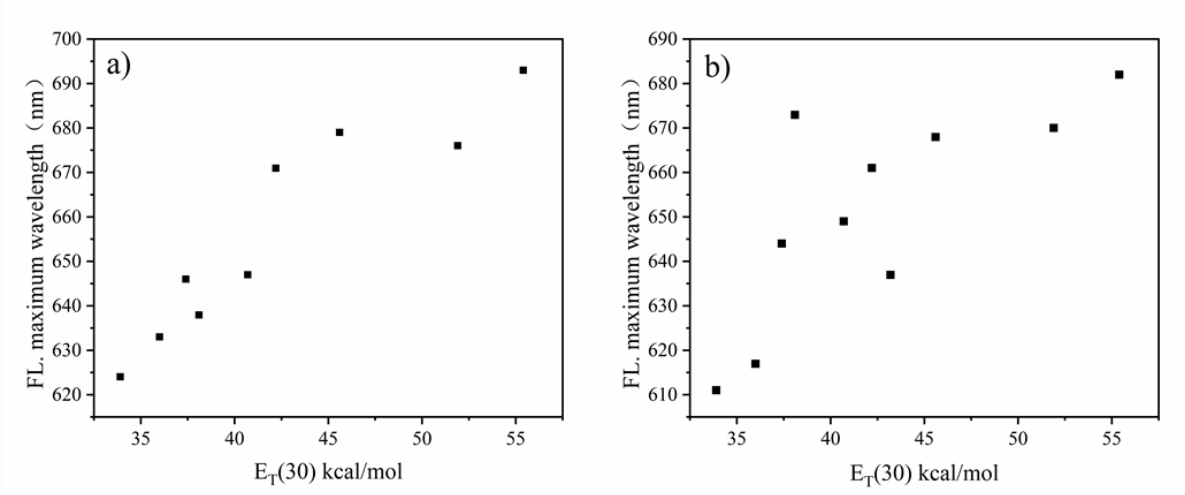

Figure3.2. Plot of the maximum emission wavelength of (a).LDP-1and (b).LDP-2 depending on the $E_T(30)$.

Table 3.1. Photophysical properties of theprobe**LDP-1** in different solvents.

LDP-1	Dioxane	Toluene	THF	DCM	Acetone	EtOH	CH_3CN	DMSO
λ_{em} (nm)	634	632	642	647	669	677	691	708
λ_{abs} (nm)	503	510	514	513	509	508	520	531
$E_T(30)^a$	36	33.9	37.4	40.7	42.2	51.9	45.6	45.1
Dielectric constant (ε)^b	2.25	2.38	7.58	8.93	20.7	24.8	37.5	46.7
Stokes shift	131	122	128	134	160	169	171	177

[a]$E_T(30)$ of each solvent was collected from the reference.[136][b]The data was collected from the reference.[137]

Table 3.2. Photophysical properties of theprobe**LDP-2** in different solvents.

LDP-2	Dioxane	Toluene	THF	DCM	Acetone	EtOH	CH_3CN	DMSO
λ_{em} (nm)	621	623	632	638	653	660	672	687
λ_{abs} (nm)	522	510	537	522	516	542	533	563
$E_T(30)^a$	36	33.9	37.4	40.7	42.2	51.9	45.6	45.1
Dielectric constant (ε)^b	2.25	2.38	7.58	8.93	20.7	24.8	37.5	46.7
Stokes shift	99	113	95	116	137	118	139	124

[a]$E_T(30)$ of each solvent was collected from the reference.[136][b]The data was collected from the reference.[137]

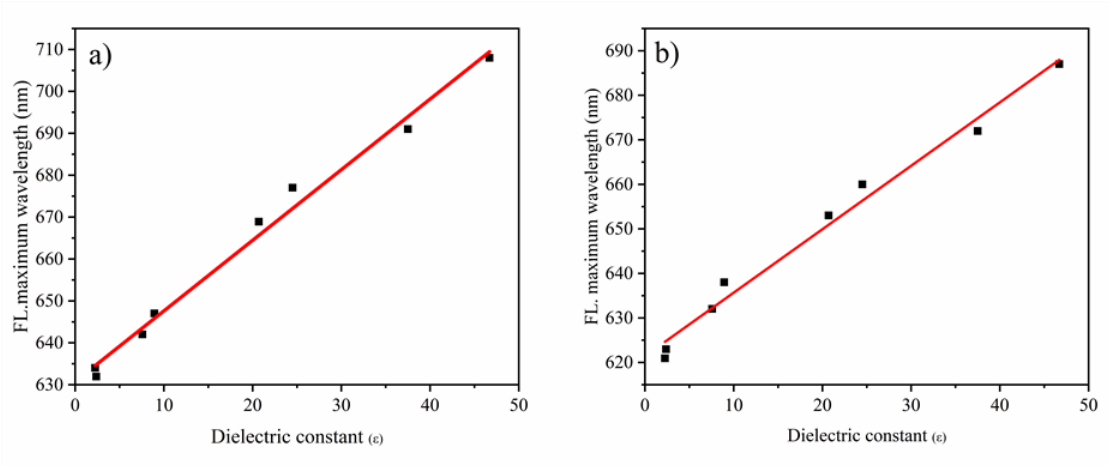

Figure 3.3.Plot of the maximum emission wavelength of (a).LDP-1 and(b).LDP-2 depending on the dielectric constant (ε) of the solvents.

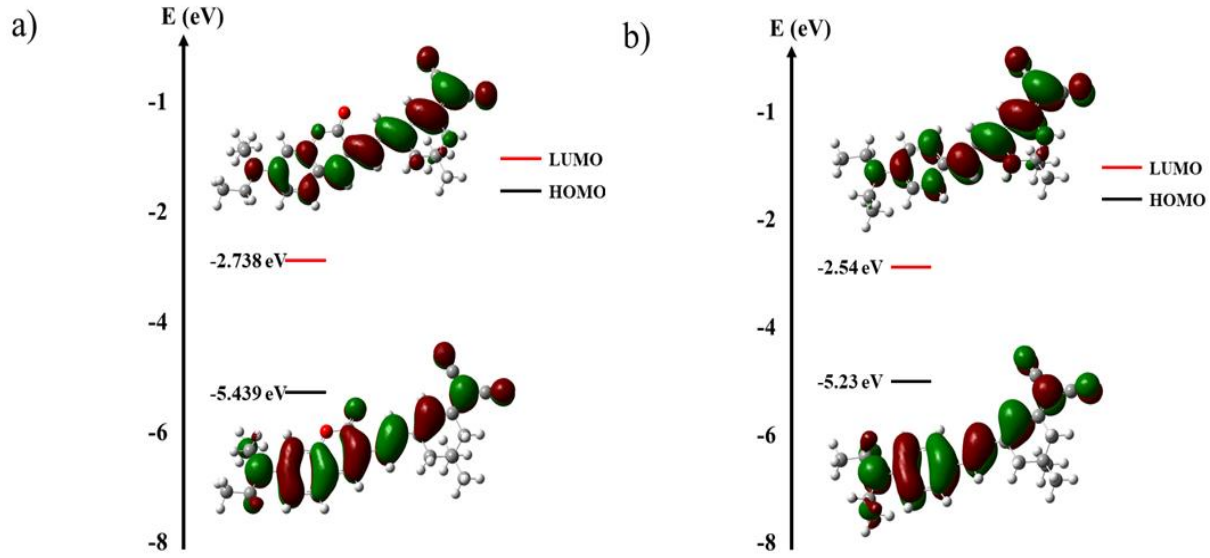

Figure3.4. Frontier molecular orbitals of the probe (a) LDP-1, (b) LDP-2 calculated with Gaussian'09 using hybrid B3LYP functional and 6-31 G(d,p) basis set.

3.3.5 Emission behavior of theprobe in PBS and CH_3CN

LDs contains almost no water, so as to store triglycerides and cholesterol esters more efficiently in the neutral core which provides a scheme for labeling LDs. The emission behavior of the probes in PBS-CH3CN mixed solvents with different volume ratios were tested.

(Figure 3.5a-3.5b). Transfer 20.0 μL of the stock solution to a test tube, and then dilute it to 2.0 mL with PBS-CH3CN mixture. According to the experimental data, we found that with the decrease of water content in the mixed solvent, the emission intensity gradually increased (Figure 3.5c-3.5d). From the figure, we can observe that the fluorescence intensity of the probe in acetonitrile is 150 times stronger than that in water. The result may be due to the formation of aggregates.[138-139] The relation between fluorescence emission intensity and probe concentration was studied (Figure 3.6). If the solubility is good, the fluorescence intensity will increase with the increase of concentration. From the detection results, we can see that when the concentration is lower than 100 μM, the fluorescence intensity does increase with the increase of the concentration, but once the concentration is higher than 100 μM, the fluorescence becomes weaker.Then, we proceeded to examine the particle size distribution of the probes in CH3CN and CH3CN-PBS (1/9) (Figure 3.7). We found that when the content of PBS were 0 % and 90 %, the particle size waschanged significantly. That is to say, the aggregation of probe LDP-1 and LDP-2 in CH3CN-PBS (1/9) was occured clearly.

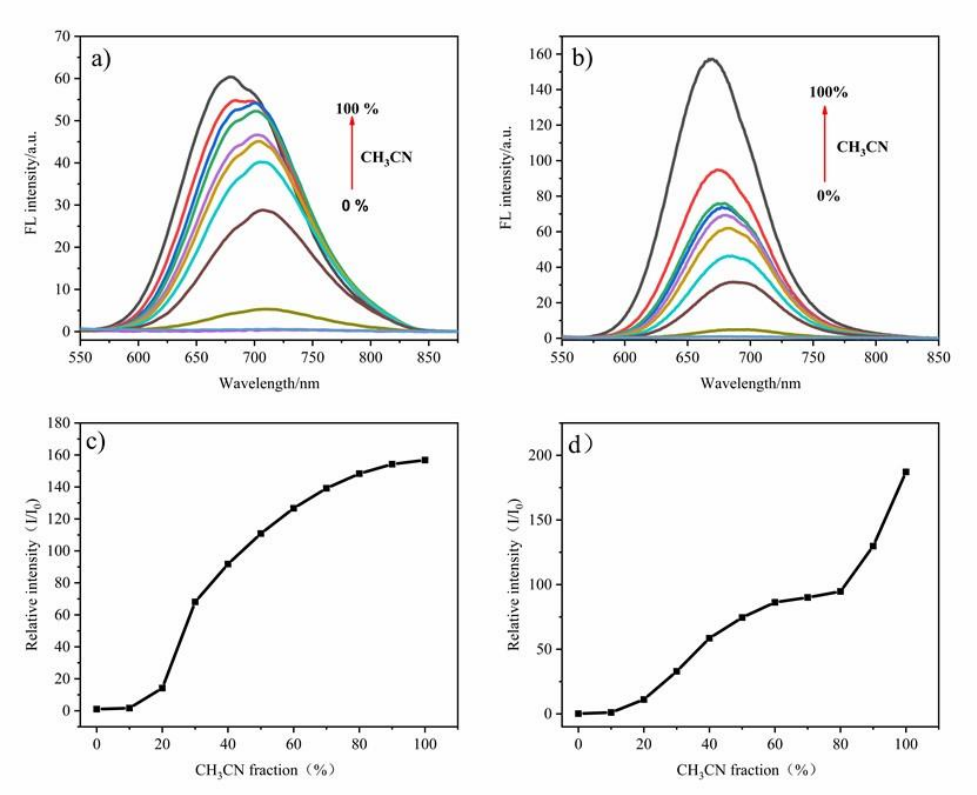

Figure 3.5. Fluorescence emission spectra of (a) LDP-1 (10 μM, λex= 520 nm).(b) LDP-2 (10 μM, λex= 530 nm) in varying concentrations of CH3CN in PBS. Relative maximum intensity of (c) LDP-1 (d) LDP-2. I0 is the fluorescence intensity of the probe in water.

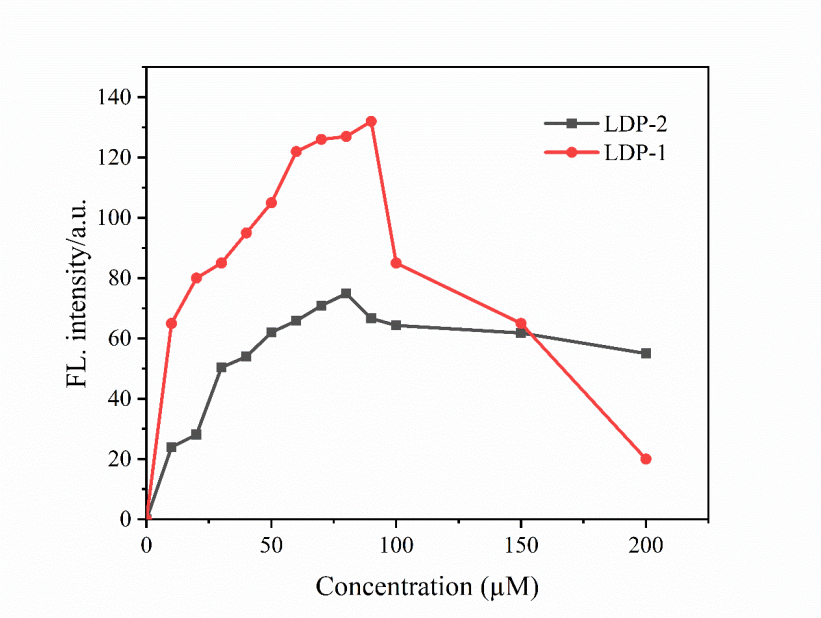

Figure3.6. Therelationship between maximum fluorescence emission intensity and probe concentration in CH_3CN.

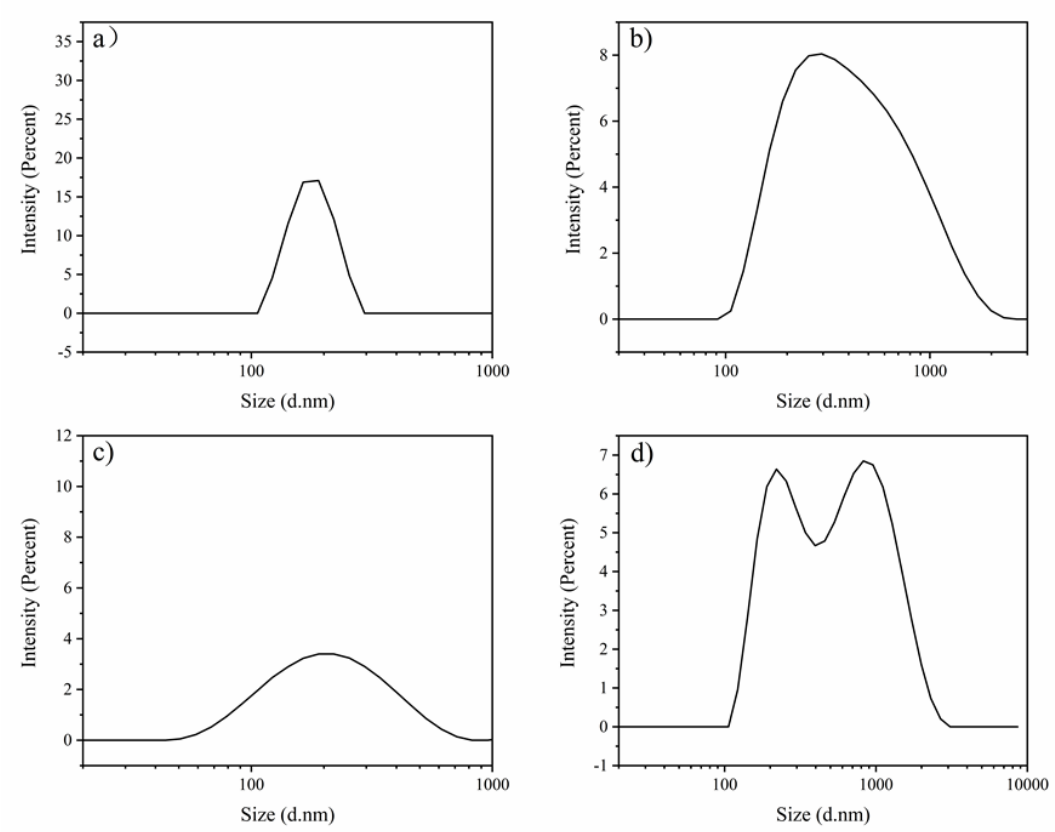

Figure 3.7. (a) particle size distribution of LDP-1 (10 μM) in CH3CN. (b) particle size distribution of LDP-1 (10 μM) in mixture of PBS and CH3CN (9/1). (c) particle size distribution of LDP-2 (10 μM) in CH3CN. (d) particle size distribution of LDP-2 (10 μM) in mixture of PBS and CH3CN (9/1).

3.3.6 Emission behavior of the probe in different viscosity

The viscosity of cytoplasm (1 cp) is much lower than that of LDs (57 cp).[140-141] Therefore, it will provide another way to distinguish LDs. Next, the relationship between viscosity and fluorescence intensity we studied in methanol-glycerol binary medium system.[142] Transfer 20.0 μL of the stock solution to a test tube, and then dilute it to 2.0 mL with methanol-glycerol mixture. According to the results, we found that there was a small red shift phenomenon

(~25nm). This was due to the increase in polarity of the medium. Andthe experimental results were consistent with the conclusion of polarity sensitive experiment. We found that the fluorescence intensity of probeswere positively related to viscosity (Figure 3.8). LDP-1 showed a ~4 folds intensity increment while LDP-2 showed a ~9 folds rise in intensity along with a ~25 nm red shifts. The cells contained a large amount of water, so we tested PBS-Glycerol system again (Figure3.9). With the increase of viscosity, the fluorescence intensity of the probe increased by nearly 40 times. The experimental results were consistent. In order to further study the sensitivity of the probe to viscosity. The fluorescence intensity of probes in different solvents were also studied (Figure3.10). The probe emitted strongly in glycerol with high viscosity.

The emission intensity of the probeswere affected by viscosity because of the molecular rotor. The novel fluorescent materials with twisted intramolecular charge transfer effect generally contained a rotatable D-π-A conjugated structure.[143]In low-viscosity medium, intramolecular rotation results in relaxation of excitation energy, which significantly weakens fluorescence emission. But, in high-viscosity medium, free rotation was prevented, and the molecules release energy mainly by radiation, resulting in significant enhancement of fluorescence.[144]

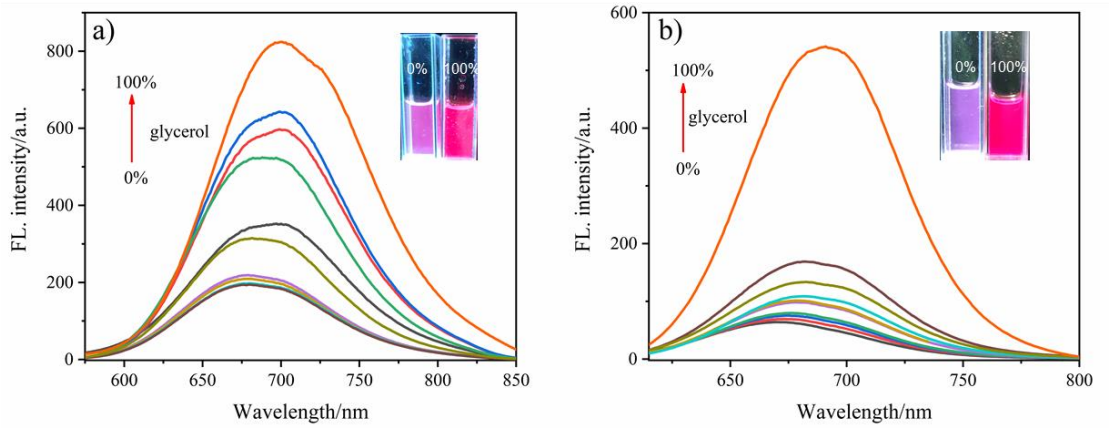

Figure 3.8. (a) Changes of fluorescence spectra of LDP-1 (10 μM, λex= 520 nm) with the variation of solution viscosity (methanol-glycerol system). (b) Changes of fluorescence spectra of LDP-2 (10 μM, λex= 530 nm) with the variation of solution viscosity (methanol-glycerol system).

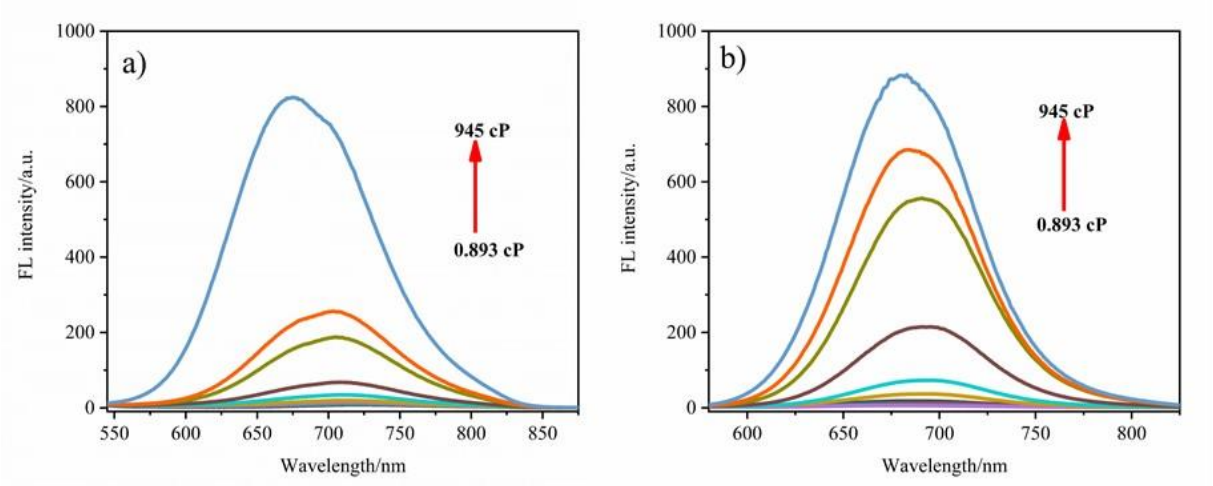

Figure 3.9. (a) Changes of fluorescence spectra of LDP-1 (10 μM, λex= 520 nm) with the variation of solution viscosity (PBS-glycerol system). (b) Changes of fluorescence spectra of LDP-2 (10 μM, λex= 530 nm) with the variation of solution viscosity (PBS-glycerol system).

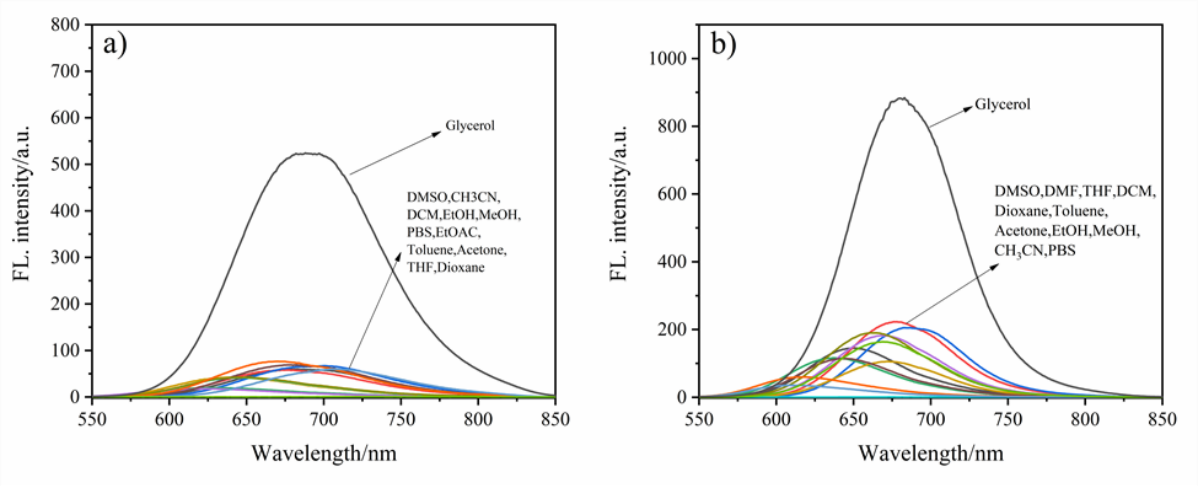

Figure3.10. Fluorescence emission of the probe (a) LDP-1 and (b) LDP-2 in various solvents withdifferent polarities.

3.3.7 Anti-interference of the probe and effect of different pH

High selectivity for analytes in biological imaging is very important. Many aromatic groups linked by vinyl groups are known to react with nucleophilic molecules such as bisulfites, and biological thiols.[145-148] Under the same external conditions in each group, we studied the fluorescence intensity changes of the probes LDP-1 and LDP-2 to potentially interfering chemicals (Figure 3.11). Addition of ions and potentially interfering chemicals to the solution of the probe did not induce any obvious change in the fluorescence intensity of the probe in PBS-CH_3CN(1:1).The emission behaviors of LDP-1 and LDP-2were hardly affected by other chemicals. Subsequently, the effect of different pH was investigated. As shown in Figure12. In mixture of PBS and CH_3CN (1:1), when pH changes from 1 to 12, there were almost no changes of probe LDL-1 and LDL-2, indicating that the two probes were

not affected by pH.

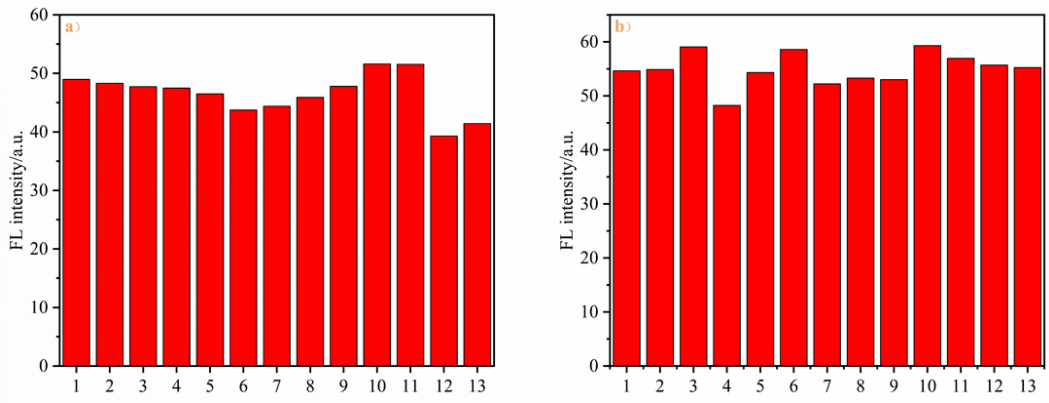

Figure 3.11.In CH_3CN-PBS (1:1), (a) the fluorescent intensity of LDP-1 (10 μM, λex= 520 nm, at 705 nm) and (b)LDP-2 (10 μM, λex= 530 nm, at 690 nm) upon addition of various species (100 μM) including: 1, Blank; 2, Arg; 3, H_2O_2; 4, HSO_3^-; 5, Cys; 6, Ser; 7, Zn^{2+}; 8, N_2H_4; 9, K^+; 10, GSH; 11, Fe^{3+}; 12, Cu^{2+}; 13, Al^{3+}.

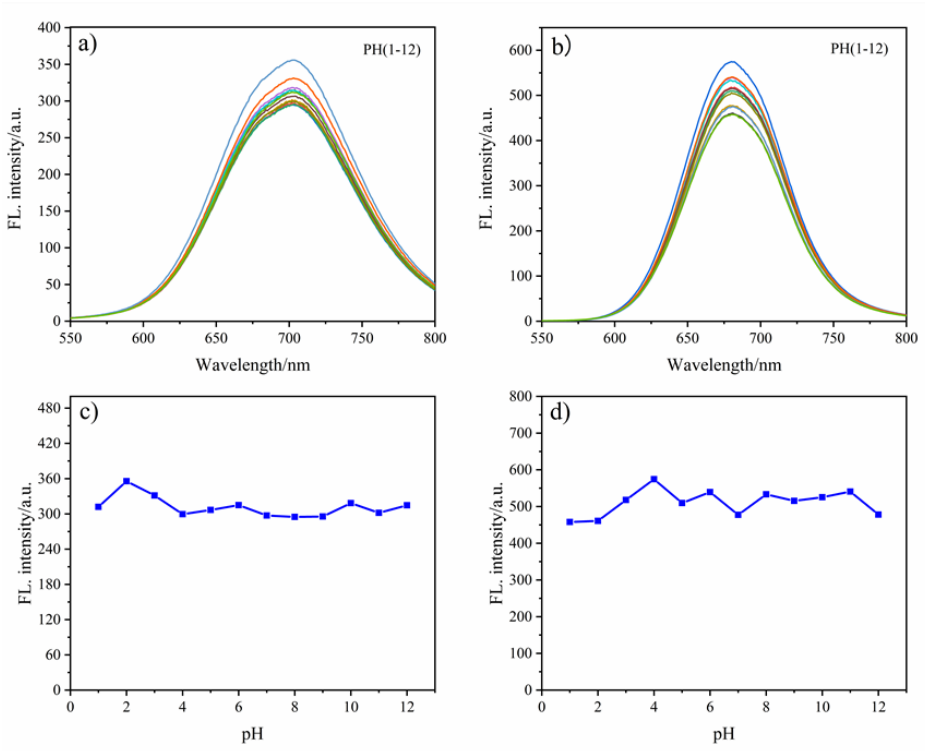

Figure 3.12. The maximum emission intensity of probe (a) (c) LDP-1 (10 Mm, λex= 520 nm) and (b) (d) LDP-2 (10 Mm, λex= 530 nm) in 50 % water mixtures at various pH (1-12).

3.3.8 Cellular imaging of the probe

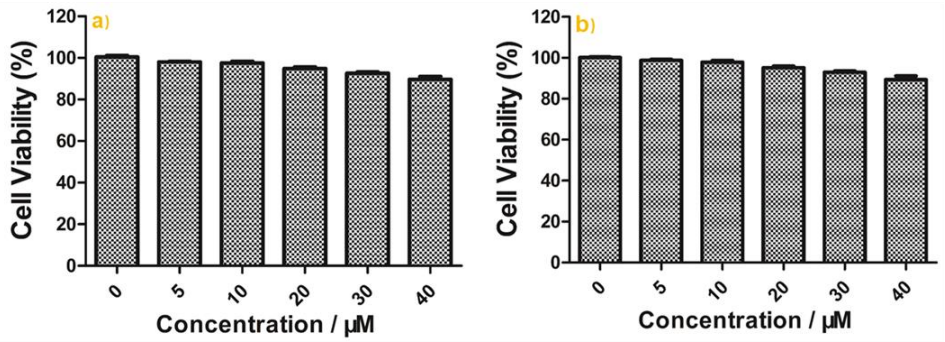

Figure 3.13. Cytotoxicity assays of probe (a) LDP-1and (b) LDP-2 at different concentrations (0 μM; 5μM; 10 μM; 20 μM;30 μM; 40 μM) for HeLa cells

Before imaging living cells, we must test the biotoxicity of probes. The cytotoxicity of the probes were evaluated by MTT method. (Figure 3.13). HeLa cells were cultured with probes at different concentrations for 24 hours, and the cell survival rate was observed. As shown in Figure3.13, the survival rate were over 85%.To sum up, the two probes with low biotoxicity were suitable for cell imaging.

To further prove that our designed probes could be used for selectively labelling LDs in cells, co-localization experiments in living HeLa cells were carried out by purchasing the commercially available LDs probe BODIPY 493/503 (Figure 3.14-3.15). Thered fluorescence imaging were stained by probesLDP-1 (Figure 3.14c) andLDP-2(Figure 3.15c). The green fluorescence imaging were stained by BODIPY493/503.The images after co-localization were depicted in Figure 14d and Figure 15d.In addition, the Pearson's correlation coefficients were up to 0.97

(LDP-1) and 0.89 (LDP-2). The experimental results showed that the two probes could selectively sense LDs distribution in living HeLa cells.

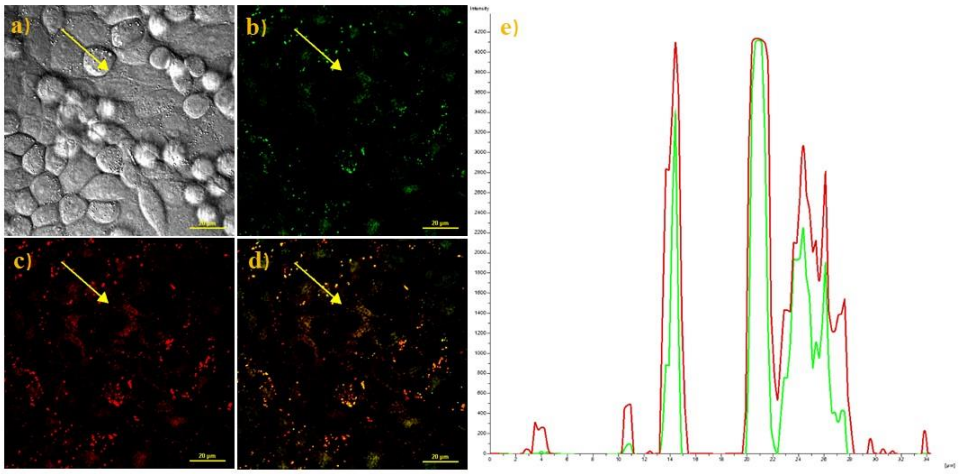

Figure 3.14. Fluorescence image of live HeLa cells incubated with both LDP-1 (10 μM) and BODIPY 493/503 for 30 min at 37 ℃. (a) bright field image.(b) Emissions from the BODIPY (480-510 nm, λex=488 nm). (c) Emissions from LDP-1 (680-710 nm, λex= 520 nm). (d) Merged image. (e) Fluorescence intensity profile along the ROI line (10 μm).

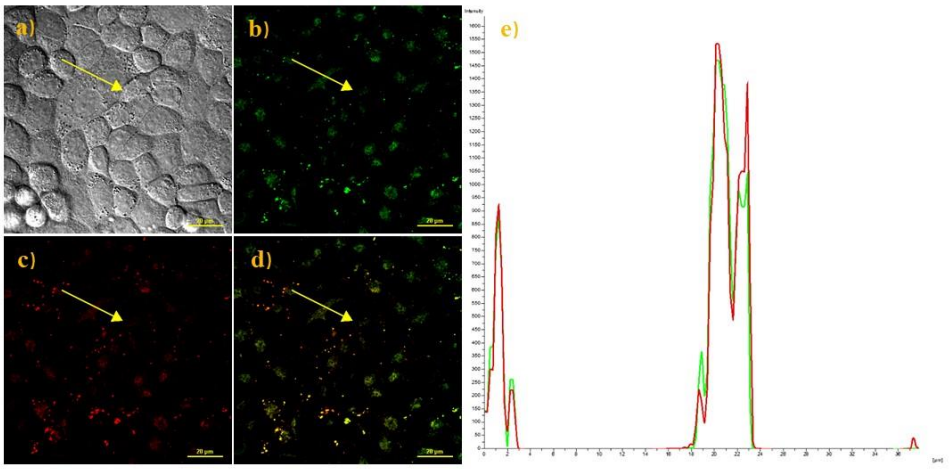

Figure 3.15. Fluorescence image of live HeLa cells incubated with both LDP-2 (10 μM) and BODIPY 493/503 for 30 min at 37 ℃. (a) bright field image.(b) Emissions from the BODIPY (480-510 nm, λex=488 nm). (c) Emissions from LDP-1 (660-700 nm, λex= 530 nm). (d) Merged image. (e) Fluorescence intensity profile along the ROI line (10 μm).

3.4 Conclusion

In this chapter, two organic bio-probes LDP-1 and LDP-2 were designed and synthesized for LDs cell imaging. The two probes could sense the hydrophobicity and high viscosity environment of LDs at the same time. The two probes showed good characteristics, including long emission wavelengths, large Stokes shifts, good anti-interference ability and low biotoxicity. In addition, the two probes could also selectively be applied for tracing LDs. This work provides a new method for monitoring LDs at organ and body levels.

SECTION 4. A novel polarity sensitive lipid droplets fluorescent probe synthesized by a rational design strategy and its application in cell imaging

4.1 Introduction

As key organelles that store and supply lipids, lipid droplets serve to buffer intracellular lipid concentrations and control their release to meet specific cellular demands. Lipids represent a special class of hydrophobic substances that are constantly performing tasks required for cellular functions to maintain the dynamic balance within the cell[149-153]. As precursors for the synthesis of many signaling molecules in cells, lipids may cause cytotoxicity leading to cellular dysfunction and apoptosis if not properly controlled, and this term is known as lipotoxicity, and thus lipid droplets are key intracellular organelles that store and supply lipids[154]. Interestingly, lipid droplets also exhibit the function of helping to transport intracellular proteins[155-157]. Moreover, cancer cells are constantly robbing the surrounding nutrients, which inevitably take up excess lipids and cholesterol and store them in lipid droplets[158-160]. Therefore, detection of LDs content in cells could also be a potential method for tumor treatment and monitoring.

Polarity is a very important parameter and indicator for normal cells, playing a key role in numerous biological processes such as cell

differentiation, cell migration, and tissue and organ formation. Moreover, loss of cell polarity is associated with cancer and other related disease states[161-164]. Numerous studies have shown that the development of certain diseases is closely related to abnormal changes in polarity, such as inflammation[165-168]. The unique function of the lipid droplet and the unique environment in which it resides dictate that it is closely related to the level of polarity in the microenvironment, and there are increasing data suggesting that abnormalities in LDs polarity are inseparable from the tumor process, and the low polarity of LDs has been certified to be associated with cancer cells[169-172]. Therefore, the rational development of a tool that can monitor the polarity of lipid droplets is important to discriminate between normal and abnormal cells.

As a technique developed in recent years, fluorescence probe technology has the advantages of sensitivity, convenience, accuracy, ease of operation and non-destructive characteristics, and it is gradually became an important reference tool for in vivo and in vitro biomedical research[173-183]. In the present study, a novel polarity-sensitive lipid droplet fluorescent probe, ATOP-LD, was synthesized based on the design of coumarin fluorophore with 3-Pyridinecarbonitrile. The probe exhibits excellent photostability in terms of photophysical properties, and the probe emission wavelength is accompanied by a significant red shift with increasing polarity of the dispersed solvent. In addition, the probe

ATOP-LD exhibited effective targeting of lipid droplets, favorable biocompatibility, remarkable pH stability and reasonable selectivity.

4.2 Synthesis of probes

4.2.1 Reagent

Short name	Name	Supplier
DCM	Dichloromethane	Damao Chemical Reagent Factory
THF	Tetrahydrofuran	Damao Chemical Reagent Factory
EtOAC	ethyl acetate	Damao Chemical Reagent Factory
EtOH	Etanol	Damao Chemical Reagent Factory
CH_3CN	Acetonitrile	Damao Chemical Reagent Factory
DMSO	Dimethyl Sulfoxide	Damao Chemical Reagent Factory
DMF	N,N-DiMethylforMaMide	Damao Chemical Reagent Factory
Arg	L-Arginine	J&K Scientific
Cys	L-Cysteine	J&K Scientific
Ser	L-Serine	J&K Scientific
GSH	L-Glutathione	Energy Chemical
Pip	Piperidine	Energy Chemical

4.2.2 Materials

The 1H NMR and 13C NMR spectrums were obtained from INOVA-

400 MHz nuclear magnetic resonance instruments, respectively. High-resolution electrospray mass spectra (HRMS) were obtained from Bruker APEX IV-FTMS 7.0T mass spectrometer. All the UV–vis absorption spectra and emission spectra were obtained from Shimadzu UV-1800 spectrometer and Shimadzu RF-5301PC spectroscope respectively. The fluorescence images of cells were obtained with Nikon A1MP confocal microscopy with a CCD camera, Both TLC and silica gel were purchased from the Qingdao Ocean Chemicals.

4.2.3 Synthesis of probes

Synthesis of the compound 1

A mixture of ethyl acetoacetate (1.30 g, 10 mmol), ethyl cyanoacetate (1.13 g, 10 mmol), methylamine (0.31 g, 10 mmol), ethanol (15 mL), and piperidine (0.25 g, 3 mmol) was reacted under nitrogen at reflux for 8 hours. After the reaction was completed, excess ethanol was removed using a rotary evaporator and the viscous residue was slowly poured into cold 10 % hydrochloric acid (30 mL) to precipitate the crude product product. Finally, the crude product was recrystallized from ethanol three times to obtain pure white crystals (1.46 g, 89%). 1H NMR (400 MHz, DMSO-d6) δ 9.56 (s, 1H), 5.65 (s, 1H), 3.28 (s, 3H), 2.23 (s, 3H). 13C NMR (101 MHz, DMSO-d6) δ 160.59, 160.40, 157.79, 117.41, 91.83, 88.30, 27.47, 20.44. （Fig. S2-S3）

Synthesis of compound 2

The mixture of diethyl malonate (1.60 g, 10 mmol), 4-(diethylamino)-2-hydroxybenzaldehyde (1.93 g, 10 mmol), anhydrous ethanol (15 mL) and piperidine (0.25 g, 3 mmol) was reacted at reflux under nitrogen for 6 h. After the reaction, the remaining solvent was removed by evaporation under reduced pressure. Then, 30 mL of the mixed solution HCl/glacial acetic acid (1:1, v/v) was added to the reaction system at 120°C and the reaction was continued for 7 h. After the reaction, the resulting mixture was poured into 40 mL of deionized water and the pH was adjusted to neutral with 40 % sodium hydroxide solution and a dark brown precipitate was produced. The precipitate was filtered and washed several times with water and ethanol to obtain the target product (1.98 g, 91 %). 1H NMR (400 MHz, CDCl3) δ 7.54 (d, J = 9.3 Hz, 1H), 7.24 (d, J = 8.8 Hz, 1H), 6.56 (d, J = 8.8 Hz, 1H), 6.46 (s, 1H), 6.02 (d, J = 9.3 Hz, 1H), 3.40 (q, J = 7.2 Hz, 4H), 1.20 (t, J = 7.2 Hz, 6H). (Fig. S4)

Synthesis of compound 3

DMF (1 mL) was added to the dry eggplant bottle after three cycles of vacuum and nitrogen filling, POCl3 (1.61 g, 10.5 mmol) dissolved in DMF (1 mL) was slowly added to the eggplant bottle with a syringe and stirred for 45 min at 50 °C. Compound 2 (0.76 g, 3.5 mmol) was dissolved in DMF (5 mL) and added to the above mixed system and

stirred for 2 h at 60 °C. After the reaction, the mixture was slowly poured into 100 mL of ice water and the pH was adjusted to neutral with 20% NaOH. The precipitate was filtered and washed several times with deionized water and anhydrous ethanol to obtain a yellow solid powder. Yield : 81 %. 1H NMR (400 MHz, CDCl3) δ 10.13 (s, 1H), 8.26 (s, 1H), 7.43 (d, J = 9.0 Hz, 1H), 6.68 (dd, J = 9.0, 2.6 Hz, 1H), 6.53 (d, J = 2.7 Hz, 1H), 3.48 (q, J = 7.1 Hz, 4H), 1.26 (t, J = 7.2 Hz, 6H). (Fig. S5)

Synthesis of probe ATOP-LD

Compound 3 (0.12 g 0.5 mmol) and compound 1 (0.075 g 0.5 mmol) were dissolved in glacial acetic acid (2 mL) and stirred for 1 h at 100 °C, then isopropanol (2 mL) was added and reacted at room temperature for 2 h. After the reaction was completed, petroleum ether (5 mL) was added to produce a large amount of precipitation, and the product was obtained by filtration and recrystallization with ethanol. Yield : 86 %. 1H NMR (400 MHz, CDCl3) δ 9.56 (s, 1H), 8.18 (s, 1H), 7.47 (d, J = 9.0 Hz, 1H), 6.71 (d, J = 9.2 Hz, 1H), 6.50 (s, 1H), 3.53 (q, J = 7.2 Hz, 4H), 3.35 (s, 3H), 2.61 (s, 3H), 1.30 (t, J = 7.2 Hz, 6H). 13C NMR (101 MHz, CDCl3) δ 162.76, 162.34, 160.81, 159.89, 158.46, 154.08, 150.29, 148.01, 133.27, 121.35, 114.88, 112.08, 110.82, 109.73, 103.43, 97.41, 45.74, 27.04, 19.53, 12.57. (Fig. S6-S7)

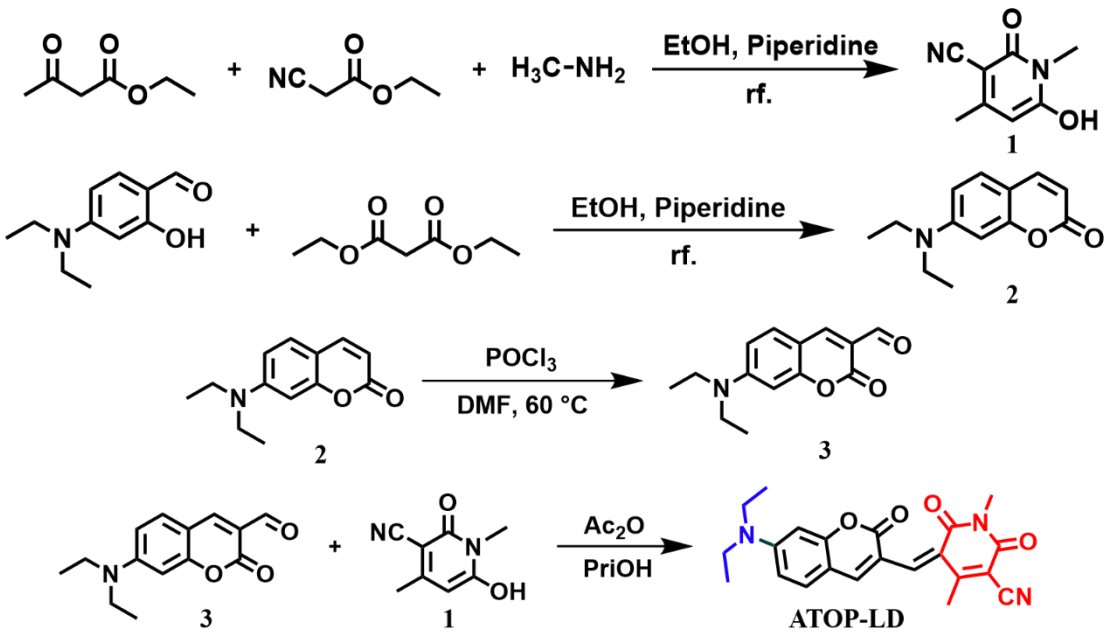

Scheme 4.1. Synthetic route of probe ATOP-LD .

4.2.4 Probe design

The probe ATOP-LD is composed of a coumarin derivative and a 1,4-dimethyl-3-cyano-6-hydroxypyridin-2-one group with strong electron-absorbing properties. Specifically, the diethylamine group is used as a functional group for precise targeting of lipid droplets and also as a strong electron-donating group for probe ATOP-LD. The fluorescent probe ATOP-LD obtained by condensation reaction of compound 1, which contains a strong electron-absorbing structure, with coumarin-derived compound 3. Due to the design of the special D-π-A chemical structure of the probe ATOP-LD and the addition of the diethylamine functional group, the probe exhibited not only effective detection of lipid droplets, but also polarity-sensitive properties.

4.3 Result and Discussion

4.3.1 General procedure for analysis

Parent stock solution of the fluorescent probe ATOP-LD (1.0 mM) wasprepared in absolute DMSO 20.0 μL of stock solution was transferred into atest tube, and then diluted to 2.0 mL with the mixture of organic solvent. All spectra were obtained in a quartzcuvette (path length = 1 cm).

The solutions of K+, Zn2+, Al3+, Cu2+, Fe3+andwere prepared from their chloride salts. Hydrogen peroxide (H2O2) was provided from its commercially available 30% aqueous solution to afford the desired concentration. Cysteine (Cys) and glutathione (GSH) and L-Serine (Ser) and L-Arginine (Arg) were prepared by dissolving the corresponding solid in ultrapure water. PBS solution was prepared withNa2HPO4and KH2PO4, and adjusted to pH 7.4.

4.3.2 Photophysical properties of the probe in different solvents

In order to verify the feasibility of the probe design we first performed absorption spectra and fluorescence spectra in different solvents, respectively toluene (Tol), tetrahydrofuran (THF), dimethyl sulfoxide (DMSO), N,N-dimethylformamide (DMF), dichloromethane (DCM), PBS buffers (pH = 7.4), 1,4-Dioxane, acetone, ethanol (EtOH), acetonitrile (CH3CN), ethyl acetate (EtOAc), Methanol (MeOH). The

detection results showed that the maximum absorption wavelength of the probe ATOP-LD in different solvents changed accordingly with the change of the solvent and the pattern is more obvious in the fluorescence spectra. The fluorescence emission intensity of the probe ATOP-LD is significantly higher in lipid solvents than in protonic solvents. As shown in Fig. 1, the fluorescence intensity of the probe in Tol, dioxane, EtOAc solvents is even 65 fold higher than that in PBS buffers, MeOH, EtOH solvents (Fig. 4.1b)). In addition, the maximum emission wavelength of the fluorescence spectrum of the probe ATOP-LD was blue-shifted by about 35 nm with the change of solvent polarity (as the polarity decreased) (Fig. 4.1a)). These results indicated that the probe ATOP-LD provides effective detection of lipid droplets.

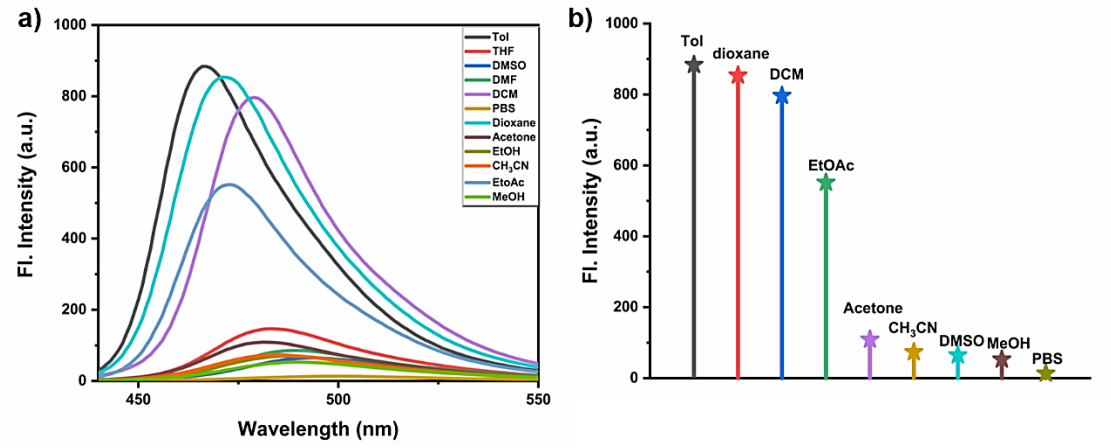

Figure.4.1. a) Fluorescence spectra of probe ATOP-LD (10 μM) in different solvents. b) Effect of different solvents on the fluorescence emission intensity of probe ATOP-LD (10 μM).

4.3.3. Fluorescence spectra of probe ATOP-LD in different ratio of EtOAc/MeOH and Dioxane/PBS buffers.

To further investigate the properties of the probe on lipid droplets, we added the fluorescence spectral properties of the probe in different ratios of EtOAc/MeOH and Dioxane/PBS buffers tests. As a result of the analysis, the fluorescence emission intensity of the probe ATOP-LD showed a significant increment with the increase of EtOAc and Dioxane in the solvent mixture and the maximum emission wavelength was accompanied by a slight blue shift of 20-35 nm (Fig. 4.2). These experimental phenomena revealed that the sensitivity of the fluorescent probe ATOP-LD to the effect of lipid droplets is favourable enough to be suitable for labeling lipid droplets.

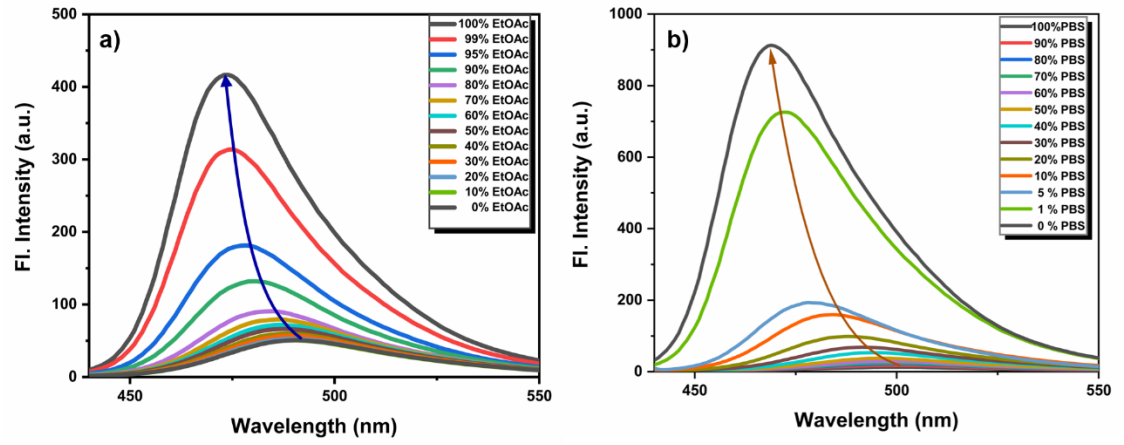

Figure. 4.2. a) The fluorescence spectra of probe ATOP-LD (10 μM) in different ratios of EtOAc/MeOH. b) The fluorescence spectra of probe ATOP-LD (10 μM) in different ratios of Dioxane/PBS buffers.

4.3.4 Study of the polarity-sensitive properties of the probe ATOP-LD

To investigate whether the probe ATOP-LD exhibited positive sensitivity to solvent polarity, we have measured the dependence of its fluorescence emission intensity and fluorescence maximum emission wavelength on polarity by fluorescence spectroscopy. As shown in Fig. 4.3, The maximum fluorescence emission wavelength of the probe ATOP-LD in different polarity solvents shifts significantly, becoming larger with increasing solvent polarity (Fig. 4.3a)). Moreover, as the polarity of the probe ATOP-LD solution changed, the fluorescence color transformed from blue to dark green under 365nm UV lamp, and the fluorescence also showed a variation from bright to weak (Fig. 4.3a)). In order to investigated the sensitivity of the probe ATOP-LD to polarity in more detail, two empirical parameters (ET(30), dielectric constant (ε)) are quoted as the polarity parameter and the dielectric constant, respectively. We discussed the relationship between the fluorescence properties of the probe and them separately. What can be obtained is that the fluorescence intensity of the probe decreases as ET(30) increased (Fig. 4.3b)). At the same time, the maximum fluorescence emission wavelength of the probe shows a significant red shift and a good linear relationship with the change of ET(30) (Fig. 4.3c)). In addition, the dielectric constant also exhibited a clear regular variation with the fluorescence intensity of the probe, which gradually decreased as the dielectric constant increased (Fig.

4.3d)). These results suggested thatdue to the unique design of the probe ATOP-LD and the strong intramolecular charge transfer mechanism, the probe showed effective sensitivity to solvents polarity.

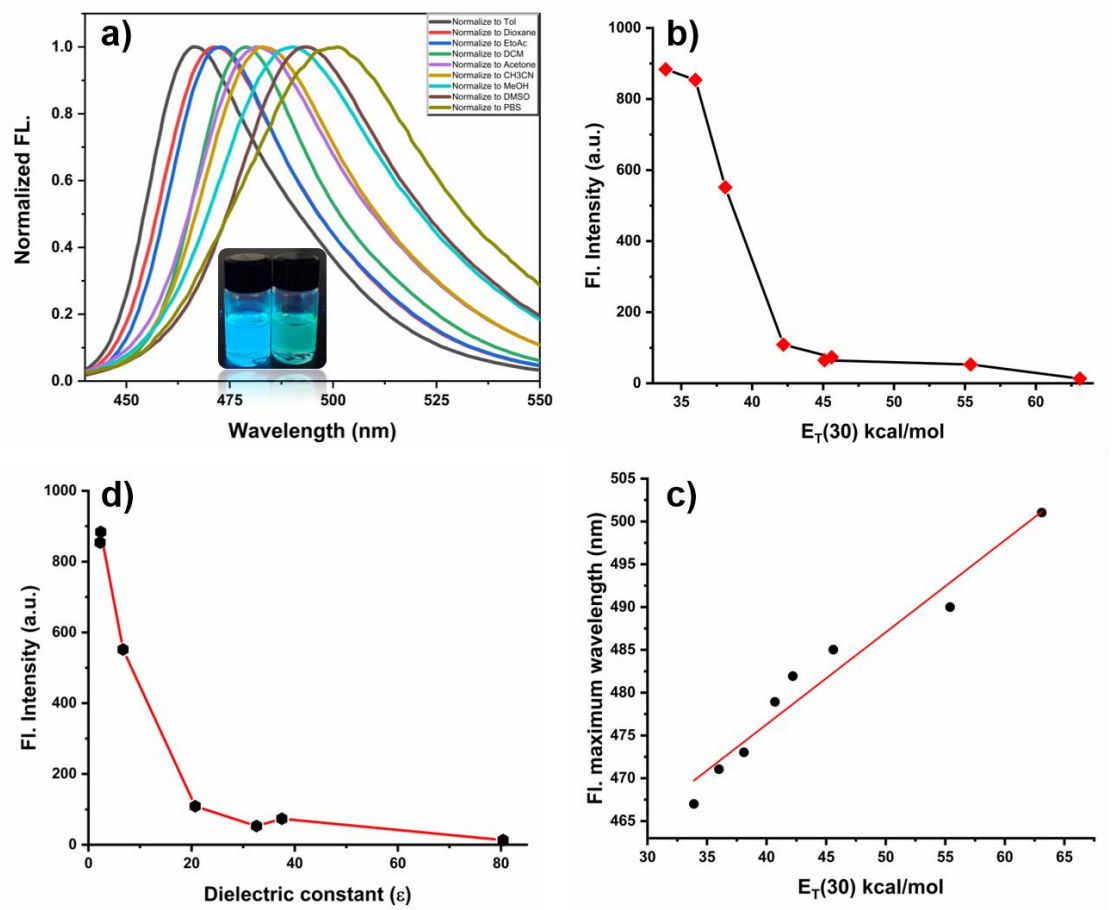

Figure. 4.3. a) Fluorescence normalized spectra of the probe ATOP-LD (10 μM) in different solvents. b) Dotted line plot of empirical polarity parameters versus probe ATOP-LD (10 μM) fluorescence emission intensity. c) Fitted curve of the relationship between the fluorescence maximum emission wavelength of the probe ATOP-LD (10 μM) and the empirical parameter of polarity. d) Dotted line plot of the fluorescence emission intensity of the probe ATOP-LD (10 μM) versus the dielectric constant of different solvents. ET(30) and dielectric constant (ε) were collected from reference. [34-35].

4.3.5 Probe ATOP-LD interference immunity test

Since the complex environment inside the cells of the organism's machinery, fluorescent probes must be highly resistant to interference. To explore the anti-interference ability of the probe ATOP-LD, we added different analytes to the test solution to detect changes in the fluorescence spectrum. As shown in Fig. 4.4, The fluorescence spectra were collected by adding different analytes to the Dioxane/PBS buffers (v/v=1/1) solvent mixture and pure PBS buffers solution respectively, and the test results showed that the change of fluorescence intensity was very minor, and the probe ATOP-LD provided favorable anti-interference ability.

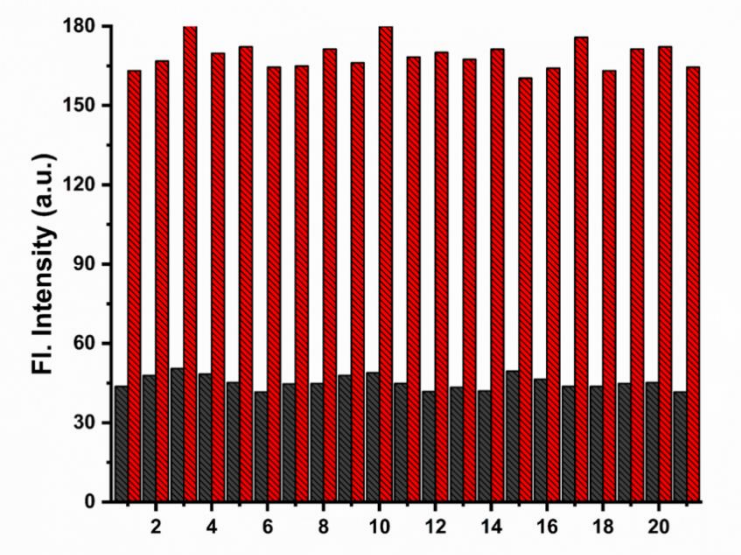

Figure. 4.4. Fluorescence intensity of the probe ATOP-LD (10 μM) in the presence of different analytes (100 μM). Black column: in dioxane/PBS buffers (v/v=1/1). red column: in dioxane/PBS buffers (v/v=9/1). Where 1-21 represent Fe^{3+},HCO^{3-}, Ca^{2+},Mg^{2+},Cu^{2+},Al^{3+},Fe^{2+},CO_3^{2-}, GSH, Cys, Arg, CIO^-, HS^-, H_2O_2, N_2H_4•H_2O, NO^{2-}, TBHP, SO_4^{2-}, Na^+, Cl^-,$(NO_3)^{2-}$ respectively.

4.3.6 Probe ATOP-LD pH and kinetic stability research

The extremely complex intracellular physiological and pathological environment requires fluorescent sensors equipped with excellent kinetic stability and pH stability to ensure that the probes remain functional in the complex physiological environment. Thus, we examined the probe ATOP-LD by fluorescence spectroscopy in terms of kinetic stability and pH stability respectively. The experimental results indicated that the probe ATOP-LD exhibited excellent kinetic stability in different solvents and even maintained a stable fluorescence emission intensity after 3 h (Fig. 4.5a). As shown in Fig. 4.5b, the fluorescence intensity of the probe varies very rarely in the range of pH1-12 and was almost independent of pH, indicating that the probe structure was designed with a good pH applicability range. These results suggested that the probe ATOP-LD can be effectively used in biological environments and maintain good stability.

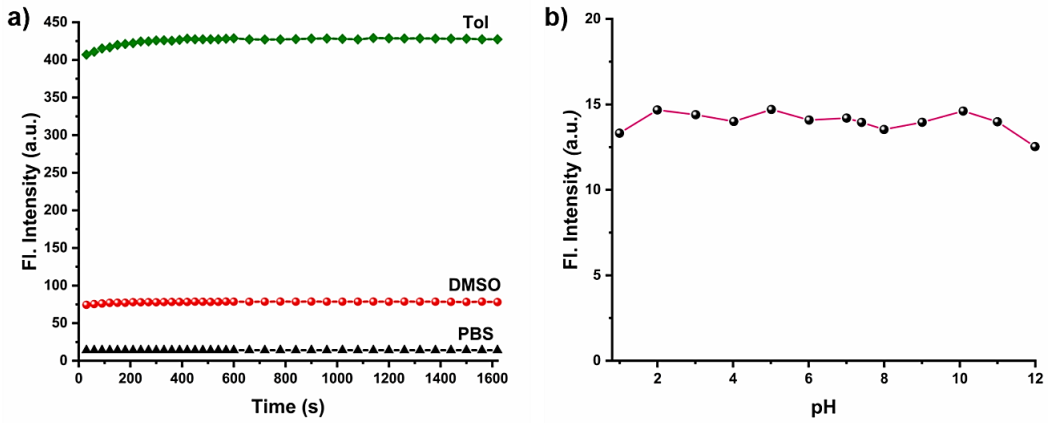

Figure. 4.5. a) Detection of kinetic stability fluorescence spectra of the probe ATOP-LD (10 μM) in different solvents. b) The pH effects of fluorescence spectra of probe ATOP-LD (10 μM) in pure PBS buffers (pH=7.4).

4.4 Conclusion

In this chapter, we developed a novel fluorescent chemosensor that can effectively label intracellular lipid droplets. interestingly, it also exhibited polarity-sensitive properties due to the rational design of the probe ATOP-LD molecular structure, which itself has strong electron-giving and electron-absorbing groups. In addition, the probe itself had excellent interference resistance, pH stability and Kinetic stability.

CONCLUSION

1. A novel organic bio-probe Cou-LDs was designed and constructed for LDs cell imaging with much more hydrophobic and viscous environment compared to cytosol. The presence of diethylamino electron donating groups helps in shiftingthe intramolecular charge transfer bands to the red-wavelength regions. This probe exhibited favorable merits including large Stokes shift (over 100 nm), good selectivity, low biological toxicity, and LDs-specificity.

2. Two organic bio-probes LDP-1 and LDP-2 were designed and synthesized for LDs cell imaging. The two probes could sense the hydrophobicity and high viscosity environment of LDs at the same time. The two probes showed good characteristics, including long emission wavelengths, large Stokes shifts, good anti-interference ability and low biotoxicity. In addition, the two probes could also selectively be applied for tracing LDs. This work provides a new method for monitoring LDs at organ and body levels.

3. Developed a novel fluorescent chemosensor that can effectively label intracellular lipid droplets. interestingly, it also exhibited polarity-sensitive properties due to the rational design of the probe ATOP-LD molecular structure, which itself has strong electron-giving and electron-absorbing groups. In addition, the probe itself had excellent interference resistance, pH stability and Kinetic stability.

List of literature sources

[1] HUANG X, LAN M, WANG J, et al. A dual-mode strategy for sensing and bio-imaging of endogenous alkaline phosphatase based on the combination of photoinduced electron transfer and hyperchromic effect [J]. Anal Chim Acta, 2021, 1142: 65-72.

[2] Zhou T, Yang Y, Zhou K, et al. Efficiently mitochondrial targeting fluorescent imaging of H2S in vivo based on a conjugate-lengthened cyanine NIR fluorescent probe[J]. Sensors and Actuators B Chemical, 2019, 301:127116-127122.

[3] YUE L, HUANG H, SONG W, et al. A near-infrared endoplasmic reticulum-targeted fluorescent probe to visualize the fluctuation of SO2 during endoplasmic reticulum stress [J]. Chemical Engineering Journal, 2021.

[4] VALEUR B, LERAY I J C C R. Design principles of fluorescent molecular sensors for cation recognition [J]. 2000, 205(1): 3-40.

[5] JIA X, CHEN Q, YANG Y, et al. FRET-Based Mito-Specific Fluorescent Probe for Ratiometric Detection and Imaging of Endogenous Peroxynitrite: Dyad of Cy3 and Cy5 [J]. J Am Chem Soc, 2016, 138(34): 10778-81.

[6] FAN J, HU M, ZHAN P, et al. Energy transfer cassettes based on organic fluorophores: construction and applications in ratiometric sensing [J]. Chem Soc Rev, 2013, 42(1): 29-43.

[7] 陈忠林, 李红玲, 韦驾, et al. 基于激发态能量转移机理比率型荧光探针的研究进展 [J]. 2015, 35(004): 789-801.

[8] ZHOU L, ZHANG X, WANG Q, et al. Molecular engineering of a TBET-based two-photon fluorescent probe for ratiometric imaging of living cells and tissues [J]. 2014, 136(28): 9838-41.

[9] ZHANG S, QIN A, SUN J, et al. Mechanism study of aggregation-induced emission [J]. 2011, 23(4): 623.

[10] DONG Y, LAM J W, QIN A, et al. Aggregation-induced and crystallization-enhanced emissions of 1, 2-diphenyl-3, 4-bis (diphenylmethylene)-1-cyclobutene [J]. 2007, (31): 3255-7.

[11] ZHAO J, JI S, CHEN Y, et al. Excited state intramolecular proton transfer (ESIPT): from principal photophysics to the development of new chromophores and applications in fluorescent molecular probes and luminescent materials [J]. 2012, 14(25): 8803-17.

[12] 王瑞祥, 赖晓静, 有机化学 刘 J. 基于激发态分子内质子转移 (ESIPT) 原理的反应型荧光探针研究进展 [J]. 2019, 39(4): 952-60.

[13] SHENG H, HU Y, ZHOU Y, et al. A highly selective ESIPT-based fluorescent probe with a large Stokes shift for the turn-on detection of cysteine and its application in living cells [J]. 2019, 160: 48-57.

[14] CHEN L, YIN S-Y, PAN M, et al. A naked eye colorimetric sensor for alcohol vapor discrimination and amplified spontaneous emission (ASE) from a highly fluorescent excited-state intramolecular proton

transfer (ESIPT) molecule [J]. 2016, 4(29): 6962-6.

[15] YIN S-Y, SUN S-S, PAN M, et al. An imidazole based ESIPT molecule for fluorescent detection of explosives [J]. 2018, 355: 377-81.

[16] MISHRA V R, GHANAVATKAR C W, SEKAR N J J O L. ESIPT clubbed azo dyes as deep red emitting fluorescent molecular rotors: Photophysical properties, pH study, viscosity sensitivity, and DFT studies [J]. 2019, 215: 116689.

[17] BARTZ R, LI W-H, VENABLES B, et al. Lipidomics reveals that adiposomes store ether lipids and mediate phospholipid traffic1, s [J]. 2007, 48(4): 837-47.

[18] BOSTRöM P, ANDERSSON L, RUTBERG M, et al. SNARE proteins mediate fusion between cytosolic lipid droplets and are implicated in insulin sensitivity [J]. 2007, 9(11): 1286-93.

[19] BRASAEMLE D L J J O L R. Thematic review series: adipocyte biology. The perilipin family of structural lipid droplet proteins: stabilization of lipid droplets and control of lipolysis [J]. 2007, 48(12): 2547-59.

[20] FARESE JR R V, WALTHER T C J C. Lipid droplets finally get a little RESPECT [J]. 2009, 139(5): 855-60.

[21] GUO Y, CORDES K R, FARESE JR R V, et al. Lipid droplets at a glance [J]. 2009, 122(6): 749-52.

[22] GUO Y, WALTHER T C, RAO M, et al. Functional genomic

screen reveals genes involved in lipid-droplet formation and utilization [J]. 2008, 453(7195): 657-61.

[23] KURAT C F, WOLINSKI H, PETSCHNIGG J, et al. Cdk1/Cdc28-dependent activation of the major triacylglycerol lipase Tgl4 in yeast links lipolysis to cell-cycle progression [J]. 2009, 33(1): 53-63.

[24] CERMELLI S, GUO Y, GROSS S P, et al. The lipid-droplet proteome reveals that droplets are a protein-storage depot [J]. 2006, 16(18): 1783-95.

[25] MIYANARI Y, ATSUZAWA K, USUDA N, et al. The lipid droplet is an important organelle for hepatitis C virus production [J]. 2007, 9(9): 1089-97.

[26] CHO S Y, SHIN E S, PARK P J, et al. Identification of mouse Prp19p as a lipid droplet-associated protein and its possible involvement in the biogenesis of lipid droplets [J]. 2007, 282(4): 2456-65.

[27] NISHIMURA H, SALTIS J, HABBERFIELD A, et al. Phosphorylation state of the GLUT4 isoform of the glucose transporter in subfractions of the rat adipose cell: effects of insulin, adenosine, and isoproterenol [J]. 1991, 88(24): 11500-4.

[28] SCHAFFER J E J C O I L. Lipotoxicity: when tissues overeat [J]. 2003, 14(3): 281-7.

[29] GONG J, SUN Z, LI P J C O I L. CIDE proteins and metabolic disorders [J]. 2009, 20(2): 121-6.

[30] KELLER P, PETRIE J T, DE ROSE P, et al. Fat-specific protein 27 regulates storage of triacylglycerol [J]. 2008, 283(21): 14355-65.

[31] MAXFIELD F R, TABAS I J N. Role of cholesterol and lipid organization in disease [J]. 2005, 438(7068): 612-21.

[32] BOULANT S, MONTSERRET R, HOPE R G, et al. Structural determinants that target the hepatitis C virus core protein to lipid droplets [J]. 2006, 281(31): 22236-47.

[33] YANG H-J, HSU C-L, YANG J-Y, et al. Monodansylpentane as a blue-fluorescent lipid-droplet marker for multi-color live-cell imaging [J]. 2012, 7(3): e32693.

[34] BECERRA-RUIZ M, VARGAS V, JARA P, et al. Blue-Fluorescent Probes for Lipid Droplets Based on Dihydrochromeno-Fused Pyrazolo-and Pyrrolopyridines [J]. 2018, 2018(34): 4795-801.

[35] SK B, THAKRE P K, TOMAR R S, et al. A Pyridoindole-Based Multifunctional Bioprobe: pH-Induced Fluorescence Switching and Specific Targeting of Lipid Droplets [J]. 2017, 12(18): 2501-9.

[36] WANG E, ZHAO E, HONG Y, et al. A highly selective AIE fluorogen for lipid droplet imaging in live cells and green algae [J]. 2014, 2(14): 2013-9.

[37] JIANG M, GU X, LAM J W, et al. Two-photon AIE bio-probe with large Stokes shift for specific imaging of lipid droplets [J]. 2017, 8(8): 5440-6.

[38] LEE J H, SO J-H, JEON J H, et al. Synthesis of a new fluorescent small molecule probe and its use for in vivo lipid imaging [J]. 2011, 47(26): 7500-2.

[39] SPANDL J, WHITE D J, PEYCHL J, et al. Live cell multicolor imaging of lipid droplets with a new dye, LD540 [J]. 2009, 10(11): 1579-84.

[40] SHARMA A, UMAR S, KAR P, et al. A new type of biocompatible fluorescent probe AFN for fixed and live cell imaging of intracellular lipid droplets [J]. 2016, 141(1): 137-43.

[41] NIU G, ZHANG R, KWONG J P, et al. Specific two-photon imaging of live cellular and deep-tissue lipid droplets by lipophilic AIEgens at ultralow concentration [J]. 2018, 30(14): 4778-87.

[42] APPELQVIST H, STRANIUS K, BORJESSON K, et al. Specific imaging of intracellular lipid droplets using a benzothiadiazole derivative with solvatochromic properties [J]. 2017, 28(5): 1363-70.

[43] YAMAGUCHI E, WANG C, FUKAZAWA A, et al. Environment-Sensitive Fluorescent Probe: A Benzophosphole Oxide with an Electron-Donating Substituent [J]. 2015, 127(15): 4622-6.

[44] NIKO Y, DIDIER P, MELY Y, et al. Bright and photostable push-pull pyrene dye visualizes lipid order variation between plasma and intracellular membranes [J]. 2016, 6(1): 1-9.

[45] ÖBERG E, APPELQVIST H, NILSSON K P R J F I C. Non-fused

phospholes as fluorescent probes for imaging of lipid droplets in living cells [J]. 2017, 5: 28.

[46] DE MOLINER F, KING A, DIAS G G, et al. Quinone-derived π-extended phenazines as new fluorogenic probes for live-cell imaging of lipid droplets [J]. 2018, 6: 339.

[47] KIM E, LEE S, PARK S B J C C. A Seoul-Fluor-based bioprobe for lipid droplets and its application in image-based high throughput screening [J]. 2012, 48(17): 2331-3.

[48] WANG Z, GUI C, ZHAO E, et al. Specific fluorescence probes for lipid droplets based on simple AIEgens [J]. 2016, 8(16): 10193-200.

[49] MOTA A A, CORREA J R, DE ANDRADE L P, et al. From live cells to Caenorhabditis elegans: selective staining and quantification of lipid structures using a fluorescent hybrid benzothiadiazole derivative [J]. 2018, 3(4): 3874-81.

[50] GAO M, SU H, LI S, et al. An easily accessible aggregation-induced emission probe for lipid droplet-specific imaging and movement tracking [J]. 2017, 53(5): 921-4.

[51] LI S, LING X, LIN Y, et al. In situ generation of photoactivatable aggregation-induced emission probes for organelle-specific imaging [J]. 2018, 9(26): 5730-5.

[52] TANG J, ZHANG Y, YIN H Y, et al. Precise labeling and tracking of lipid droplets in adipocytes using a luminescent ZnSalen complex [J].

2017, 12(19): 2533-8.

[53] MANDAL S, JANA N R J T J O P C C. Quantum dot-based designed nanoprobe for imaging lipid droplet [J]. 2017, 121(42): 23727-35.

[54] GAO M, SU H, LIN Y, et al. Photoactivatable aggregation-induced emission probes for lipid droplets-specific live cell imaging [J]. 2017, 8(3): 1763-8.

[55] RYAN T, CHRIS W, JACKY W, et al. A near-infrared AIEgen for specific imaging of lipid droplets [J]. 2016, 52(35): 5957-60.

[56] WANG D, SU H, KWOK R T, et al. Facile synthesis of Red/NIR AIE luminogens with simple structures, bright emissions, and high photostabilities, and their applications for specific imaging of lipid droplets and image-guided photodynamic therapy [J]. 2017, 27(46): 1704039.

[57] ZHENG Z, ZHANG T, LIU H, et al. Bright near-infrared aggregation-induced emission luminogens with strong two-photon absorption, excellent organelle specificity, and efficient photodynamic therapy potential [J]. 2018, 12(8): 8145-59.

[58] GUO R, YIN J, MA Y, et al. A novel NIR probe for detection of viscosity in cellular lipid droplets, zebra fishes and living mice [J]. 2018, 271: 321-8.

[59] S. Martin, R. G. Parton, Lipid droplets: a unified view of a dynamic organelle, Nat. Rev. Mol. Cell Bio. 2006, 7, 373-378.

[60] A. R. Thiam, R. V. Farese Jr, T. C. Walther, The biophysics and cell biology of lipid droplets,Nat. Rev. Mol. Cell Bio. 2013, 14, 775-786.

[61] T. C. Walther, R. V. Farese Jr, Lipid droplets and cellular lipid metabolism, Annu. Rev. Biochem. 2012, 81, 687-714.

[62] R. V. Farese Jr, T. C. Walther, Lipid droplets finally get a little R-E-S-P-E-C-T, Cell 2009, 139, 855-860.

[63] J. K. Zehmer, Y. Huang, G. Peng, J. Pu, R. G. Anderson, P. Liu, A role for lipid droplets in inter-membrane lipid traffic. Proteomics, 2009, 9, 914-921.

[64] Z. Li, K. Thiel, P. J. Thul, M. Beller, R. P. Kühnlein, M. A. Welte, Lipid droplets control the maternal histone supply of *Drosophila* embryos. Curr. Biol. 2012, 22, 2104-2113.

[65] B. M. Spiegelman, J. S. Flier, Obesity and the regulation of energy balance. Cell 2001, 104, 531-543.

[66] L. Liu, K. Zhang, H. Sandoval, S. Yamamoto, M. Jaiswal, E. Sanz, H. J. Bellen, Glial lipid droplets and ROS induced by mitochondrial defects promote neurodegeneration, Cell 2015, 160, 177-190.

[67] A. S. Greenberg, R. A. Coleman, F. B. Kraemer, J. L. McManaman, M. S. Obin, V. Puri, D. G. Mashek, The role of lipid droplets in metabolic disease in rodents and humans, J. Clin. Invest. 2011, 121, 2102-2110.

[68] L. Tirinato, F. Pagliari, T. Limongi, M. Marini, A. Falqui, J. Seco, E. Di Fabrizio, An overview of lipid droplets in cancer and cancer stem cells, Stem Cells Int. 2017, 2017.

[69] N. E. Wolins, D. Rubin, D. L. Brasaemle, TIP47 associates with lipid droplets, J.Biol. Chem. 2001, 276, 5101–5108.

[70] M. C. Wang, W. Min, C. W. Freudiger, G. Ruvkun, X. S. Xie, RNAi screening for fatregulatory genes with SRS microscopy, Nat. Methods 2011, 8, 135–138.

[71] I. Barba, M. E. Cabanas, C. Arus, The relationship between nuclear magneticresonance-visible lipids, lipid droplets, and cell proliferation in cultured C6cells, Cancer Res. 1999, 59, 1861–1868.

[72] J. A. Levitt, M. K. Kuimova, G. Yahioglu, P. H. Chung, K. Suhling, D. Phillips, Membrane-Bound molecular rotors measure viscosity in live cells via fluorescence lifetime imaging, J. Phys. Chem. C 2009, 113, 11634–11642.

[73] J. A. Levitt, P. H. Chung, K. Suhling, Spectrally resolved fluorescence lifetime imaging of Nile red for measurements of intracellular polarity, J. Biomed. Opt. 2015, 20.

[74] S. M. Borisov, O. S. Wolfbeis, Optical biosensors, Chem. Rev. 2008, 108, 423–461.

[75] M. Jiang, X. Gu, J. W. Y. Lam, Y. Zhang, R. T. K. Kwok, K. S. Wong, B. Z. Tang, Chem. Sci. 2017, 8, 5440–5446.

[76] A. Loudet, K. Burgess, BODIPY dyes and their Derivatives: syntheses and spectroscopic properties, J. Chem. Rev. 2007, 107, 4891–4932.

[77] P. Greenspan, E. P. Mayer, S. D. Fowler, Nile red: a selective fluorescent stain for intracellular lipid droplets, J. Cell Biol. 1985, 100, 965–973.

[78] M. Collot, T. K. Fam, P. Ashokkumar, O. Faklaris, T. Galli, L. Danglot, A. S. Klymchenko, Ultrabright and fluorogenic probes for multicolor imaging and tracking of lipid droplets in cells and tissues, J. Am. Chem. Soc. 2018, 140, 5401–5411.

[79] O. A. Kucherak, P. Didier, Y. M´ely, A. S. Klymchenko, Fluorene analogues of prodan with superior fluorescence brightness and solvatochromism, J. Phys. Chem. Lett. 2010, 1, 616–620.

[80] H. Tian Jr, A. C. Sedgwick, H. H. Han, S. Sen, G. R. Chen, Y. Zang, J. L. Sessler, T. D. James, J. Li, X. P. He, Fluorescent probes for the imaging of lipid droplets in live cells. Coord. Chem. Rev. 2021, 427, 213577.

[81] M. Collot, T. K. Fam, P. Ashokkumar, O. Faklaris, T. Galli, L. Danglot, A. S. Klymchenko, Ultrabright and fluorogenic probes for multicolor imaging and tracking of lipid droplets in cells and tissues. J. Am. Chem. Soc. 2018, 140, 5401–11.

[82] X. Zheng, W. Zhu, F. Ni, H. Ai, S. Gong, X. Zhou, J. L. Sessler, C. Yang, Simultaneous dual-colour tracking lipid droplets and lysosomes dynamics using a fluorescent probe. Chem. Sci. 2019, 10, 2342–8.

[83] R. Hu, B. Chen, Z. Wang, A. Qin, Z. Zhao, X. Lou, B. Z. Tang, Intriguing "chameleon" fluorescent bioprobes for the visualization of lipid droplet-lysosome interplay. Biomaterials 2019, 203, 43–51.

[84] N. Zhao, Y. Li, W. Yang, J. Zhuang, Y. Li, N. Li, Multifunctional pyrazoline based AIEgens: real-time tracking and specific protein “fishing” of lipid droplets. Chem. Sci. 2019, 10, 9009–16.

[85] L. Guo, M. Tian, Z. Zhang, Q. Lu, Z. Liu, G. Niu, X. Yu, Simultaneous two-color visualization of lipid droplets and endoplasmic reticulum and their interplay by single fluorescent probes in lambda mode. J. Am. Chem. Soc. 2021, 143, 3169–79.

[86] M. Ye, W. Hu, M. He, C. Li, S. Zhai, Z. Liu, Y. Wang, H. Zhang, C. Li, Deep imaging for visualizing nitric oxide in lipid droplets: discovering the relationship between nitric oxide and resistance to cancer chemotherapy drugs. Chem. Commun. 2020, 56, 6233–6.

[87] M. K. Cho, M. J. Seo, V. Juvekar, J. H. Jo, W. Kim, K. S. Choi, H. M. Kim, Screening of drug-induced steatosis and phospholipidosis using lipid droplet-selective two-photon probes. Anal. Chem. 2020, 92, 11223–31.

[88] G. Jiang, Y. Jin, M. Li, H. Wang, M. Xiong, W. Zeng, H. Yuan, C. Liu, Z. Ren, C. Liu, Faster and more specific: excited-state intramolecular proton transfer-based dyes for high-fidelity dynamic imaging of lipid droplets within cells and tissues. Anal. Chem. 2020, 92, 10342–9.

[89] X. Zhang, L. Yuan, J. Jiang, J. Hu, A. du Rietz, H .Cao, R. Zhang, X. Tian, F. Zhang, Y. Ma, Z. Zhang, K. Uvdal, Z. Hu, Light-up lipid droplets dynamic behaviors using a red-emitting fluorogenic probe. Anal. Chem. 2020, 92, 3613–9.

[90] K. Wang, S. Ma, Y. Ma, Y. Zhao, M. Xing, L. Zhou, D. Cao, W. Lin, Aurone derivative revealing the metabolism of lipid droplets and monitoring oxidative stress in living cells. Anal. Chem. 2020, 92, 6631–6.

[91] T. Yoshihara, R. Maruyama, S. Shiozaki, K. Yamamoto, S. Kato, Y. Nakamura, S. Tobita, Visualization of lipid droplets in living cells and fatty livers of mice based on the fluorescence of π-extended coumarin using fluorescence lifetime imaging microscopy. Anal. Chem. 2020, 92, 4996–5003.

[92] X. Wang, F. Qi, Z. Jiang, M. Yan, L. Xu, Highly fluorescent bisboron complexes in both solution and solid-state: synthesis, photophysical properties and lipid droplet imaging in living cells. Dyes Pigments 2021, 186, 108999.

[93] W. Ren, D. Wang, W. Huang, J. Li, X. Tian, Z. Liu, G. Han, B. Liu, M. Han, Z. Zhang, R. Zhang, Real-time tracking of lipid droplets

interactions with other organelles by a high signal/noise probe. Dyes Pigments 2021, 191, 109366.

[94] B. Dong, W. Song, Y. Lu, Y. Sun, W. Lin, Revealing the viscosity changes in lipid droplets during ferroptosis by the real-time and in situ near-infrared imaging. ACS Sens 2021, 6, 22–6.

[95] P. Tan, W. Zhuang, S. Li, J. Zhang, H. Xu, L. Yang, Y. Liao, M. Chen, Q. Wei, A lipid droplet targeted fluorescent probe for high-efficiency image-guided photodynamic therapy of renal cell carcinoma. Chem. Commun. 2021, 57, 1046–9.

[96] M. Waltermann, A. Steinbuchel, Neutral lipid bodies in prokaryotes: recent insights into structure, formation, and relationship to eukaryotic lipid depots, J. Bacteriology 2005, 187, 3607–3619.

[97] D. J. Murphy, The dynamic roles of intracellular lipid droplets: from archaea to mammals， Protoplasma 2012, 249, 541-585.

[98] S. Martin, R. G. Parton, Lipid droplets: a unified view of a dynamic organelle, Nat. Rev. Mol. Cell Biol. 2006, 7, 373-378.

[99] R. V. Farese, T. C. Walther, Lipid droplets finally get a little R-E-S-P-E-C-T, Cell 2009, 139, 855-860.

[100] L. Liu, K. Zhang, H. Sandoval, S. Yamamoto, M. Jaiswal, E. Sanz, et al. Glial lipid droplets and ROS induced by mitochondrial defects promote neurodegeneration, Cell 2015, 160, 177-190.

[101] T. Fujimoto, Y. Ohsaki, J. Cheng, M. Suzuki, Y. Shinohara, Lipid

droplets: a classic organelle with new outfits, Histochem. Cell Biol. 2008, 130, 263-279.

[102] N. Krahmer, R. V. Farese, T. C. Walther, Balancing the fat: lipid droplets and human disease, EMBO Mol Med 2013, 5, 973-983.

[103] P. T. Bozza, J. P. B. Viola, Lipid droplets in inflammation and cancer, Prostag. Leukotr. Ess. 2010, 82, 243-250.

[104] H. Abramczyk, J. Surmacki, M. Kopeć, A. K. Olejinik, P. L. Pietruszewska, K. F. Majewska, The role of lipid droplets and adipocytes in cancer raman imaging of cell cultures: MCF10A, MCF7, and MDA-MB-231 compared to adipocytes in cancerous human breast tissue, Analyst 2015, 140, 2224-2235.

[105] S. Beloribi-Djefaflia, S. Vasseur, F. Guillaumond, Lipid metabolic reprogramming in cancer cells, Oncogenesis 2016, 5, e189.

[106] T. C. Walther, R. V. Farese Jr., Lipid droplets and cellular lipid metabolism, Annu. Rev. Bio. 2012, 81,687−714.

[107] P. Greenspan, E. P. Mayer, S. D. Fowler, Nile red: a selective fluorescent stain for intracellular lipid droplets, J. Cell. Biol. 1985, 100, 965-973.

[108] Z. Wang, C. Gui, E. Zhao, J. Wang, X. Li, A. Qin, et al. Specific fluorescence probes for lipid droplets based on simple AIEgens, ACS Appl. Mater. Interfaces 2016, 8, 10193-10200.

[109] M. Gao, H. Su, S. Li, Y. Lin , X. Ling, A. Qin, et al. An easily

accessible aggregation-induced emission probe for lipid droplet-specific imaging and movement tracking, Chem. Commun. 2017, 53, 921-924.

[110] M. Gao, H. Su, Y. Lin, X. Ling, S. Li, A. Qin, et al. Photoactivatable aggregation-induced emission probes for lipid droplets-specific live cell imaging, Chem. Sci. 2017, 8, 1763-1768.

[111] M. Jiang, X. Gu, J. W. Y. Lam, Y. Zhang, R. T. K. Kwok, K. S. Wong, et al. Two-photon AIE bio-probe with large Stokes shift for specific imaging of lipid droplets, Chem. Sci. 2017, 8, 5440-5446.

[112] Z. Zheng, T. Zhang, H. Liu, Y. Chen, R. T. K. Kwok, C. Ma, et al. Bright near-infrared aggregation-induced emission luminogens with strong two-photon absorption, excellent organelle specificity, and efficient photodynamic therapy potential, ACS Nano 2018, 12, 8145-8159.

[113] C. W. Song, U. Tamima, Y. J. Reo, M. Dai, S. Sarkar, K. H. Ahn, A rationally designed polarity–viscosity sensitive probe for imaging lipid droplets, Dyes and Pigments 2019, 171, 107718.

[114] Y. Yan, S. Li, Z. Zhang, J. Qu, J. Wang, A sensitive bio-probe for tracking lipid droplets with large Stokes shift and its application in cell imaging, Spectrochim. Acta Part A. 2021, 260, 119988.

[115] M. Collot, T. K. Fam, P. Ashokkumar, O. Faklaris, T. Galli, et al.Ultrabright and fluorogenic probes for multicolor imaging and tracking of lipid droplets in cells and tissues, J. Am. Chem. Soc. 2018,140, 5401-

5411.

[116] D. Wang, H. Su, R. T. K. Kwok, G. Shan, A. C. S. Leung, et al.Facile synthesis of Red/NIR AIE luminogens with simple structures, bright emissions, and high photostabilities, and their applications for specific imaging of lipid droplets and image-guided photodynamic therapy, Adv. Funct. Mater. 2017, 27, 1704039.

[117] J. Luo, Z. Xie, J. W. Y. Lam, L. Cheng, B. Z. Tang, et al. Aggregation-induced emission of 1-methyl-1,2,3,4,5-pentaphenylsilole, Chem. Commun. 2001,1740-1741.

[118] Y. W. Jun, H. R. Kim, Y. J. Reo, M. Dai, K. H. Ahn, Addressing the autofluorescence issue in deep tissue imaging by two-photon microscopy: the significance of far-red emitting dyes, Chem. Sci. 2017, 8, 7696-7704.

[119] R. Chowdhury, B. Jana, A. Saha, S. Ghosh, K. Bhattacharyya, Confocal microscopy of cytoplasmic lipid droplets in a live cancer cell: number, polarity, diffusion and solvation dynamics, Med. Chem. Comm. 2014, 5, 536-539.

[120] S. Chen, Y. Hong, Y. Zeng, Q. Sun, Y. Liu, et al. Mapping live cell viscosity with an aggregation-induced emission fluorogen by means of two-photon fluorescence lifetime imaging, Chem. Eur. J. 2015, 21, 4315-4320.

[121] C. Reichardt, Solvatochromic dyes as solvent polarity indicators, Chem. Rev. 1994, 94, 2319-2358.

[122] D. Yao, Z. Lin, J. Wu, Near-infrared fluorogenic probes with polarity-sensitive emission for in vivo imaging of an ovarian cancer biomarker, ACS Appl. Mater. Interfaces 2016, 8, 5847-5856.

[123] M. Li, J. Fan, H. Li, J. Du, S. Long, X. Peng, A ratiometric fluorescence probe for lysosomal polarity, Biomaterials 2018, 164, 95-108.

[124] A. Jimenez-Sanchez, E. K. Lei, P. S. O. Kelley, A multifunctional chemical probe for the measurement of local micropolarity and microviscosity in mitochondria, Angew. Chem., Int. Ed. 2018, 57, 8891-8895.

[125] T. B. Ren, W. Xu, Q. L. Zhang, X. Zhang, S. Yu, H. Yi, et al. Enhancing the anti-solvatochromic two-photon fluorescence for cirrhosis imaging by forming a hydrogen-bond network, Angew. Chem., Int. Ed. 2018, 57, 7473-7477.

[126] L. Liu, Y. Zhang, J. Zhou, J. Yang, C. Zhong, Y. Zhang, et al. Design of a quinazolinone-based environment-sensitive fluorescent dye: solvatochromic fluorescence and application for one-photon and two-photon bioimaging, Dyes and Pigments 2019, 165, 58-64.

[127] W. Y. Kim, H. Shi, H. S. Jung, D. Cho, P. Verwilst, J. Y. Lee, et al. Coumarin-decorated schiff base hydrolysis as an efficient driving force for the fluorescent detection of water in organic solvents, Chem. Commun. 2016, 52, 8675-8678.

[128] S. Osella, S. Knippenberg, Laurdan as a molecular rotor in biological environments, ACS Appl. Bio Mater. 2019, 2, 5769-5778.

[129] M. Hornum, J. Kongsted, P. Reinholdt, Computational and photophysical characterization of a laurdan malononitrile derivative, P. C. C. P. 2021, 23, 9139-9146.

[130] S. Sasaki, G. P. C. Drummen, G. Konishi, Recent advances in twisted intramolecular charge transfer (TICT) fluorescence and related phenomena in materials chemistry, J. Mater. Checm. C. 2016, 14, 2731-2743.

[131] M. Fu, W. Shen, Y. Chen, W. Yi, C. Cai, L. Zhu, et al. A highly sensitive red-emitting probe for the detection of viscosity changes in living cells, zebrafish, and human blood samples, J. Mater. Chem. B, 2020, 8, 1310-1315.

[132] S. Ludwanowski, A. Samanta, S. Loescher, C. B. Kowollik, A. Walther, A modular fluorescent probe for viscosity and polarity sensing in DNA hybrid mesostructures, Advanced Science, 2021, 8, 2003740.

[133] S. Ye, H. Zhang, J. Fei, C. H. Wolstenholme, P. X. Zhang, A general strategy to control viscosity sensitivity of molecular rotor-based fluorophores, Angew. Chem., Int. Ed. 2021, 60, 1339-1346.

[134] C. Reichardt, Solvatochromic dyes as solvent polarity indicators, Chem. Rev. 1994, 94, 416-431.

[135] C. Reichardt, Polarity of ionic liquids determined empirically by

means of solvatochromic pyridinium N-phenolate betaine dyes, Green Chem. 2005, 7, 339-351.

[136] J. P. Cerón-Carrasco, D. Jacquemin, C. Laurence, A. Planchat, C. Reichardt, K. Sraïdi, Solvent polarity scales: determination of new $E_T(30)$ values for 84 organic solvents, J. Phys. Org. Chem. 2014, 27, 512-518.

[137] C. Reichardt, Solvatochromic dyes as solvent polarity indicators, Chem. Rev. 1994, 21, 2319.

[138] I. M. Smallwood, Handbook of organic solvent properties, Headline Publishing Group, 1996.

[139] B. K. An, J. Gierschner, S. Y. Park, π-conjugated cyanostilbene derivatives: a unique self-assembly motif for molecular nanostructures with enhanced emission and transport, Acc. Chem. Res. 2012, 45, 544-554.

[140] B. Xu, J. He, Y. Dong, F. Chen, W. Yu, W. Tian, Aggregation emission properties and self-assembly of conjugated oligocarbazoles, Chem. Comm. 2011, 47, 6602-6604.

[141] K. Luby-Phelps, S. Mujumdar, R. Mujumdar, L. Ernst, W. Galbraith, A. Waggoner, A novel fluorescence ratiometric method confirms the low solvent viscosity of the cytoplasm, Biophys. J. 1993, 65, 236-242.

[142] C. Jüngst, M. Klein, A. Zumbusch, Long-term live cell microscopy studies of lipid droplet fusion dynamics in adipocytes, J. Lipid. Res. 2013,

54, 3419-3429.

[143] J. B. Segur, H. E. Oberstar, Viscosity of glycerol and its aqueous solutions, Ind. Eng. Chem. Res. 1951, 43, 2117-2120.

[144] G. Zhang, Y. Ni, D. Zhang, H. Li, N. Wang, C. Yu, et al. Rational design of NIR fluorescence probes for sensitive detection of viscosity in living cells, Spectrochim. Acta Part A. 2019, 214, 339-347.

[145] G. Zhang, Y. Sun, X. He, W. Zhang, M. Tian, R. Feng, et al. Red-emitting mitochondrial probe with ultrahigh signal-to-noise ratio enables high-fidelity fluorescent images in two-photon microscopy, Anal. Chem. 2015, 87, 12088-12095.

[146] J. Liu, Y. Q. Sun, Y. Y. Huo, H. Zhang, L. Wang, P. Zhang, et al. Simultaneous fluorescence sensing of Cys and GSH from different emission channels, J. Am. Chem. Soc. 2014, 136, 574-577.

[147] H. Huang, W. Liu, X. J. Liu, Y. Q. Kuang, J. H. Jiang, A novel mitochondria-targeted near-infrared fluorescence probe for ultrafast and ratiometric detection of SO_2 derivatives in live cells, Talanta 2017, 3, 203-209.

[148] J. Lv, Y. Chen, F. Wang, T. Wei, Z. Zhang, J. Qiang, et al. A mitochondria-targeted fluorescent probe based on fluorescein derivative for detection of hypochlorite in living cells, Dyes and Pigments 2018, 148, 353-358.

[149] C. Thiele, J. Spandl, Cell biology of lipid droplets, Curr. Opin. Cell

Biol. 20 (2008) 378–385. https://doi.org/10.1016/j.ceb.2008.05.009.

[150] A.R. Thiam, R. V. Farese, T.C. Walther, The biophysics and cell biology of lipid droplets, Nat. Rev. Mol. Cell Biol. 14 (2013) 775–786. https://doi.org/10.1038/nrm3699.

[151] T. Yang, Y. Zuo, Y. Zhang, Z. Gou, X. Wang, W. Lin, AIE-active polysiloxane-based fluorescent probe for identifying cancer cells by locating lipid drops, Anal. Chim. Acta. 1091 (2019) 88–94. https://doi.org/10.1016/j.aca.2019.09.020.

[152] R. Guo, J. Yin, Y. Ma, G. Li, Q. Wang, W. Lin, A novel NIR probe for detection of viscosity in cellular lipid droplets, zebra fishes and living mice, Sensors Actuators, B Chem. 271 (2018) 321–328. https://doi.org/10.1016/j.snb.2018.05.055.

[153] W.L. Wu, H.L. Ma, L.L. Xi, M.F. Huang, K.M. Wang, J.Y. Miao, B.X. Zhao, A novel lipid droplets-targeting ratiometric fluorescence probe for hypochlorous acid in living cells, Talanta. 194 (2019) 308–313. https://doi.org/10.1016/j.talanta.2018.10.006.

[154] C.W. Song, U. Tamima, Y.J. Reo, M. Dai, S. Sarkar, K.H. Ahn, A rationally designed polarity–viscosity sensitive probe for imaging lipid droplets, Dye. Pigment. 171 (2019) 107718. https://doi.org/10.1016/j.dyepig.2019.107718.

[155] P. Greenspan, E.P. Mayer, S.D. Fowler, Nile red: A selective fluorescent stain for intracellular lipid droplets, J. Cell Biol. 100 (1985)

965–973. https://doi.org/10.1083/jcb.100.3.965.

[156] S. Martin, R.G. Parton, Late Endosome, Definitions. 7 (2020) 373–378. https://doi.org/10.32388/4fgx6b.

[157] T. Fujimoto, Y. Ohsaki, J. Cheng, M. Suzuki, Y. Shinohara, Lipid droplets: A classic organelle with new outfits, Histochem. Cell Biol. 130 (2008) 263–279. https://doi.org/10.1007/s00418-008-0449-0.

[158] N. Krahmer, R. V. Farese, T.C. Walther, Balancing the fat: Lipid droplets and human disease, EMBO Mol. Med. 5 (2013) 973–983. https://doi.org/10.1002/emmm.201100671.

[159] M.A. Welte, Expanding roles for lipid droplets, Curr. Biol. 25 (2015) R470–R481. https://doi.org/10.1016/j.cub.2015.04.004.

[160] S. Beloribi-Djefaflia, S. Vasseur, F. Guillaumond, Lipid metabolic reprogramming in cancer cells, Oncogenesis. 5 (2016) e189–e189. https://doi.org/10.1038/oncsis.2015.49.

[161] P.T. Bozza, J.P.B. Viola, Lipid droplets in inflammation and cancer, Prostaglandins Leukot. Essent. Fat. Acids. 82 (2010) 243–250. https://doi.org/10.1016/j.plefa.2010.02.005.

[162] F. Boschi, V. Rizzatti, M. Zamboni, A. Sbarbati, Lipid droplets fusion in adipocyte differentiated 3T3-L1 cells: A Monte Carlo simulation, Exp. Cell Res. 321 (2014) 201–208. https://doi.org/10.1016/j.yexcr.2013.12.023.

[163] Y. Saito, R.R. Desai, S.K. Muthuswamy, Reinterpreting polarity

and cancer: The changing landscape from tumor suppression to tumor promotion, Biochim. Biophys. Acta - Rev. Cancer. 1869 (2018) 103–116. https://doi.org/10.1016/j.bbcan.2017.12.001.

[164] S.O. Olofsson, P. Boström, L. Andersson, M. Rutberg, J. Perman, J. Borén, Lipid droplets as dynamic organelles connecting storage and efflux of lipids, Biochim. Biophys. Acta - Mol. Cell Biol. Lipids. 1791 (2009) 448–458. https://doi.org/10.1016/j.bbalip.2008.08.001.

[165] T.C. Walther, R. V. Farese, Lipid droplets and cellular lipid metabolism, Annu. Rev. Biochem. 81 (2012) 687–714. https://doi.org/10.1146/annurev-biochem-061009-102430.

[166] F. Baenke, B. Peck, H. Miess, A. Schulze, Hooked on fat: The role of lipid synthesis in cancer metabolism and tumour development, DMM Dis. Model. Mech. 6 (2013) 1353–1363. https://doi.org/10.1242/dmm.011338.

[167] C. Ghosh, S. Nandi, K. Bhattacharyya, Probing micro-environment of lipid droplets in a live breast cell: MCF7 and MCF10A, Chem. Phys. Lett. 670 (2017) 27–31. https://doi.org/10.1016/j.cplett.2016.12.068.

[168] R. Chowdhury, M.A. Amin, K. Bhattacharyya, Intermittent Fluorescence Oscillations in Lipid Droplets in a Live Normal and Lung Cancer Cell: Time-Resolved Confocal Microscopy, J. Phys. Chem. B. 119 (2015) 10868–10875. https://doi.org/10.1021/jp5120042.

[169] J. Yin, M. Peng, W. Lin, Two-photon fluorescence imaging of lipid

drops polarity toward cancer diagnosis in living cells and tissue, Sensors Actuators, B Chem. 288 (2019) 251–258. https://doi.org/10.1016/j.snb.2019.02.122.

[170] S. Mandal, N.R. Jana, Quantum Dot-Based Designed Nanoprobe for Imaging Lipid Droplet, J. Phys. Chem. C. 121 (2017) 23727–23735. https://doi.org/10.1021/acs.jpcc.7b07571.

[171] M. Jiang, X. Gu, J.W.Y. Lam, Y. Zhang, R.T.K. Kwok, K.S. Wong, B.Z. Tang, Two-photon AIE bio-probe with large Stokes shift for specific imaging of lipid droplets, Chem. Sci. 8 (2017) 5440–5446. https://doi.org/10.1039/c7sc01400g.

[172] F. Gai, Y. Zuo, W. Lin, Detecting lipid droplets polarity: Silicone-based unique fluorescent probe for cancer diagnosis in living cells, Talanta. 225 (2021) 122059. https://doi.org/10.1016/j.talanta.2020.122059.

[173] X. Zhang, L. Yuan, J. Jiang, J. Hu, A. Du Rietz, H. Cao, R. Zhang, X. Tian, F. Zhang, Y. Ma, Z. Zhang, K. Uvdal, Z. Hu, Light-Up Lipid Droplets Dynamic Behaviors Using a Red-Emitting Fluorogenic Probe, Anal. Chem. 92 (2020) 3613–3619. https://doi.org/10.1021/acs.analchem.9b04410.

[174] Y. Dai, Z. Zhan, Q. Li, R. Liu, Y. Lv, Simultaneous monitoring of polarity changes of lipid droplets and lysosomes with two-photon fluorescent probes, Anal. Chim. Acta. 1136 (2020) 34–41.

https://doi.org/10.1016/j.aca.2020.08.033.

[175] H. Xu, H. Zhang, G. Liu, L. Kong, X. Zhu, X. Tian, Z. Zhang, R. Zhang, Z. Wu, Y. Tian, H. Zhou, Coumarin-Based Fluorescent Probes for Super-resolution and Dynamic Tracking of Lipid Droplets, Anal. Chem. 91 (2019) 977–982. https://doi.org/10.1021/acs.analchem.8b04079.

[176] H. Tian, A.C. Sedgwick, H.H. Han, S. Sen, G.R. Chen, Y. Zang, J.L. Sessler, T.D. James, J. Li, X.P. He, Fluorescent probes for the imaging of lipid droplets in live cells, Coord. Chem. Rev. 427 (2021) 213577. https://doi.org/10.1016/j.ccr.2020.213577.

[177] K.N. Wang, X.J. Peng, Y. Li, H.T. Tang, Y.M. Pan, L. He, Photostable fluorescent probes for 3D imaging and monitoring the metabolism of lipid droplets, Dye. Pigment. 180 (2020). https://doi.org/10.1016/j.dyepig.2020.108502.

[178] F. Meng, J. Niu, H. Zhang, R. Yang, Q. Lu, Y. Yu, Z. Liu, G. Niu, X. Yu, Simultaneous visualization of lipid droplets and lysosomes using a single fluorescent probe, Sensors Actuators, B Chem. 329 (2021). https://doi.org/10.1016/j.snb.2020.129148.

[179] L. Liu, K. Zhang, H. Sandoval, S. Yamamoto, M. Jaiswal, E. Sanz, Z. Li, J. Hui, B.H. Graham, A. Quintana, H.J. Bellen, Glial lipid droplets and ROS induced by mitochondrial defects promote neurodegeneration, Cell. 160 (2015) 177–190. https://doi.org/10.1016/j.cell.2014.12.019.

[180] Y. Yan, S. Li, Z.H. Zhang, J. Qu, J.Y. Wang, A sensitive bio-probe

for tracking lipid droplets with large Stokes shift and its application in cell imaging, Spectrochim. Acta - Part A Mol. Biomol. Spectrosc. 260 (2021) 119988. https://doi.org/10.1016/j.saa.2021.119988.

[181] W.-L. Cui, Z.-H. Zhang, L. Wang, J. Qu, J.-Y. Wang, A novel and stable fluorescent probe for tracking Hg2+ with large Stokes shift and its application in cell imaging, Spectrochim. Acta Part A Mol. Biomol. Spectrosc. 267 (2021) 120516. https://doi.org/10.1016/j.saa.2021.120516.

[182] C. Reichardt, Solvatochromic dyes as solvent polarity indicators, Chem. Rev. 94 (1994) 2319–2358. https://doi.org/10.1021/cr00032a005.

[183] I.M. Smallwood, Handbook of Organic Solvent Properties, Handb. Org. Solvent Prop. (2012) 1–306. https://doi.org/10.1016/C2009-0-23646-4.